APPLICATIONS OF SINGLE SELECTIVE INVERSION DNMR

APPLICATIONS OF SINGLE SELECTIVE INVERSION DNMR

By

Suzie S. Rigby

B.Sc.

A Thesis

Submitted to the School of Graduate Studies

in Partial Fulfilment of the Requirements

for the Degree

Master of Science

McMaster University

August, 1994

MASTER OF SCIENCE McMASTER UNIVERSITY

(Chemistry) Hamilton, Ontario

TITLE: Applications of Single Selective Inversion DNMR

AUTHOR: Suzie S. Rigby, B.Sc. (Brock University)

Supervisors: Professor A.D. Bain, Professor M.J.M. McGlinchey

Number of pages: xii, 125

Abstract

The single selective inversion recovery experiment, developed by Bain and Cramer, has been used with great success in elucidating the molecular dynamics of three systems.

The isomerization of *d,l* bis(1-indenyl)dimethylsilane to its *meso* isomer proceeds through sequential [1,5]-suprafacial shifts; $\Delta H^{\ddagger}$ for the process was evaluated as 21.9 ± 0.5 kcal/mol. There is only one mechanism operating at a detectable rate below about 150 °C. Below 100 °C this process is too slow to be detected by DNMR, but it is readily followed by classical kinetics methods. Above 100 °C, the isomerization may be followed by 1D selective inversion experiments. The isoindene intermediate is conveniently trapped as its double Diels-Alder adduct showing that the rearrangement occurs relatively rapidly on the chemical time-scale.

The barrier to hindered rotation about the Mn - C(4) sigma bond in (η^1-Cpp)$Mn(CO)_3(PEt_3)_2$ was measured. The observed value of $\Delta H^{\ddagger}$ was 13.1 ± 0.2 kcal/mol. $\Delta S^{\ddagger}$ was determined to be -11.2 ± 0.7 eu. As the compound is thermally sensitive, it would have been impossible to use lineshape analysis to determine the barrier. 1D selective inversion recovery experiments were used.

A combination of ^{13}C NOESY, ^{13}C single selective inversion, and ^{13}C lineshape analysis experiments identified the exchange pathways and determined temperature-dependent rate constants for the *N,N'*-[dimethyl-(2,2'-dithiobisacetyl)]ethylenediamine (DADS) system. DADS exists as five exchanging rotamers in solution. Two of the conformers are symmetric, with C_2 symmetry (*ZZ1* and *ZZ2*). The other three conformers are asymmetric, with one amide group cis and the other trans (*ZE1, ZE2, ZE3*).

The NOESY experiments gave a site-to-site map of the exchange processes at several temperatures. At room temperature, *ZE1* is exchanging

with both *ZE2* and *ZE3*, but there appears to be no exchange between *ZE2* and *ZE3*. This process seems to occur via hindered rotation about the disulfide bond, with $\Delta H^{\ddagger} = 15.3 \pm 0.4$ kcal/mol, and $\Delta S^{\ddagger} = -6.3 \pm 1.1$ eu.

At higher temperatures, *ZZ1* and *ZZ2* start to exchange with *ZE1* via hindered rotation about the amide bonds. $\Delta H^{\ddagger}$ for the process was determined to be 19.8 ± 0.4 kcal/mol, and $\Delta S^{\ddagger}$ was found to be 0.7 ± 1.2 eu. The barrier agrees quite well with that measured for the uncyclized precursor to DADS. $\Delta H^{\ddagger}$ was found to be 19.3 ± 0.7 kcal/mol, while $\Delta S^{\ddagger}$ was determined to be 2.5 ± 2.1 eu.

ACKNOWLEDGEMENTS

I would like to thank my two supervisors, Professor A.D. Bain, and Professor M.J. McGlinchey. Besides being patient and understanding, they created a working environment which was very pleasant and conducive to getting things done.

I would also like to thank my coworkers: Dr. Janice Cramer, Dr. Gregory Duns, Frank Rathgeb, Dr. Luc Girard, Dr. Hari Gupta, Ralph Ruffolo, Pippa Lock and Lisa Chao.

I would like to thank Dr. R. Bell, Dr. R. Maharajh, Dr. A. Decken and John Valliant for the molecules.

Thanks go to Dr. Donald Hughes and Mr. Brian Sayer for the NMR time, and advice.

Finally, I would like to thank my parents, family and friends, without whom graduate school would have ended before this project began.

TABLE OF CONTENTS

LIST OF FIGURES

LIST OF TABLES

CHAPTER ONE

Introduction

1.1 Chemical Exchange

Molecules in solution often exist as an equilibrium mixture of two or more species. These species may possess different conformations, different ionized forms, different positions of protonation, etc. Some of the atoms in such a molecule will be in one environment in one conformation, and a different environment in another conformation. For example, an axial hydrogen in cyclohexane becomes an equatorial hydrogen upon ring inversion of the molecule. These atoms are said to undergo chemical exchange.

There are many methods available for studying the kinetics of chemically exchanging systems. Nuclear magnetic resonance (NMR) spectroscopy is an excellent method for several reasons.

While NMR can be used to follow the time course of concentrations during a chemical reaction, it is one of the few methods available for studying rates of reactions when the system observed is at equilibrium. Under conditions of dynamic equilibrium, the exchange process is proceeding at a detectable rate, although there is no net reaction. Most kinetics methods such as stopped flow, temperature or pressure jump methods, follow the transformation of one substance into another substance.[1] There are NMR spectral changes caused by kinetic processes, even when the system being observed is at equilibrium. Dynamic nuclear magnetic resonance (DNMR) spectroscopy makes use of these spectral changes to determine rate constants and mechanisms for chemical exchange processes.[2]

NMR differs from other methods for studying chemical exchange in that separate signals due to nuclei in different chemical environments may be resolved and assigned.[2] The NMR spectrum can give information about the parts of the molecule that are involved in the exchange process. Furthermore, a wide range of nuclei may be observed.

It should be noted that in many cases, it is possible to obtain kinetic information over a very wide temperature range. Errors in the thermodynamic parameters obtained from such data are likely to be small. Of course this is the case with any technique which permits the measurement of rate constants over a wide temperature range, not just NMR.

DNMR has experienced a boom since the late 1960's, because of the introduction of FT NMR spectrometers, and the accessibility of high speed computers.[3] Fast computers have made the calculation of exchange-broadened spectra routine, thereby eliminating the need to use approximate expressions for obtaining rate constants. With FT NMR, it is possible to manipulate a spin system to get it to provide information other than that obtained from a continuous wave spectrum. Experiments can thus be tailored to give the specific information that is required. More will be said about this in chapter two, when DNMR methods are discussed in detail.

1.2 Dynamic Nuclear Magnetic Resonance

Chemical exchange processes between the different species of a molecule may affect the NMR spectrum of that molecule. Based on the changes in the shape of the NMR spectra of the system under study, rate constants for these chemical exchange processes may be determined using dynamic nuclear

magnetic resonance (DNMR) methods.[4] As well as these kinetic data, DNMR methods may give mechanistic information about the exchange pathways involved in the process.

In a system which is not undergoing chemical exchange, separate NMR signals will be observed for each of the species present in solution. If a reversible chemical process which exchanges nuclei between some environments or sites occurs, the NMR signals arising from those exchanging nuclei (and also from nuclei which are spin-coupled to them) will be affected by the exchange.[3] If the rate of chemical exchange between the species being observed is small, one will see broadening in the signals. As the rate of exchange increases, with increasing temperature, the signals gradually merge or coalesce, until only one averaged signal is seen.

Rate constants in the range 10^{-1} to 10^{8} may be measured, depending upon the DNMR method used. These reaction rates correspond to a range of rates of reactions and isomerizations that occur widely in chemistry, making NMR a convenient method of studying the kinetics of many exchanging systems. For example, DNMR has been used to study hindered rotation about partial double bonds in amides, rotation about sterically hindered single bonds, ring inversion in cyclohexane, pyramidal inversions of sulfur atoms, etc.[5]

1.3 Introduction to the Systems Studied in this Thesis

The molecular dynamics of three systems were investigated in this thesis work. In all three systems, the slow exchange regime was accessible, and some of the rate constants were determined using the single selective inversion recovery method of Bain and Cramer.[6,7] This method, along with other DNMR

methods will be discussed in chapter two. Following chapter two, there are three chapters, one for each of the molecules mentioned below. These chapters describe the exchange pathways, the determination of the rate constants, and the derivation of the activation parameters for the systems.

1.3.1 Bis(1-indenyl)dimethylsilane

The molecular dynamics of bis(1-indenyl)dimethylsilane were reported recently.[8] In solution the molecule was found to exist as a mixture of *d,l* enantiomers, exchanging with a *meso* isomer.

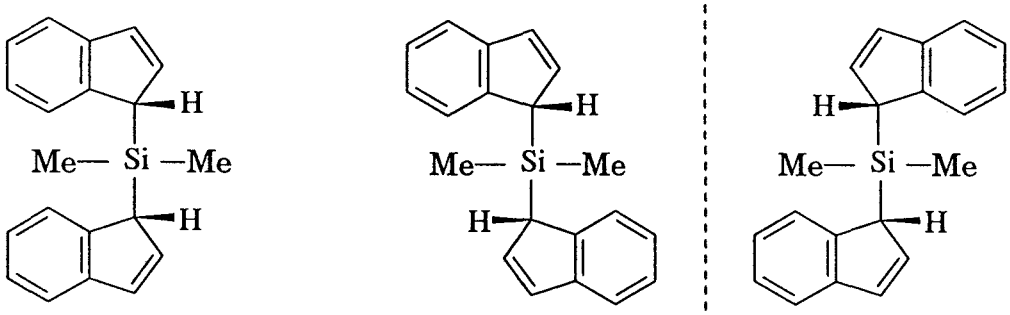

Meso *d,l*

The *d,l* isomers give rise to a single methyl NMR resonance, while the *meso* isomer gives rise to two methyl signals. Kinetic data were obtained, and thermodynamic parameters were reported for the thermal diastereomerization process for this molecule, as well as for several related molecules.

The work bore reinvestigation because the means used to obtain rate constants were questionable, and therefore, so were the activation parameters derived form them. Also, the authors reported that the mechanism for the exchange process was a symmetry forbidden [1,3]-silicon shift. The molecule was therefore prepared, in order to determine meaningful activation parameters.

Since the barrier to isomerization was so high, selective inversion experiments would be useful in measuring rate constants. Further, it was hoped that the isoindene intermediate could be trapped using a Diels-Alder reaction to confirm that the exchange process was a [1,5]-silicon shift, rather than the symmetry forbidden [1,3]-silicon shift.

1.3.2 (η^1-cpp)Mn(CO)$_3$(PEt$_3$)$_2$

The compound (η^1-cpp)Mn(CO)$_3$(PEt$_3$)$_2$ was synthesized by Andreas Decken.[9] It was found to undergo hindered rotation about the sigma bond between the manganese atom and the ligand atom bonded to it.

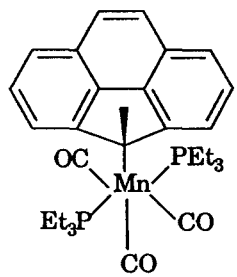

Although it was a simple 2-site equally populated exchange problem, the compound was found to be thermally sensitive. Therefore, lineshape analysis could not be used to determine the barrier to rotation. It was an ideal case for selective inversion experiments.

1.3.3 *N,N*-[dimethyl-(2,2'-dithiobisacetyl)]ethylenediamine

The heterocycle *N,N*-[dimethyl-(2,2'-dithiobisacetyl)]ethylenediamine, abbreviated to DADS, was synthesized by Rob Maharajh.[10]

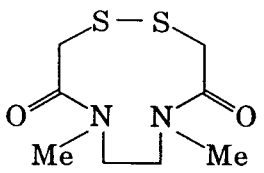

It is an extremely complex system, existing as five conformations in solution, which are exchanging through hindered rotation about the disulfide bond, as well as hindered rotation about the two amide bonds. With 24 unequally populated sites involved in the exchange processes, it would provide a challenge to the single selective inversion recovery technique of Bain and Cramer.[6,7]

CHAPTER TWO

DNMR Methods

2.1 Introduction

Rate constants associated with chemically exchanging systems may be determined using several DNMR techniques. The various DNMR methods may be classified according to the rates of exchange that they are useful in measuring; slow, intermediate and fast exchange rates. Slow rate constants of about 10^{-1} - 10^{2} s^{-1}, which are of comparable size to spin-lattice relaxation times for the exchanging sites, may be measured with 1D magnetization transfer methods. 2D EXSY is useful over about the same range, allowing rates of 10^{-2} - 10^{2} s^{-1} to be measured. Rate constants of about 1 - 10^{5} s^{-1} may be measured using lineshape analysis.[2] Systems undergoing exchange at rates faster than this may be studied through molecular correlation times from relaxation or cross-relaxation studies.

While DNMR methods give mechanisms for chemical exchange processes, and the rate constants associated with them, chemists are often interested in obtaining the standard activation parameters $\Delta G^{\ddagger}$, $\Delta H^{\ddagger}$, and $\Delta S^{\ddagger}$ for chemical exchange processes. This chapter will describe the derivation of these thermodynamic parameters, followed by a discussion of lineshape analysis and 1D and 2D magnetization transfer methods. First a short description of one-dimensional Fourier transform NMR will be given.

2.2 One-Dimensional Fourier Transform NMR (1D FT NMR)[11-13]

Nuclei with non-zero spin possess a magnetic moment which interacts

with the applied static magnetic field, $\mathbf{B}_0$. The spins give rise to different quantized energy levels in a magnetic field. For example, protons, with spin quantum number I = 1/2, give rise to two energy levels, one aligned with the static magnetic field, the other against the static magnetic field. The energy levels are separated by an amount ΔE.

$$\Delta E = h\gamma B_0/2\pi \quad (1)$$

where γ is the magnetogyric ratio, which is a characteristic property of the nucleus.

The energy states are unequally populated, with the ratio of the populations given by the Boltzmann equation:

$$N_\beta/N_\alpha = \exp(-\Delta E/kT) \quad (2)$$

where N_β is the population of the upper state and N_α is the population of the lower state for nuclei with spin quantum number I = 1/2.

The magnetic moments of all of the nuclei of a sample sum to give the bulk magnetization **M**. At equilibrium, the magnetization vector $\mathbf{M}_0$ lies along the applied static magnetic field $\mathbf{B}_0$ (the z axis). In order to observe NMR signals, the system must be perturbed. The magnetization may be perturbed away from its equilibrium position by applying a pulse of radio frequency irradiation. Any component of **M** that is now in the xy plane, will precess about $\mathbf{B}_0$ at its Larmor frequency $\omega = \gamma B_0$ (radians/second) or $\nu = \omega/2\pi$ (Hz).

Any perturbation which alters the population difference of the energy states changes the magnitude of $\mathbf{M}_Z$. After such a perturbation, the system relaxes to equilibrium, i.e. the populations of the states return to a Boltzmann

distribution, and the bulk magnetization returns to the equilibrium $\mathbf{M}_0$.

For simplicity when discussing precessing magnetizations, the coordinate system is considered to rotate at the frequency of the oscillating $\mathbf{B}_1$ field. $\mathbf{B}_1$ appears fixed in this rotating frame, and has the effect of rotating **M** about $\mathbf{B}_1$. Thus, if $\mathbf{B}_1$ is along the x axis in the rotating frame, and a 90^o pulse is delivered, **M** will rotate about the x axis, onto the y axis. Upon removal of the $\mathbf{B}_1$ field, **M** precesses about the static $\mathbf{B}_0$. Nuclei precessing at their Larmor frequencies appear to precess at a frequency equal to the difference between the Larmor frequency and the frequency of the coordinate system ($\mathbf{B}_1$).

Nuclei in different environments have different Larmor frequencies, therefore the precessing magnetization of a multisite sample is a sum of the individual oscillations, each with its own frequency, ω. This magnetization in the xy plane induces a voltage, as a function of time, in the receiver coil, which lies along an axis perpendicular to the $\mathbf{B}_0$ field. This transient signal, called the free induction decay (FID), is the signal that the spectrometer acquires and collects in its computer.

The FID is collected and digitized as a function of acquisition time, with measurements being made at regularly spaced times. The time domain data are Fourier transformed to give the frequency domain NMR spectrum.

2.3 Calculation of Thermodynamic Parameters

The DNMR methods allow one to determine rate constants at specific temperatures. Usually, however, chemists are more interested in obtaining the standard activation parameters $\Delta G^{\ddagger}$, $\Delta H^{\ddagger}$, and $\Delta S^{\ddagger}$ for a chemical exchange process. These are the differences per mole in Gibbs free energy, enthalpy and

entropy between the transition state and the reactants.

These parameters may be determined using the Eyring equation, if rate constants are known for a range of temperatures.[3]

$$k = \kappa(k_B T/h)\, \exp(\Delta H^{\ddagger} - T\Delta S^{\ddagger})\ /RT \qquad (3)$$

where k is the rate constant, κ is the transmission coefficient (usually assumed to be 1), k_B is the Boltzmann constant (1.3807×10^{-23} JK^{-1}), h is Planck's constant (6.6262×10^{-34} Js), and R is the gas constant (8.3144 $JK^{-1}mol^{-1}$). By taking the natural logarithm of k, and rearranging:

$$\ln(k/T) = -\Delta H^{\ddagger}/R(1/T) + [\Delta S^{\ddagger}/R + \ln(k_B/h)] \qquad (4)$$

A plot of $\ln(k/T)$ versus $1/T$ is linear with a slope of $-\Delta H^{\ddagger}/R$, and an intercept of $\Delta S^{\ddagger}/R + \ln(k_B/h)$.

Since the thermodynamic parameters are derived from a plot with a fairly wide range of temperatures and rate constants, they are less subject to error than the $\Delta G^{\ddagger}$ obtained from the coalescence method, discussed in section 2.4.2.

2.4.1 Lineshape Analysis

Probably, the most frequently used DNMR method is the classical line-shape analysis, or complete bandshape method, in which the bandshape of the exchange broadened spectrum is calculated for comparison to an experimentally obtained spectrum.[3,5]

Lineshape analysis makes use of the fact that exchange processes are manifested as characteristic changes in the shape of the NMR spectrum, i.e. broadening, coalescence, and resharpening.[2] In systems where there are only

two equally populated chemical environments, the method is straightforward. In more complex systems, including those with spin-spin coupling, unequal populations, and more than two exchange sites, the complete lineshape for the system must be calculated. There is no information available about the exchange mechanism, and it could be possible to fit the lineshape in many different ways.

In lineshape analysis, spectra are recorded at different temperatures. The spectrum of the exchanging system varies according to the rate of the exchange process, and the separation between the signals of the different exchanging species, $\Delta\nu$. When the exchange is rapid, the spectrum gives only the average of the resonance lines. When exchange is slow, separate resonances are obtained. At intermediate temperatures, various degrees of broadening are seen. Maximum broadening occurs at the coalescence temperature, T_C. Figure 2.1 shows calculated spectra for a two-site exchange, from slow exchange, through coalescence, to fast exchange.

Having obtained the experimental spectra, one then calculates spectra with different rate constants, and matches them to the experimental spectra, to obtain rate constants.

Computer programs for calculating lineshapes are available. One varies the rate of exchange until the calculated spectrum matches the experimental spectrum. Binsch's DNMR5[14] program contains an iteration procedure, which varies the rate, thus avoiding tedious manual comparisons of experimental and calculated spectra. Although this program allows for spin-spin coupling, it can only handle a maximum of five sites. The program EXCHANGE, by McClung can handle up to fifty sites, but cannot be used for systems with spin-spin

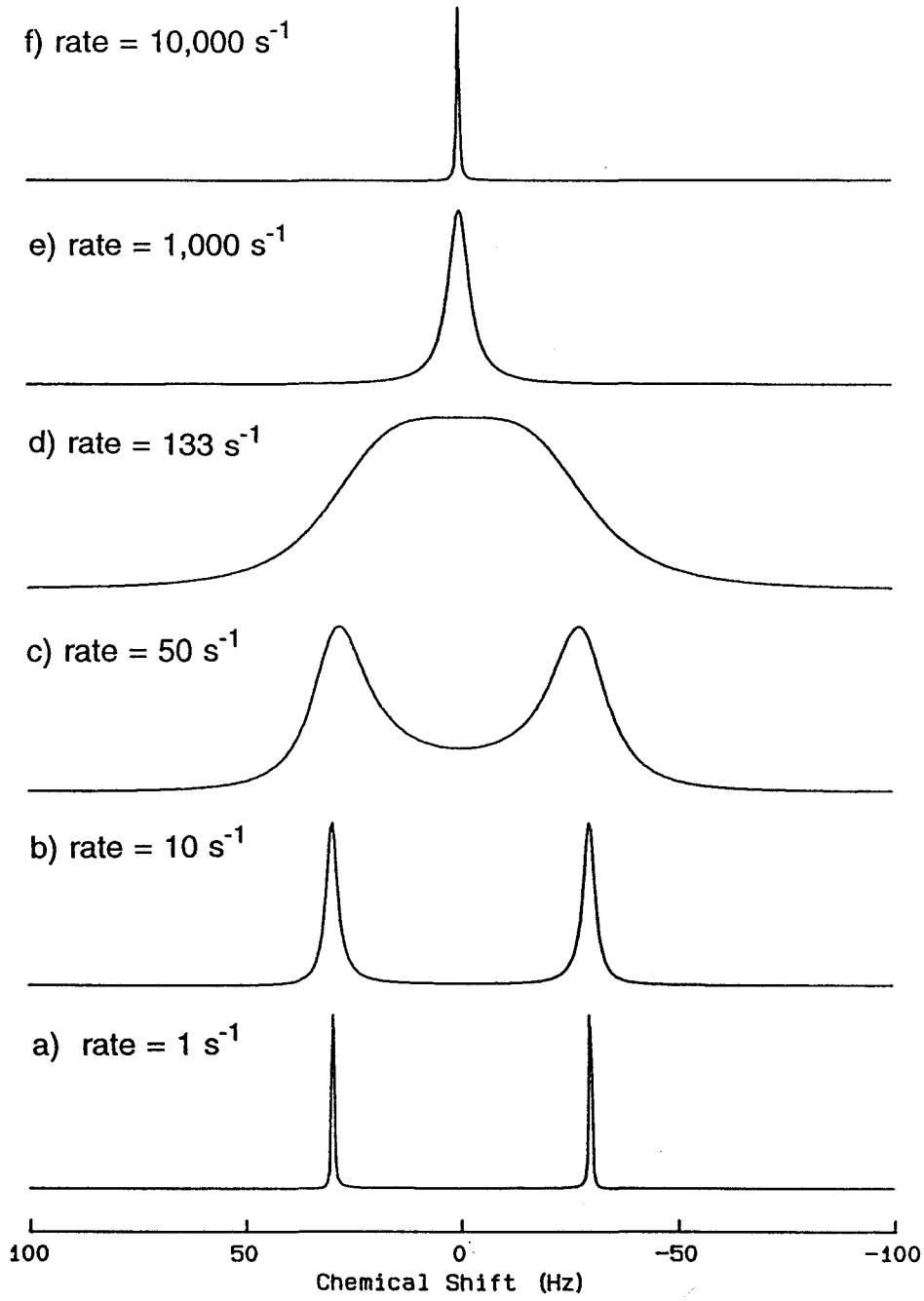

Figure 2.1 Calculated lineshapes for an equally populated 2-site exchange, with $\Delta\nu$ = 60 Hz: a-c) slow exchange, d) coalescence, e-f) fast exchange.

coupling.

The nameless program written by Bain, which was used for the lineshape analysis in this thesis, can also handle many sites, and is undergoing modification to enable calculation of lineshapes for spin-coupled systems. While the other programs calculate the frequency domain spectrum for a system, Bain's program calculates the time domain FID. This eases the analysis, since the calculated FID can readily be imported into an NMR data processing program. After Fourier transformation, the frequency domain spectrum can be overlaid with the experimental spectrum, for comparison.

From the temperature-dependent rate constants, one can obtain thermodynamic activation parameters using Eyring theory, as outlined above, or various approximations, such as the coalescence method.

2.4.2 Coalescence Method

The coalescence method allows the free energy of activation for an exchange process to be calculated from the rate constant obtained at the coalescence temperature. The rate constant, k_C, for two equally populated sites at the coalescence temperature, T_C, is given by:

$$k_C = \pi\Delta\nu/\sqrt{2}, \tag{5}$$

where $\Delta\nu$ is the distance between the two sites in the absence of exchange.[3] Using Eyring theory:

$$k_C = (k_B T_C/h) \exp(-\Delta G_C^{\ddagger}/RT_C) \tag{6}$$

Rearranging equation (6) leads to:

$$\Delta G_c^{\ddagger} = -RT_c \ln(k_c h / k_B T_c) \qquad (7)$$

Since R, *h* and k_B are constants (given in section 2.3), one obtains $\Delta G_c^{\ddagger}$ as a function of T_c and $\Delta\nu$.

This approximation is dependent upon an accurate determination of the coalescence temperature, which may be difficult to obtain.

2.5 1D Magnetization Transfer Methods

1D and 2D magnetization transfer methods have enjoyed increasing popularity recently.[1,15-17] When the rate of exchange is too slow to affect the lineshape, it may be observed upon selectively irradiating one of the sites involved in the exchange process. If the exchange rate is not much less than the spin-lattice relaxation rate, saturation is transferred from the irradiated site to sites that are chemically exchanging with it.

The various 1D magnetization transfer methods involve selective irradiation of one or more resonances of an exchanging system. The resonances may be excited either by saturation or by inversion. The time-dependent effects of that irradiation on the remaining sites are followed. Temperature-dependent rate constants are obtained, from which thermodynamic parameters can be derived, as discussed above.

2.5.1 Saturation Transfer

Forsén and Hoffman developed the 2-site magnetization transfer experiment in 1963, using a continuous wave double irradiation procedure.[17] One resonance involved in the exchange was saturated by steady state

irradiation. That saturation was transferred by exchange to the other resonance involved in the exchange process. The time dependence of the unsaturated site was monitored and a rate constant for the exchange process was derived. In order to simplify the data analysis, Forsén and Hoffman assumed that both relaxation rates in their two-site case were the same, and that there was perfect saturation at one site. In 1964, they generalized the theory for *n* sites.[15]

2.5.2 Selective Inversion

In one of the first selective inversion experiments, Dahlquist and coworkers[18] followed the two-site ring inversion of a cyclophane by exciting the resonance of interest with inversion rather than saturation. They selectively inverted one signal in the ^1H NMR spectrum by delivering a long soft pulse to that signal, before the hard 90^o observation pulse.

Inversion is advantageous because there is a longer time period for chemical exchange to occur, and the intensities of both peaks can be measured. (The intensity of the excited resonance in selective saturation experiments is zero).

Alger and coworkers[19] published the first selective inversion study in which the two exchanging sites were unequally populated, and the T_1's for the two sites were not equal. They also selectively inverted one signal with a long soft pulse, in their investigation of peptide bond isomerization.

Led and Gesmar corrected for the assumptions made by Forsén and Hoffman.[20] In particular, they stated that perfect selective saturation was not possible, and that in many cases the spin-lattice relaxation rates of the sites involved would not be equal. They inverted first one site in their two-site system,

then the other, and followed the magnetization of both sites in each case. The extra data obtained allowed for the determination of $k_{forward}$, $k_{reverse}$, and T_1's for both sites using a non-linear least squares fitting program. They later generalized this method for *n* sites.[21] This requires that each of the *n* sites in an *n*-site system be selectively inverted in turn, and this could be very time consuming for many site systems.

The methods of Grassi and coworkers[22] and McClung and coworkers[23] allowed experimental data to be fit to different mechanistic pathways. McClung's method also allows the initial magnetization, M_0, to be fitted. McClung uses his non-linear least squares fitting program, SIFIT[23], to fit experimental data. It is capable of varying the rate constants for the exchange, T_1's for each site, initial and final magnetizations, and the exchange mechanism. Because M_0 can be varied, the spin systems can be perturbed in any way, i.e., one can create any initial magnetization for each site in the system, not just $+M_\infty$ or $-M_\infty$. Also, since magnetization cannot be measured at exactly t = 0, it should be fit by the least squares fitting program.

2.5.3 Single Selective Inversion

The method of Bain and Cramer[6,7] makes use of the fact that any initial spin state can be created and fit with McClung's program. McClung uses the DANTE[24,25] pulse sequence while Bain and Cramer use hard pulses to invert their signals. For data analysis, Bain has written a non-linear least squares fitting program, FLOPSI, in the C language. FLOPSI allows the variation of the same parameters as does SIFIT.

With their single selective inversion recovery experiment, only one

experiment need be performed to get rate constants for all exchange processes occurring, provided that one can excite at least one site for each process. In the single selective inversion experiment, it is not usually possible to perfectly invert one signal for each process, therefore M_0 must be varied when fitting the data.

There should be an optimal set of parameters that will give sufficient information about each of the exchange processes of interest. Partial derivatives of the magnetizations with respect to rate coefficients will determine how sensitive a set of initial conditions are to the rate process. If the partial derivative with respect to a rate process is large, then the initial conditions are sensitive to that process.

Calculation of the complete set of partial derivatives for a system with more than three sites is complicated because both the eigenvalues and the eigenvectors are functions of the parameters. Bain and Cramer[7] have analytically solved for the partial derivatives for 2-site and 3-site cases. They found that the partial derivative is at a maximum when one site is inverted and the other(s) not perturbed, for the two and three site cases. Also, the maximum in the partial derivative curve was found to be broad, so the choice of variable delay used in the experiment is forgiving. Their results agreed with intuition for the two site and three site cases.

In this thesis work, intuition was used in setting up the initial conditions for the 24 site DADS system, rather than calculating partial derivatives for all sites. With 24 unequally populated sites, and four exchange processes, this would have meant 192 partial derivatives.

2.5.3.1 Pulse Sequence for Single Selective Inversion Experiments

With all of the 1D magnetization transfer experiments, a spin system can be perturbed from equilibrium, allowed to evolve after that perturbation, and followed by detection, to monitor what happened during the evolution period. In the single selective inversion recovery experiment the pulse sequence is as follows:

$$D1 - 90^{o} - D2 - 90^{o} - VD - 90^{o} - FID \qquad (8)$$

where D2 is $1/2\Delta\nu$, and $\Delta\nu$ is the frequency difference between the signal being inverted, and the signal left unperturbed.[6,7] D1 is a fixed delay ($5xT_1$), and VD is a variable delay.

The selective inversion of the NMR signal which is on resonance is achieved with the 90^{o} - D2 - 90^{o} sequence. The hard pulses are delivered at the frequency of the on-resonance signal. The first 90^{o} pulse rotates the magnetization onto the y axis. Since the signal to be inverted is separated from the signal to be observed by $\Delta\nu$ Hz, after $1/2\Delta\nu$ seconds, the two signals will be 180^{o} out of phase, i.e. one signal along +y, the other along -y. The second 90^{o} pulse rotates the magnetization back onto the z axis, one signal along +z, the other -z. The on resonance signal thus experiences a net 180^{o} pulse, while the signal $\Delta\nu$ Hz from the on resonance signal experiences no net excitation. All other signals follow equation (9).

$$M(0)_i = - M(\infty)_i \cos(2\pi\omega_i\tau) \qquad (9)$$

where $\omega_i = (\nu_i - \nu_o)$. ν_o is the transmitter offset (O1). τ is the time delay, $M(0)_i$ is the initial magnetization for the site *i*, and $M(\infty)_i$ is the equilibrium magnetization

for site *i*.

Z-magnetization will return to equilibrium via chemical exchange and spin-lattice relaxation. In order to monitor this return to equilibrium of the magnetization, there must be a component in the xy plane. This is achieved by a 90^{o} pulse, which rotates the z magnetization into the xy plane, producing a signal which is proportional to that z magnetization. One can follow the growth or decay of the z magnetization during the evolution time by setting up a series of experiments with different delay times (VD in the pulse sequence).

Figure 2.2 shows an initial spin state and equilibrium spectrum for the molecule bis(1-indenyl)dimethylsilane. In this system, the *d,l* isomer gives rise to a single methyl resonance while the *meso* isomer gives rise to two methyl resonances, labeled as *meso1* and *meso2* in figure 2.2. The processes to be followed are *d,l* to *meso1* and *d,l* to *meso2*. Note that the *d,l* peak is inverted, and the two *meso* peaks are left unperturbed, so information about both processes should be obtainable from this single experiment.

Figure 2.3 shows a plot of magnetization versus time delay (VD) for the system in figure 2.2.

All of these magnetization transfer techniques work because each one creates an initial perturbation of the magnetizations from their initial values. The method of analyzing the data differs from one group to another.

McConnell[26,27] and Gutowsky and Holm[28] were the first to modify the Bloch equations to describe the time dependence of magnetization under the influence of chemical exchange. The following equation describes the time course for the relaxation to equilibrium, under the influence of chemical exchange.

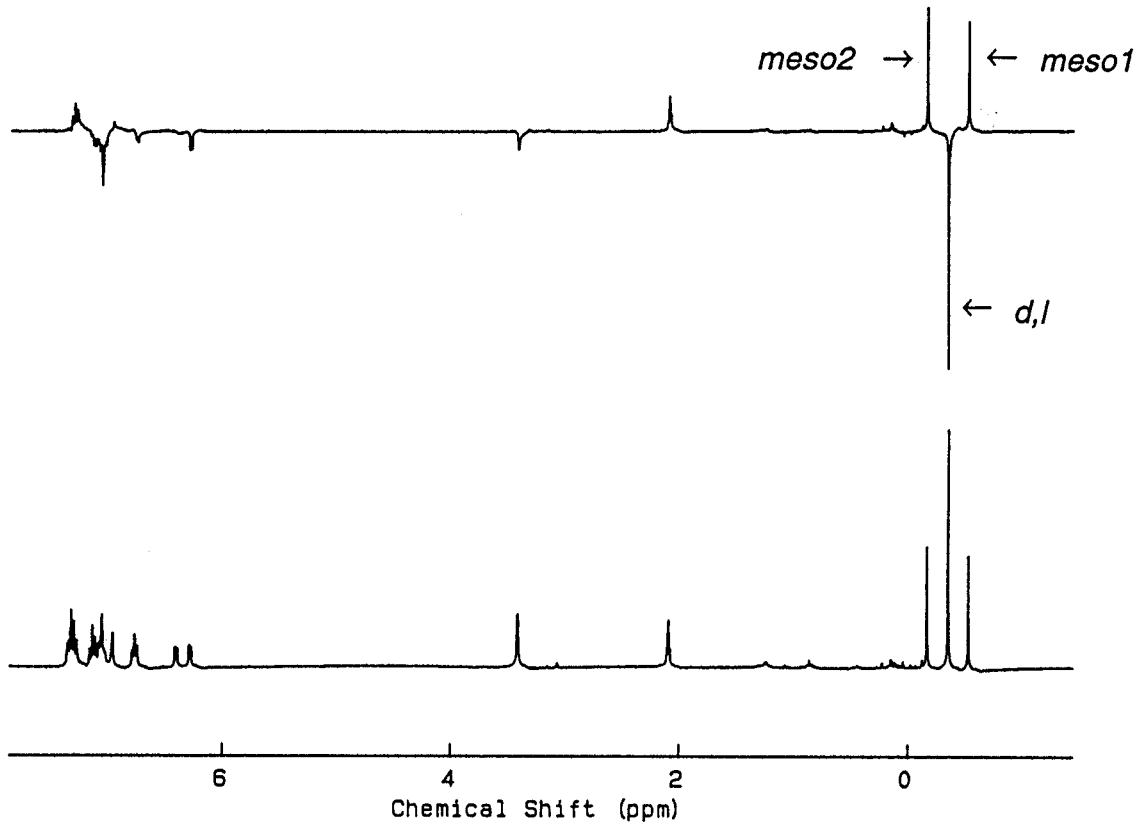

Figure 2.2 300.13 MHz ^{1}H selective inversion initial state (upper) spectrum with equilibrium (lower) spectrum for bis(1-indenyl)dimethylsilane, **3.1a**, **3.2a**, in toluene-d_8.

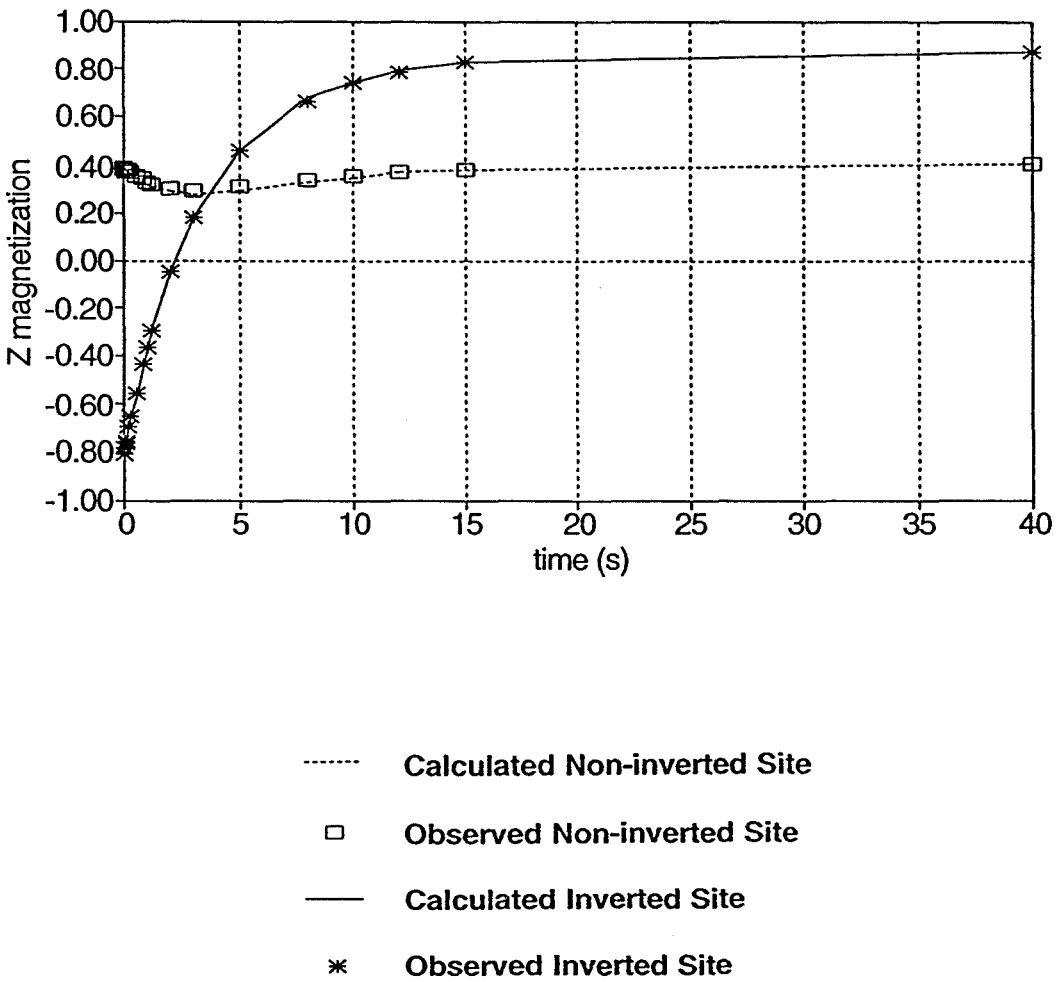

Figure 2.3 Experimental data vs. calculated data obtained from a ^{1}H selective inversion recovery experiment for bis(1-indenyl)dimethylsilane, **3.1a**, **3.2a**.

$$\frac{\partial}{\partial t}\begin{bmatrix} M_1(\infty) - M_1(t) \\ \vdots \\ M_n(\infty) - M_n(t) \end{bmatrix} = -A \begin{bmatrix} M_1(\infty) - M_1(t) \\ \vdots \\ M_n(\infty) - M_n(t) \end{bmatrix} \qquad (10)$$

$$\textit{where } A = \begin{bmatrix} R_1 & -k_{21} & -k_{31} \ldots & -k_{n1} \\ -k_{12} & R_2 & -k_{32} \ldots & -k_{n2} \\ \vdots & & & \\ -k_{1n} & -k_{2n} & -k_{3n} \ldots & R_n \end{bmatrix}$$

$$\text{and} \qquad R_i = \frac{1}{T_{1i}} + \sum_{l \neq i} k_{il}$$

This restoration to the equilibrium state can be followed by NMR, and the exchange parameters determined.

2.6 2D EXSY or NOESY

The 2D techniques NOESY (nuclear Overhauser effect spectroscopy) and EXSY (exchange spectroscopy) use the same pulse sequence to provide different information. The two procedures are sensitive to different time ranges.

NOESY provides a map of which atoms are close together in space, being a 2D display of the Overhauser interactions. The 1D spectrum appears on the diagonal, while off-diagonal peaks indicate nuclear Overhauser enhancements between pairs of nuclei.

The same pulse sequence provides a map of sites that are chemically exchanging, in EXSY. The EXSY experiment provides the same qualitative mechanistic information as 1D magnetization transfer, but does so for all spins in one experiment.

2D NMR for chemical kinetics was first proposed by Jeener, Meier, Bachmann and Ernst.[1] The cross-peaks in a 2D EXSY spectrum correspond to site to site exchange. 2D EXSY is often applicable to multisite systems which are difficult to study by lineshape or 1D magnetization transfer methods. 2D EXSY can give site-to-site rate constants if one is careful, but even qualitatively, the 2D NMR cross-peaks provide a clear picture of the exchange processes occurring in a system.[2] Especially in multisite systems, they map out the exchange pathways by showing which NMR signals exchange with which other signals, thereby giving mechanistic information. Lineshape analysis is sensitive only to lifetimes[2], therefore not as informative. Figure 2.4 shows a ^{1}H NOESY spectrum for bis(1-indenyl)dimethylsilane in the methyl region.

The pulse sequence[1] follows:

$$90^o - t_1 - 90^o - t_m - 90^o - t_2 \qquad (11)$$

where t_m = mixing time. t_2 is the same as the acquisition time in 1D NMR, i.e. the transverse magnetization is measured as a function of t_2, with measurements being made at regularly spaced, values of t_2. The evolution time, t_1, is also variable. By regularly incrementing t_1 at each successive pulse sequence, t_1 becomes a second discrete variable like t_2. The mixing time is the time during which chemical exchange occurs and is monitored by the 2D experiment.

The first 90^o pulse rotates the magnetization into the xy plane. The signals precess at their Larmor frequencies during t_1. The frequency labeled spins are then rotated onto the z axis by the second 90^o pulse, just as in 1D magnetization transfer. Chemical exchange and relaxation occur during the

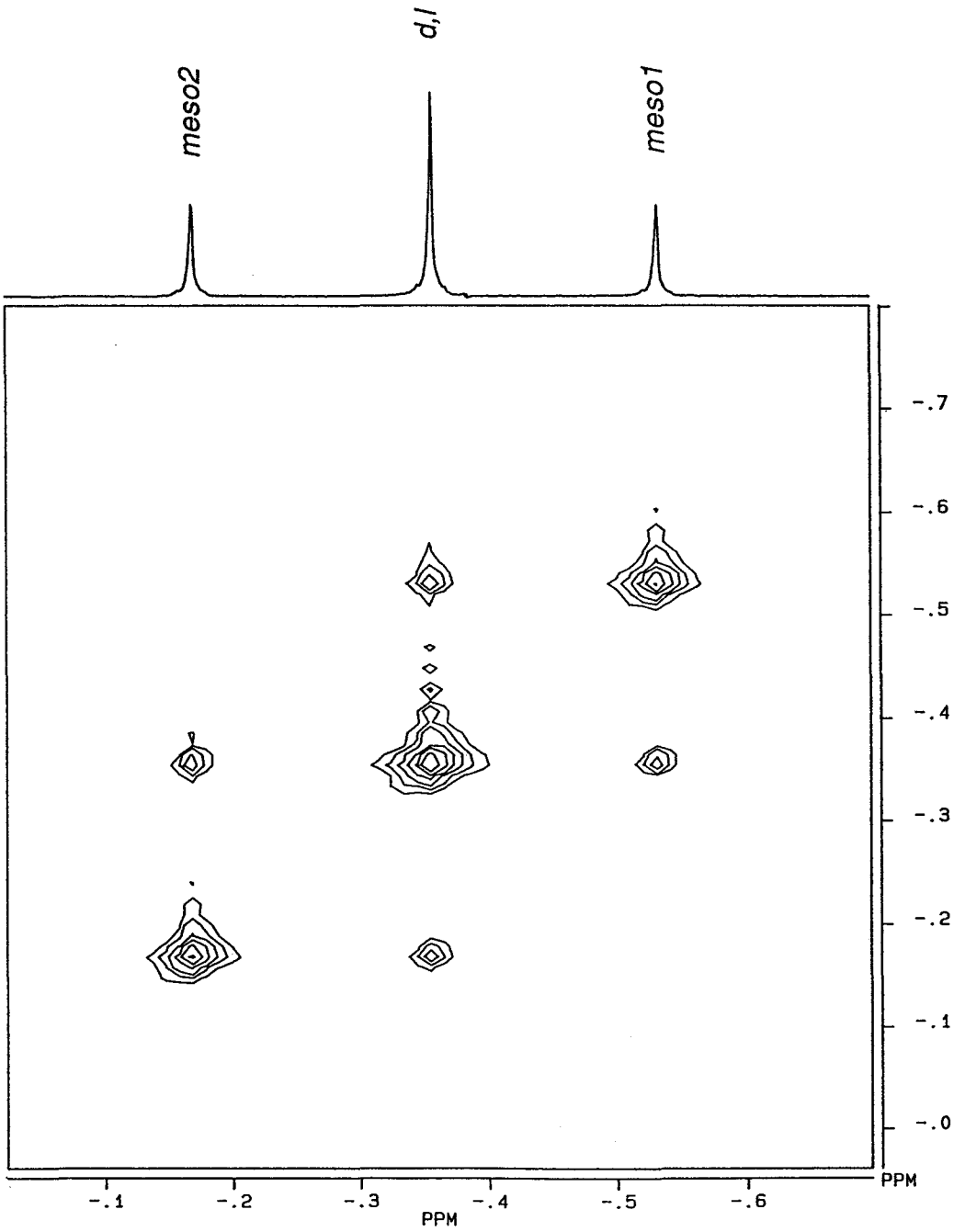

Figure 2.4 Methyl region of the 300.13 MHz ^{1}H NOESY spectrum of bis(1-indenyl)dimethylsilane, **3.1a, 3.2a**, in toluene-d_8.

fixed delay, t_m. The final 90° pulse rotates the magnetization back to the xy plane, for detection.

The measured magnetization is a function of both t_1 and t_2. Double Fourier transformation of the time domain function converts this to a 2D spectrum that is a function of two frequency variables (ω_1 and ω_2).

2.7 Selecting a DNMR Method

Each of the DNMR methods have their own strengths and weaknesses. These should be considered when there is a choice to be made between different DNMR techniques.[2] In some cases, the accessible rate of chemical exchange of the system will determine which method will be used. For example, if the system is slowly exchanging on the NMR timescale, and the signals don't broaden appreciably at the highest temperatures obtainable, then 1D or 2D magnetization transfer methods must be used. Sometimes the slow through to fast exchange regimes will be accessible, and several DNMR methods may be used. Some other factors to consider follow.

The NMR instrument time required to obtain kinetic data is important when choosing a DNMR method to study a system. 2D EXSY requires a lot of instrument time, but it can be competitive with most 1D magnetization techniques. The total time required for 1D magnetization transfer methods increases as the number of sites increases, except for the single selective inversion recovery method. The time required for a 2D experiment is independent of the number of sites, provided that the chemical shift difference between sites are not small, i.e. high resolution is not needed. Lineshape analysis requires the smallest amount of instrument time, but probably the most

amount of time for processing data. especially for problems with many site or several different processes.

In the latter case, it may not be possible to determine a unique solution to the problem, since lineshape analysis does not give direct information regarding the exchange pathways. There may be several ways to fit the various rate constants to the experimental spectrum. 2D EXSY, will give a site-to-site map of the exchange pathways.

Since 1D magnetization transfer and 2D EXSY operate on a slightly longer time scale than lineshape analysis, they are useful at lower temperatures than lineshape. This is advantageous with compounds that are thermally sensitive, such as the $(\eta^1\text{-cpp})Mn(CO)_3(PEt_3)_2$ compound studied in this work.

In 2D EXSY, one faces the problem of choosing an optimum mixing time. To choose the mixing time, one needs an estimate of the rate constant for the exchange process. If the mixing time is too short, cross peaks may be absent. If it is too long, in multisite exchanges, second order cross peaks may appear.

Another problem with EXSY is that for multisite systems, there may not be one optimum mixing time, unless all of the rate constants are equal. If they are nearly equal, an average of their mixing times will be suitable. If they are quite different, several experiments will have to be run with different mixing times.[29,30] These problems in choosing a useful mixing time can lead to misinterpretation of the exchange mechanism, but are far more serious if the cross peak intensities are to be measured to obtain rate constants.

One disadvantage of using just one of any of the methods is that they are limited to a somewhat narrow range of temperatures and therefore rate constants. The errors in the activation parameters $\Delta H^{\ddagger}$ and $\Delta S^{\ddagger}$ may be large.

1D magnetization transfer may be combined with lineshape analysis at higher temperatures, to increase the temperature range, and therefore decrease the error in the activation parameters.

CHAPTER THREE

The Molecular Dynamics of Bis(1-indenyl)dimethylsilane

3.1 Introduction

A recent report described the syntheses and molecular dynamics of a series of molecules of the type $(indenyl)_2SiR_2$, where R = Me, OMe or Cl.[8] These molecules are important because of their relevance to stereospecific polymerizations of alkenes.[8] Moreover, $(indenyl)_2SiR_2$ systems possess a particular stereochemical feature (two chiral centers) in that they can exist not only as the *meso* isomer, **3.1**, but also as the mixture of enantiomers **3.2**.

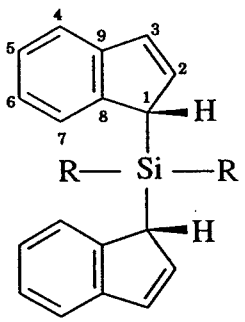

Meso

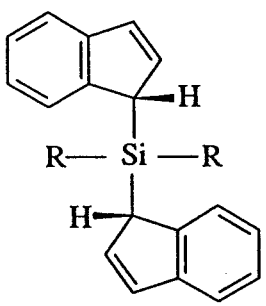

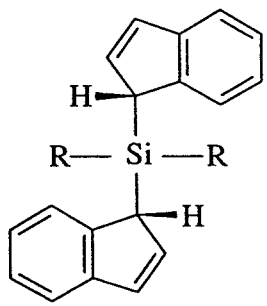

d,l

3.1a R=CH_3

3.1b R=OCH_3

3.1c R=Cl

3.2a R=CH_3

3.2b R=OCH_3

3.2c R=Cl

One can readily envisage interconversion of the *meso* and *d,l* isomers by successive [1,5]-suprafacial sigmatropic shifts of one (indenyl)$SiMe_2$ moiety over the surface of the 5-membered ring of the other indenyl unit. As depicted in Scheme 3.1, the process would pass through the isoindene intermediate **3.3**; indeed, such a [1,5]-shift mechanism has been the subject of detailed study by a number of groups.[31,32]

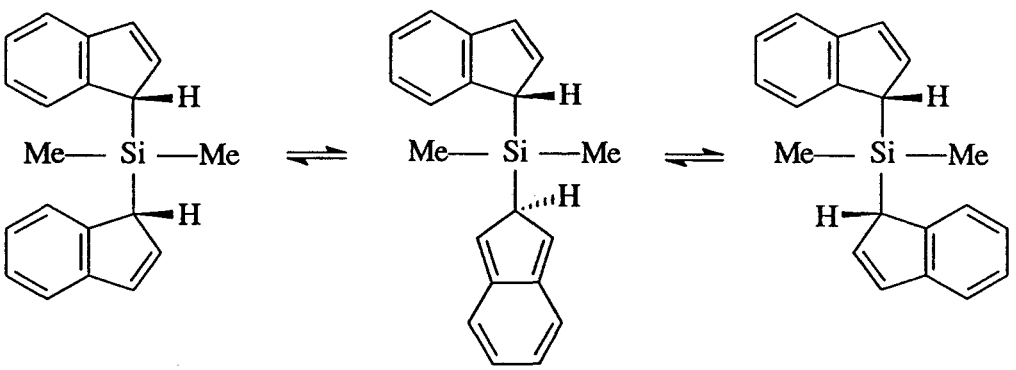

Meso **3.3** *d,l*

Scheme 3.1 [1,5]-silicon shifts in bis(1-indenyl)dimethylsilane.

There is also the possibility of [1,5]-hydrogen shifts to give the 3-silyl isomer **3.4**, but this occurs only at elevated temperatures,[8] and isomer **3.4** can only be detected after prolonged heating at 200 °C (see Scheme 3.2).

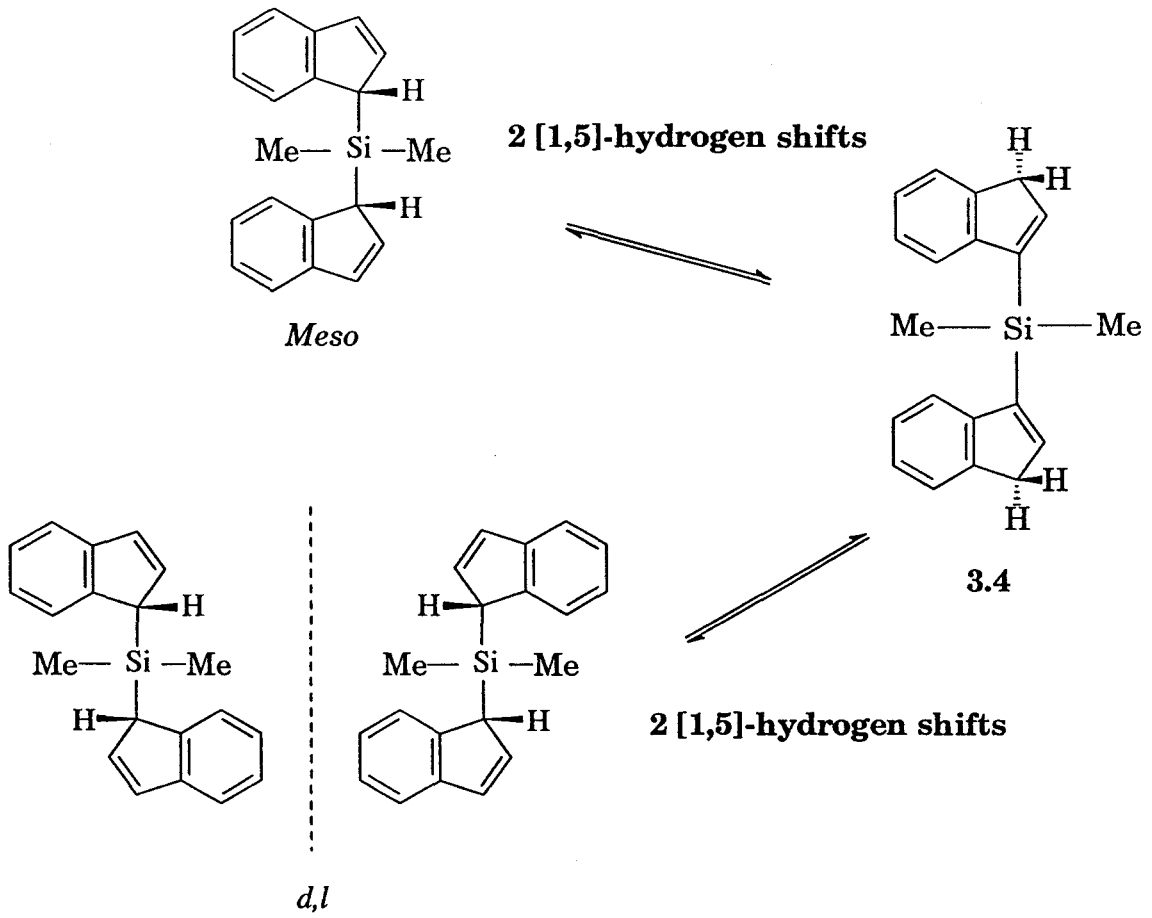

Scheme 3.2 [1,5]-hydrogen shifts in bis(1-indenyl)dimethylsilane.

As noted previously, the *meso* isomer, **3.1a**, has a single mirror plane (C_S symmetry); the two methyl groups bonded to silicon are magnetically non-equivalent and yield a pair of singlets in either the ^1H or ^{13}C NMR spectra. In contrast, the *d,l* isomers have C_2 symmetry which renders these methyl groups chemical-shift equivalent, and a single CH_3 resonance is observed in either the ^1H or ^{13}C spectrum. The *d,l* compound, **3.2a**, is readily isolable by crystallization, and the rate of its conversion into **3.1a** is conveniently followed by monitoring the intensities of the ^1H NMR methyl resonances of **3.1a** and **3.2a**.

The previous authors tried to evaluate the kinetic parameters for the *d,l* to

meso transformation, but they chose a somewhat curious approach. At temperatures well above 110 °C, there is evidence of line-broadening of the aforementioned ^{1}H NMR methyl resonances in **3.2a** and, in principle, it may be possible to extract thermodynamic parameters from these data. However, the authors tried to follow the progress of the reaction below the temperature at which line-broadening became evident.

The problems associated with this approach became apparent upon examination of the reported kinetic parameters. For (indenyl)$_2$SiMe$_2$, **3.1a**, $\Delta H^{\ddagger}$ was quoted as 18.9 kcal mol^{-1}, and $\Delta G^{\ddagger}$ as 0.2 kcal mol^{-1}; for (indenyl)$_2$Si(OMe)$_2$, **3.1b**, the values were claimed to be $\Delta H^{\ddagger}$ = 12.0 kcal mol^{-1} and $\Delta G^{\ddagger}$ = 0.6 kcal mol^{-1}; finally, for (indenyl)$_2$SiCl$_2$, **3.1c**, the values are $\Delta H^{\ddagger}$ = 7.7 kcal mol^{-1} and $\Delta G^{\ddagger}$ = 1.0 kcal mol^{-1}. These apparently remarkable results would suggest that, since $\Delta G^{\ddagger}$ remains almost constant at 0 ± 1 kcal mol^{-1}, while $\Delta H^{\ddagger}$ changes noticeably, the process involves almost exactly compensatory changes in the $T\Delta S^{\ddagger}$ term.

Another curious facet of this report was the claim that "the fluxional process" (presumably the [1,5]-suprafacial shift) only became operative at approximately 150 °C, and so the interconversion of the *meso* and *d,l* isomers, **3.1** and **3.2**, must occur via a different, lower energy mechanism below this temperature. That mechanism was assumed by the authors to be the symmetry forbidden [1,3]-suprafacial silicon shift. This whole series of inconsistencies prompted a reinvestigation of the molecular dynamics of these molecules.

3.2 Results and Discussion

It appeared that there was only one exchange process occurring at all

temperatures, and that this process was a [1,5]-suprafacial silicon shift. In order to obtain reliable activation parameters ($\Delta H^{\ddagger}$ and $\Delta S^{\ddagger}$), one needs a wide range of rates. The barrier is very high, so it is difficult to see coalescence, which would occur at about 210 °C. Rather than using lineshape analysis, as the previous authors[8] have done, single selective inversion recovery experiments were performed at high temperatures, when the molecule was slowly exchanging on the NMR timescale, and classical kinetics methods at lower temperatures, where the exchange cannot be observed even with magnetization transfer methods.

3.2.1 The Interconversion of 3.1a and 3.2a Below 100 °C

Classical kinetics methods were used below 100 °C. A pure sample of *d,l* bis(1-indenyl)dimethylsilane, **3.2a**, dissolved in toluene-d_8. It was placed in the probe of an NMR spectrometer at a constant temperature and the intensities of the methyl peaks in **3.1a** and **3.2a** were monitored at regular intervals. Figure 3.1 shows the ^{1}H NMR spectrum for a sample of almost pure *d,l* bis(1-indenyl)dimethylsilane, **3.2a**. Figure 3.2 compares the ^{1}H NMR spectrum for a mixture of *d,l* and *meso* isomers (upper spectrum), to the ^{1}H NMR spectrum of the *d,l* compound (lower spectrum), in the methyl region. Figure 3.3 compares the ^{1}H NMR spectrum for a mixture of *d,l* and *meso* isomers (upper spectrum), to the ^{1}H NMR spectrum of the *d,l* compound (lower spectrum), in the aromatic region. By this means, rate constants were obtained at a number of temperatures. Activation parameters were then determined. In this particular case, the barrier to interconversion of **3.1a** and **3.2a** is large, the rates are slow and equilibrium is not obtained within 15 minutes, as assumed by the previous

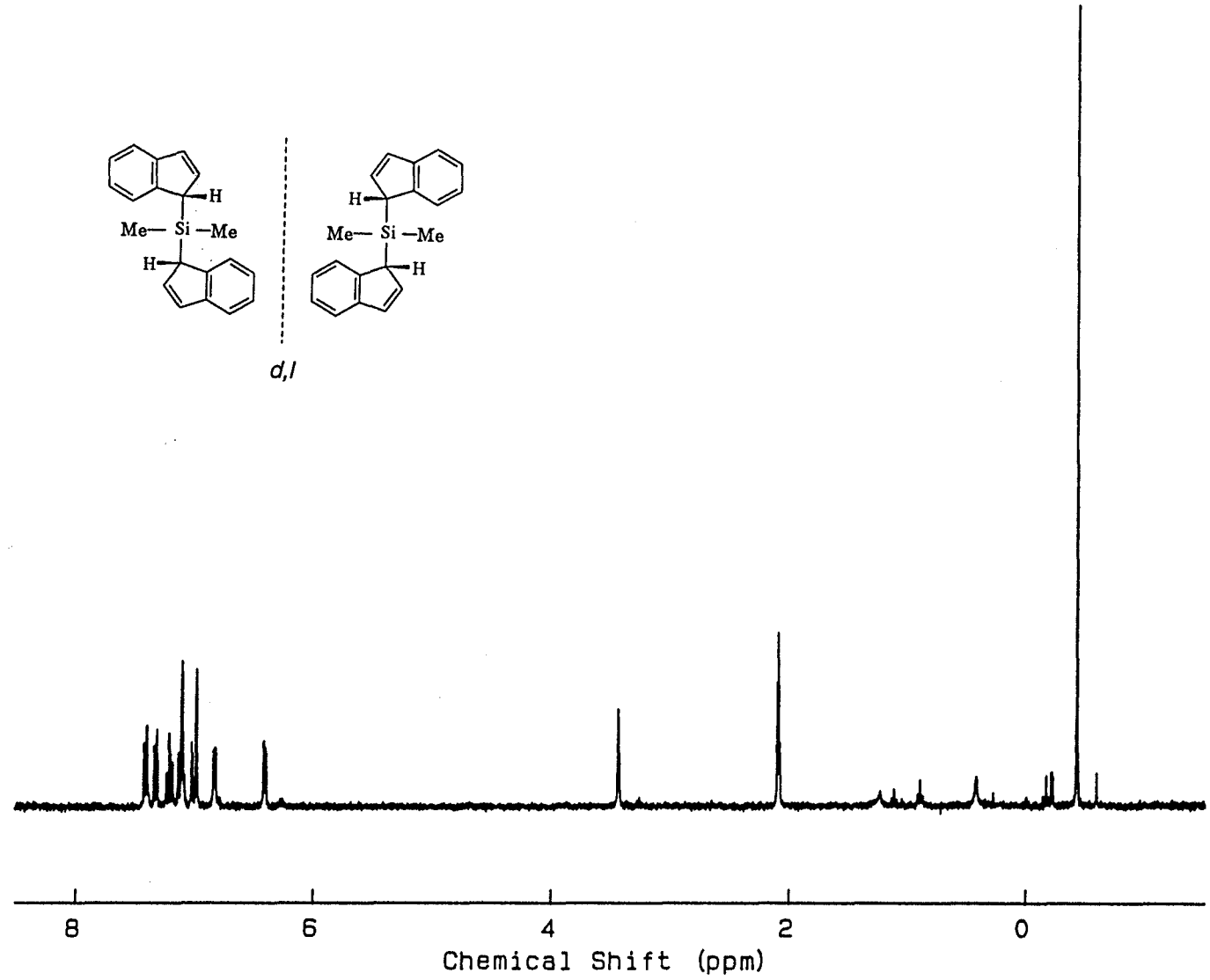

Figure 3.1 300.13 MHz ^{1}H NMR spectrum of the *d,l* enantiomers of bis(1-indenyl)dimethylsilane, **3.2a**, in toluene-d_8.

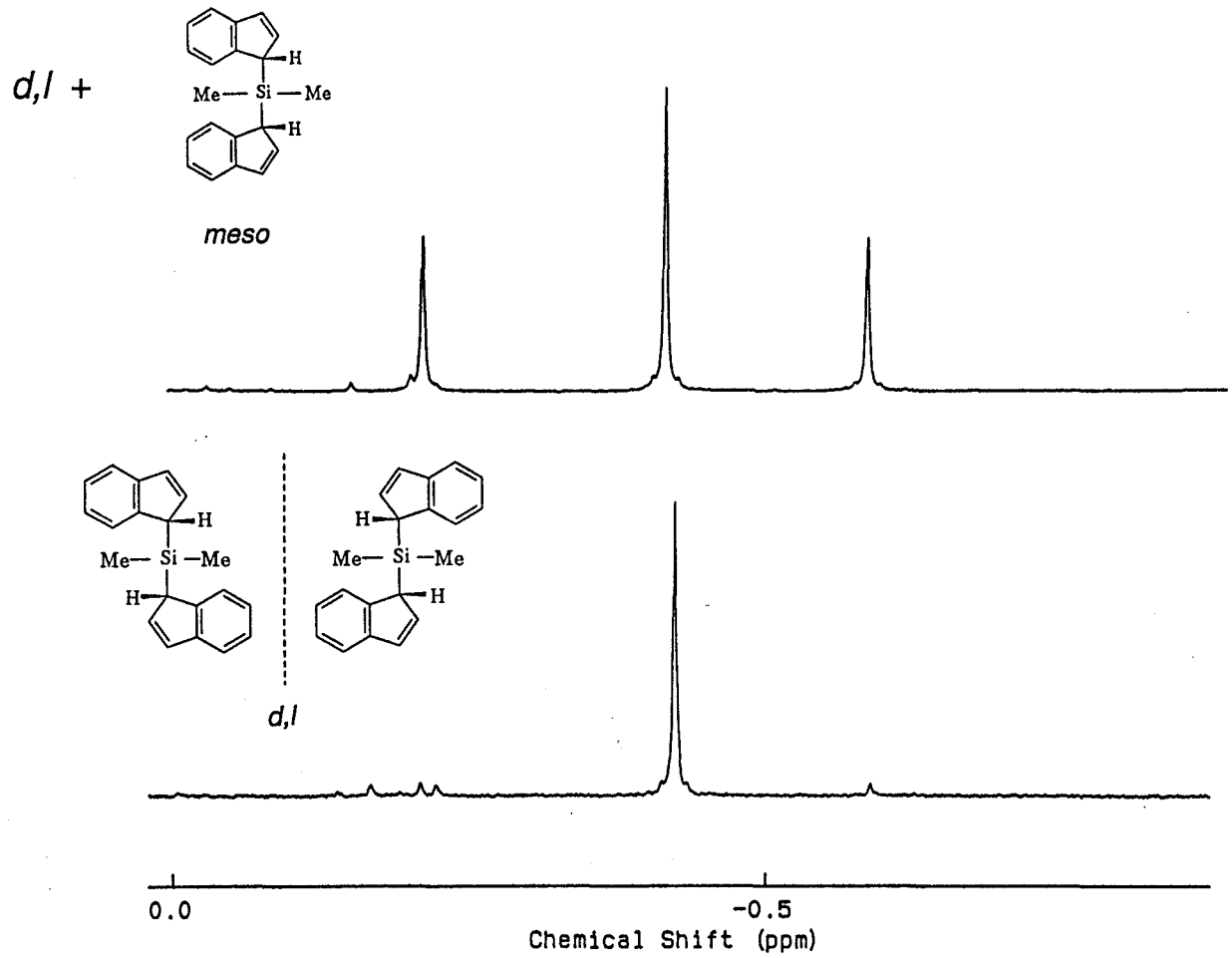

Figure 3.2 Methyl region of the 300.13 MHz ^{1}H NMR spectra of the *d,l* enantiomers, **3.2a**, (lower spectrum), and a mixture (upper spectrum) of the *d,l* and *meso*, **3.1a**, isomers of bis(1-indenyl)dimethylsilane, in toluene-d_8.

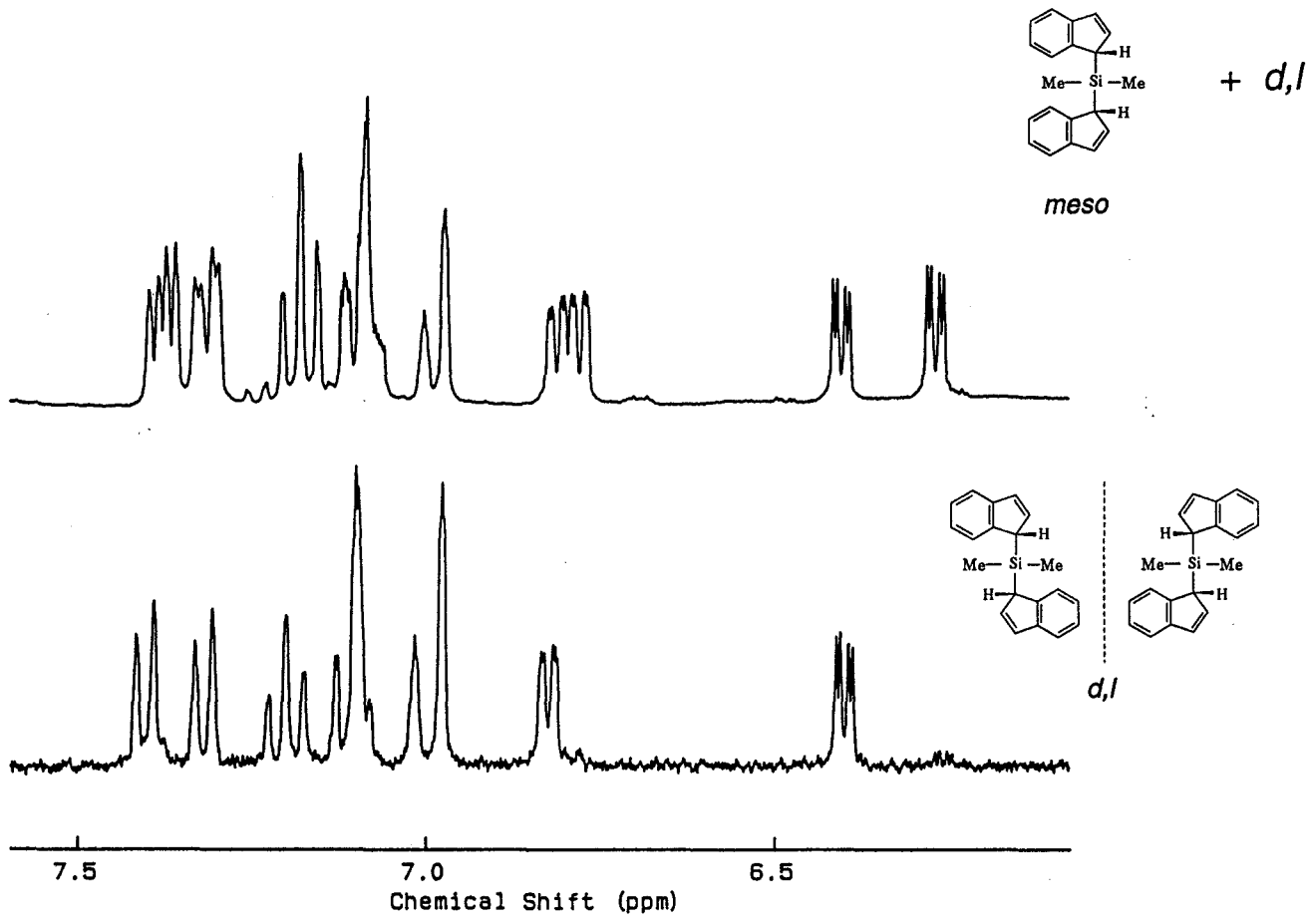

Figure 3.3 Aromatic region of the 300.13 MHz ^{1}H NMR spectra of the *d,l* enantiomers,**3.2a**, (lower spectrum), and a mixture (upper spectrum) of the *d,l* and *meso,* **3.1a**, isomers of bis(1-indenyl)dimethylsilane, in toluene-d_8.

authors; thus, their kinetic parameters are questionable. Figure 3.4 illustrates the Eyring plot obtained; the *ln k/T* values obtained at less than 100 °C are shown as open squares.

3.2.2 The Interconversion of 3.1a and 3.2a Above 100 °C

As the molecule was just starting to exchange on the NMR timescale above 100 °C, a 2D NOESY experiment was used to determine the exchange pathways and 1D ^{1}H selective inversion recovery experiments were used to measure the rate constants. The aromatic region of the ^{1}H NOESY is shown in figure 3.5. There is a crosspeak between the sp^3 proton, and the sp^2 proton H(3), as expected. The methyl region of the spectrum appears in figure 2.4. It shows the crosspeaks between the *d,l* methyl resonance and each of the *meso* methyl resonances, but no crosspeak between the two *meso* resonances.

One of the methyl resonances (the *d,l* one) was selectively inverted, and the return to equilibrium of that resonance, as well as a meso methyl peak, were followed. Figure 2.2 shows the selective inversion initial state (upper spectrum) and equilibrium (lower) spectrum. The time dependence of the z-magnetization for the two methyl peaks were fitted using a non-linear least squares fitting program, FLOPSI, from which rate constants were extracted. Figure 2.3 shows the experimental data vs. the fit calculated by FLOPSI, at a single temperature. The *ln k/T* values for the temperature range above 100 °C are shown in Figure 3.4 as filled squares. It is evident that the data are fit by a single process with the following values: $\Delta H^{\ddagger} = 21.9 \pm 0.5$ kcal mol^{-1}, $\Delta S^{\ddagger} = -7.2 \pm 1.4$ cal mol^{-1}K^{-1}, and $\Delta G^{\ddagger} = 24.2 \pm 0.5$ kcal mol^{-1} at 50 °C.

These results are consistent with the existence of a single migration

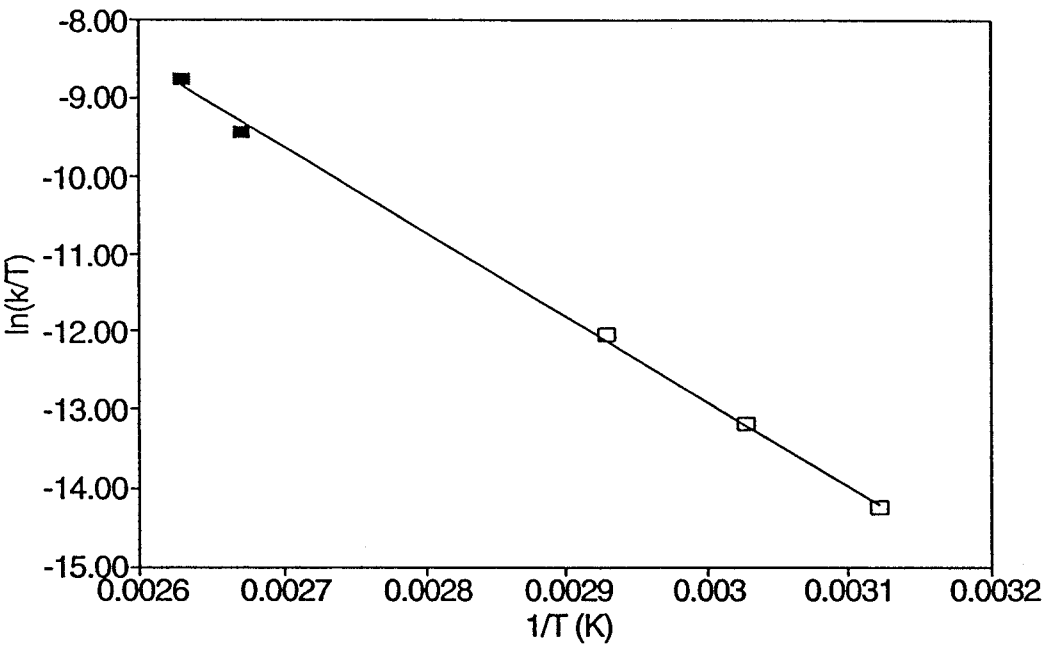

Figure 3.4 Eyring plot of ln(k/T) vs. 1000/T for bis(1-indenyl)dimethylsilane, **3.1a**, **3.2a**, in toluene-d_8. The filled squares represent rate constants derived from ^{1}H selective inversion recovery experiments, while the open squares represent rate constants derived from classical kinetics methods.

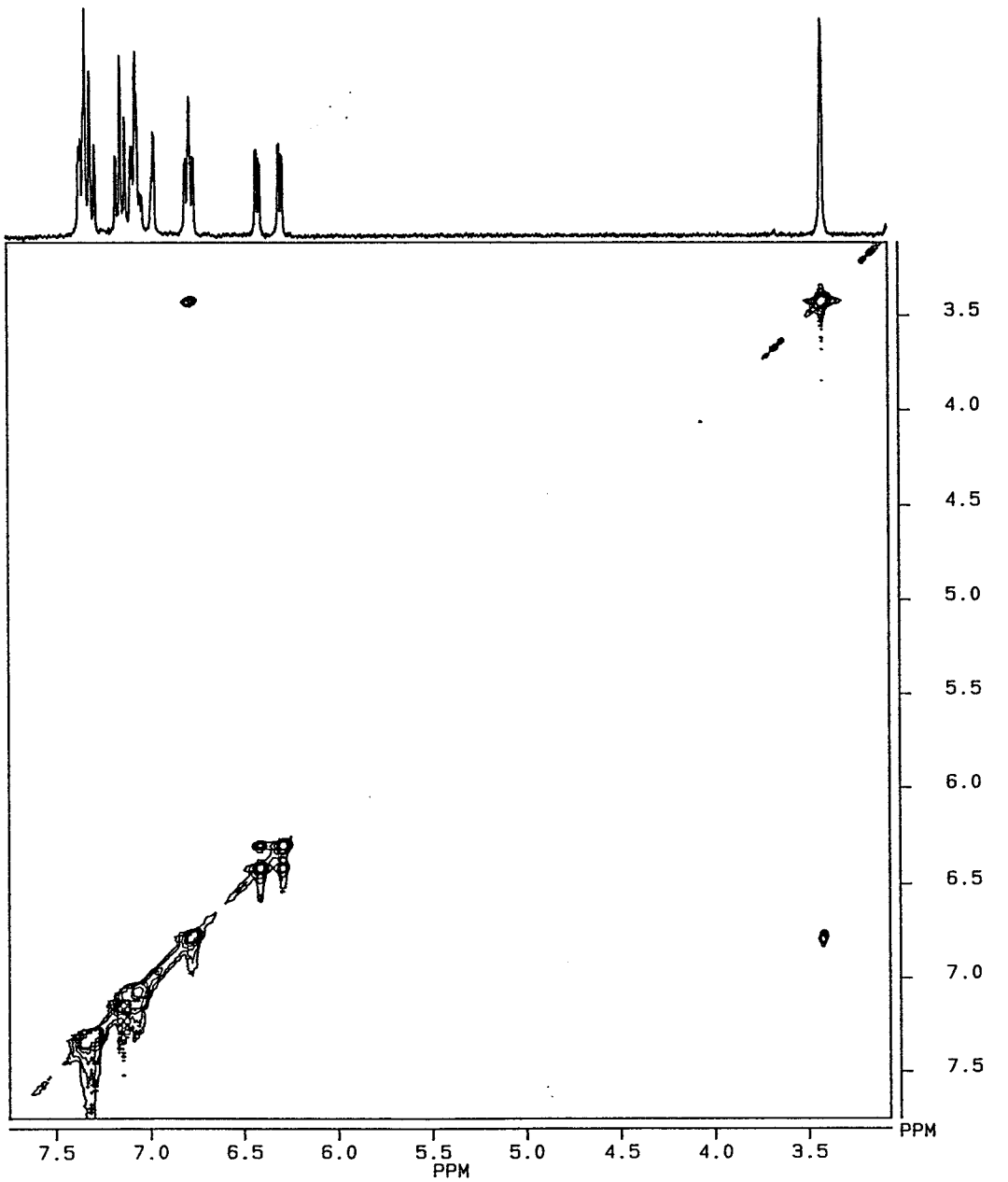

Figure 3.5 Aromatic region of the 300.13 MHz ^{1}H NOESY spectrum of bis(1-indenyl)dimethylsilane, **3.1a, 3.2a**, in toluene-d_8.

mechanism, presumably the [1,5]-suprafacial sigmatropic shift of one (indenyl)$SiMe_2$ moiety relative to the other indenyl fragment. They are also consistent with the experimental activation energies reported for the fluxional molecules 2-(trimethylsilyl)indene, 23 kcal/mol, and 1,2-bis(trimethylsilyl)indene, 26 kcal/mol.[32] If the activation energies for (trimethylsilyl)indene and bis(1-indenyl)dimethylsilane are so similar, it is not likely that the barriers for $(ind)_2SiR_2$ (R=Cl, OMe, Me) vary as widely as reported, ($\Delta H^{\ddagger}$ 7.7-18.9 kcal/mol), nor is it likely that they would be different for steric reasons, as reported.[8] The earlier speculations which invoked the symmetry-forbidden [1,3]-shift below 100 °C are not very likely.[8]

Moreover, as expected, molecular orbital calculations at the extended Hückel level show unequivocally that migration of a trimethylsilyl substituent over the 5-membered ring of an indenyl group proceeds through an isoindene intermediate.[33] Indeed, placement of the Me_3Si fragment over the center of the 5-membered ring (as postulated by the authors of reference 8) is calculated to be strongly disfavored.

3.2.3 Trapping of an Isoindene Intermediate

If the assumption of the intermediacy of an isoindene structure, **3.3**, is correct, then one should be able to trap such a species as a Diels-Alder adduct. Some years ago, it was reported that 2-trimethylsilyl-isoindene, **3.5**, could be intercepted by maleic anhydride at 150 °C; the resulting adduct was hydrolyzed in the presence of methanol and the NMR data of the final product were in accord with its formulation as the diester **3.6**, as in Scheme 3.3.[34]

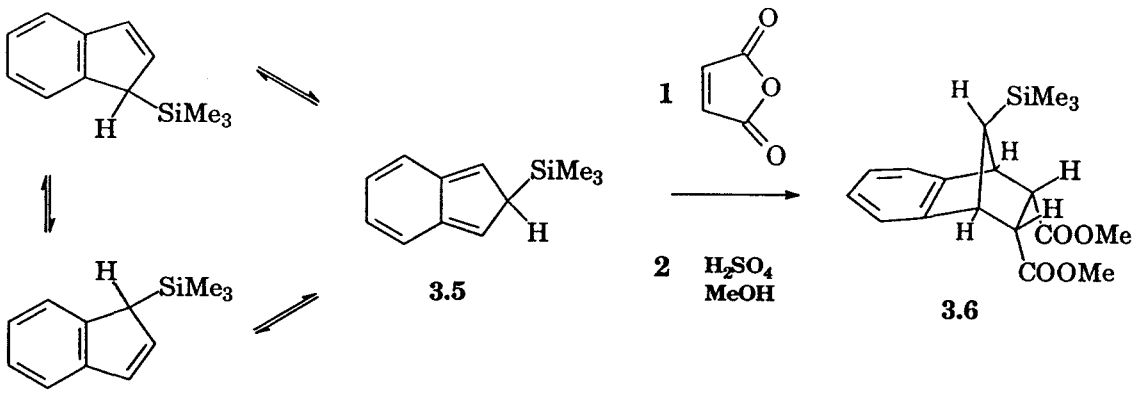

Scheme 3.3 Diels-Alder Trapping of an Isoindene

2-Trimethylsilyl-isoindene was also trapped with tetracyanoethylene at room temperature.[35] ^{1}H NMR data were consistent with the Diels-Alder adduct **3.7**.

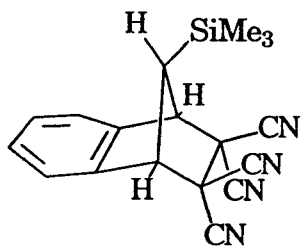

3.7

When **3.2a** was stirred with an excess of tetracyanoethylene (TCNE) at room temperature for 72 h, the ^{1}H and ^{13}C NMR spectra indicated the disappearance of the starting material and the formation of a molecule with a symmetric structure. The mass spectrum of the isolated product revealed it to be **3.8**, the adduct derived from the reaction of two TCNE's with one molecule of (indenyl)$_2$SiMe$_2$.

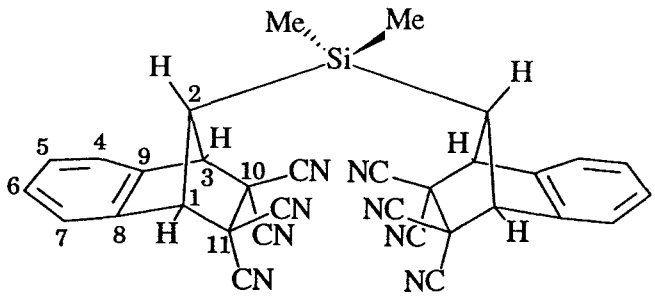

3.8

The ^{1}H (figure 3.6) and ^{13}C NMR (figure 3.7) spectra were assigned by means of ^{1}H-^{13}C shift correlated spectra (figures 3.8 and 3.9) and NOE difference experiments (figure 3.10). In particular, irradiation of the H-1, H-3 signal enhanced the methyl, H-7, H-4 and the H-2 signals.

In conclusion, the isomerization of *d,l*-(indenyl)$_2$SiMe$_2$, **3.2a**, to its *meso* isomer, **3.1a**, proceeds through sequential [1,5]-suprafacial shifts. There is only one mechanism operating at a detectable rate below about 150 °C. Below 100 °C this process is too slow to be detected by NMR line-broadening methods, but it is readily followed by selective excitation methods above 100 °C. The isoindene intermediate is conveniently trapped as its double Diels-Alder adduct showing that the rearrangement occurs relatively rapidly on the chemical time-scale.

3.3 Experimental Section

All experiments were performed under an inert atmosphere of N_2, using standard Schlenk techniques. NMR spectra were recorded on a Bruker AC 300 spectrometer with a 7.65 T superconducting magnet, equipped with a Bruker B-VT 2000 temperature controller, and a 5 mm QNP probe. Protons were

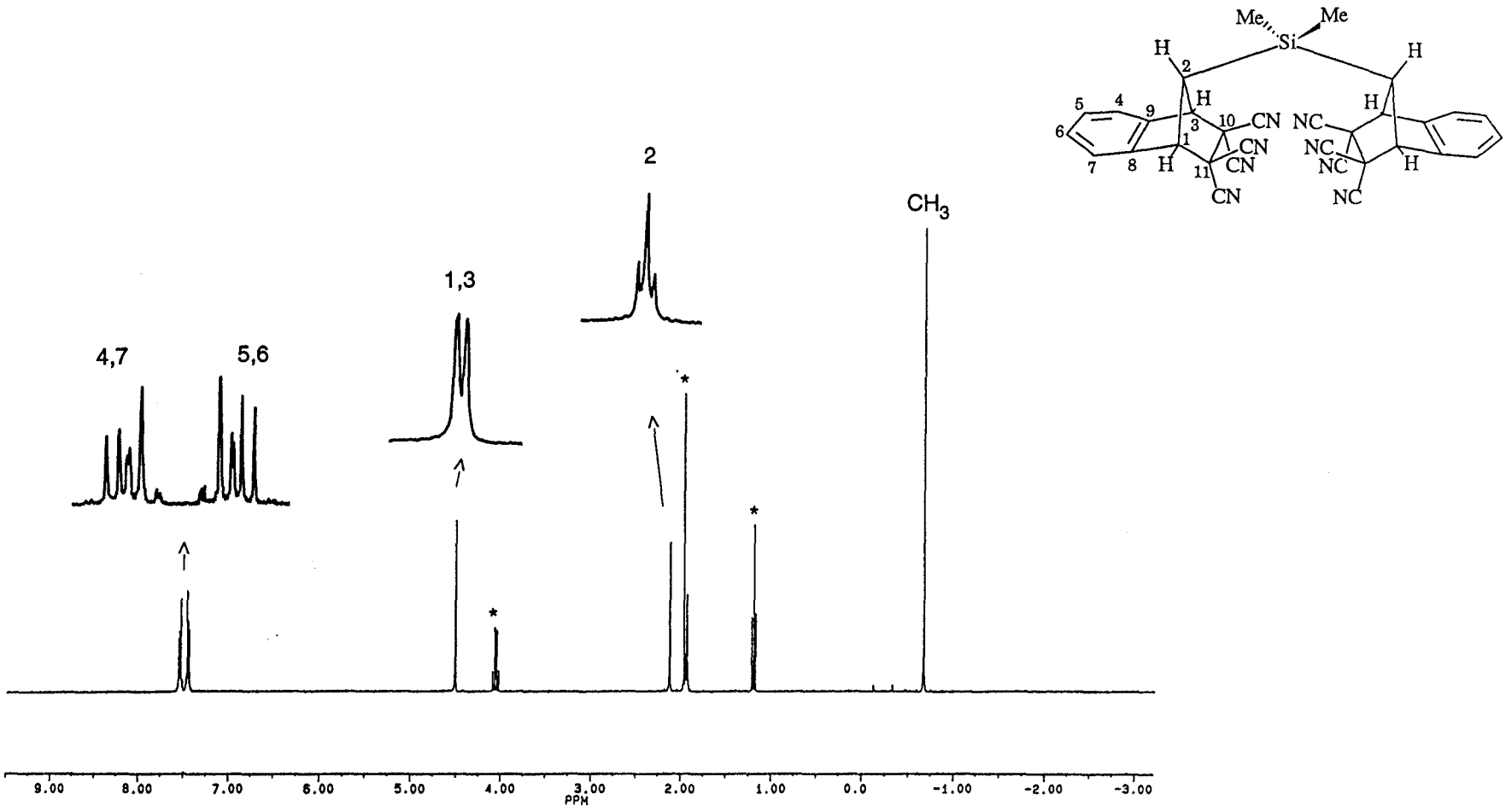

Figure 3.6 300.13 MHz ^{1}H NMR spectrum of the double Diels-Alder adduct, **3.8**, in acetonitrile-d_3.
* ethyl acetate

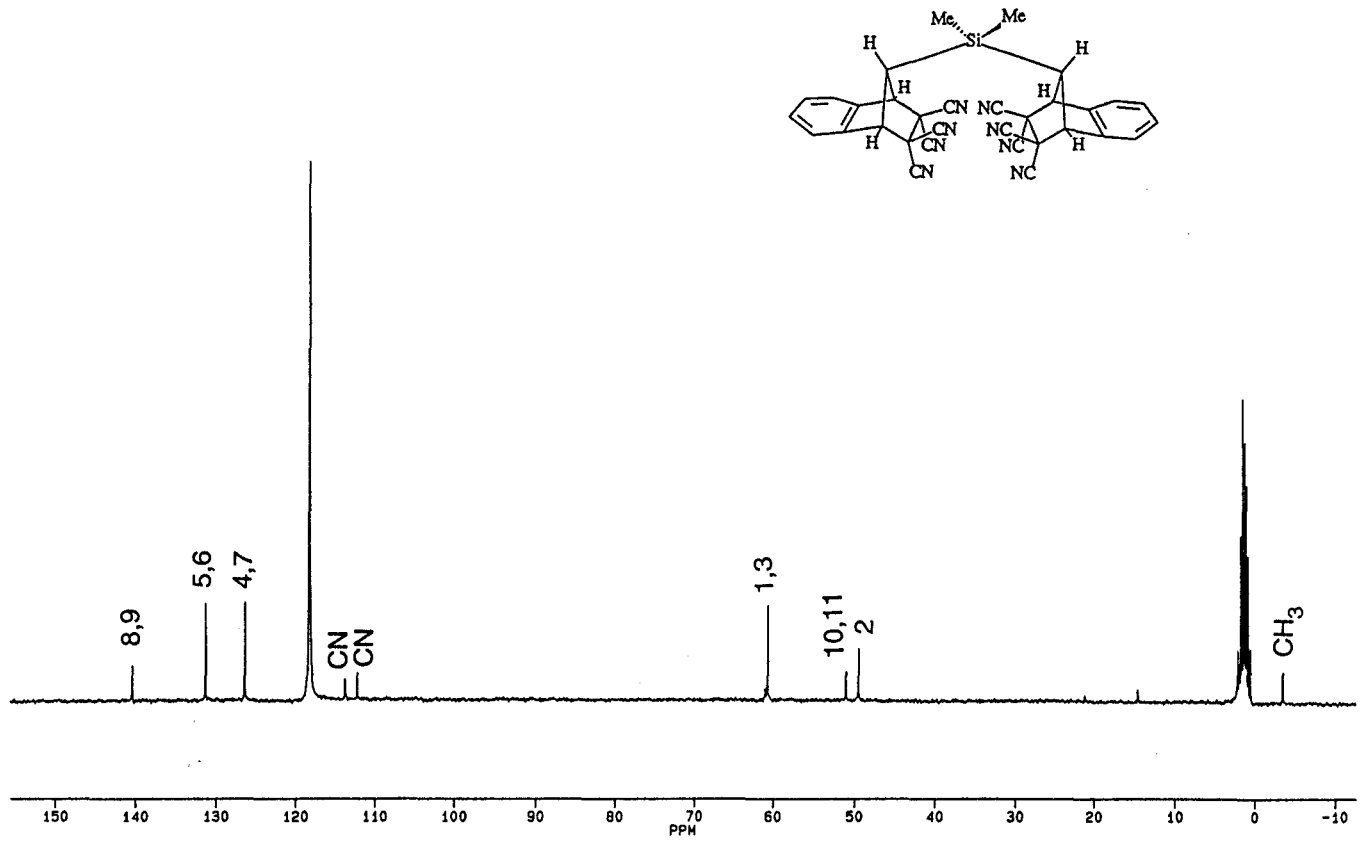

Figure 3.7 75.47 MHz ^{13}C NMR spectrum of the double Diels-Alder adduct, **3.8**, in acetonitrile-d_3.

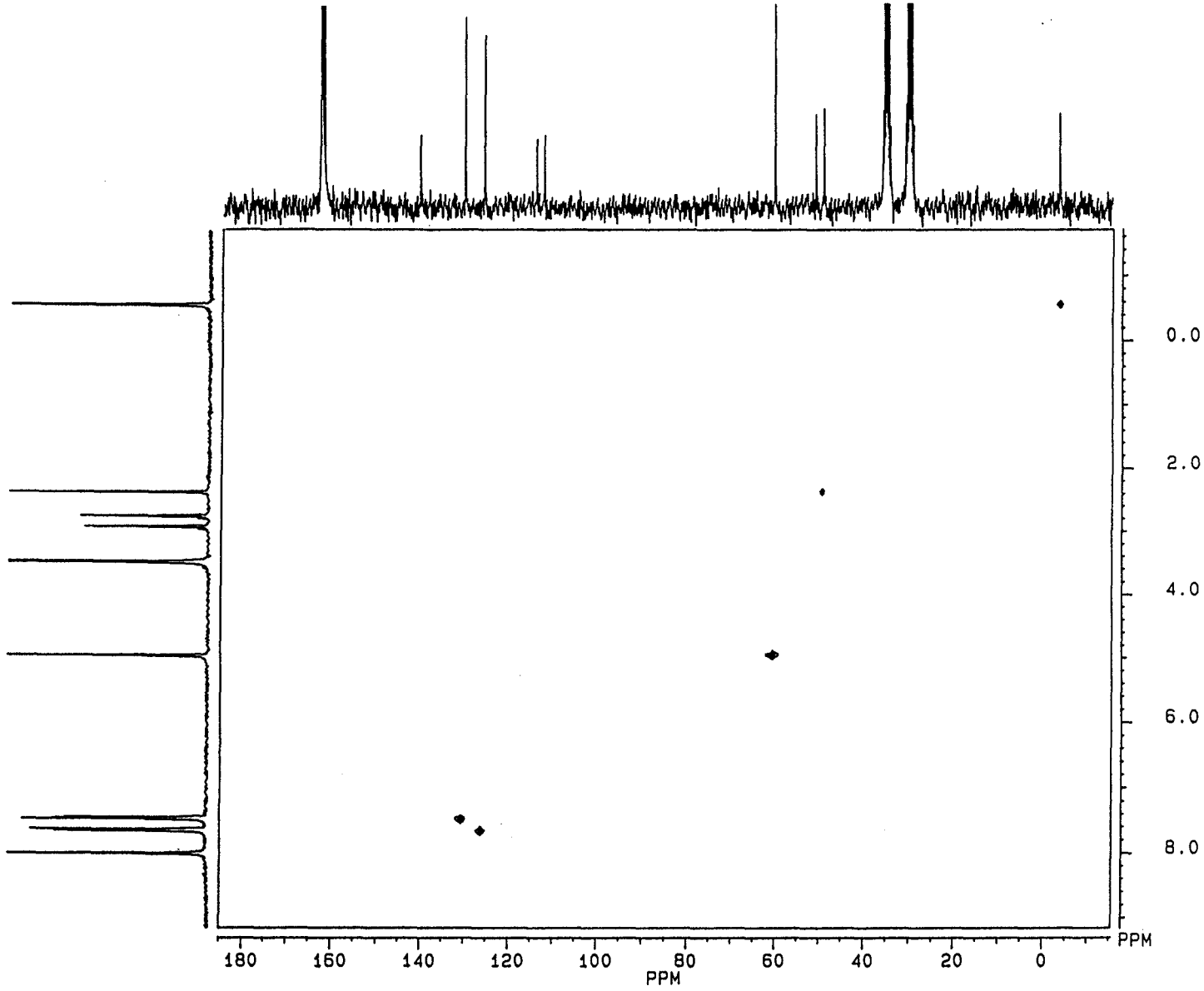

Figure 3.8 ^{1}H - ^{13}C shift correlated spectrum of the double Diels-Alder adduct, **3.8**, in *N,N*-dimethylformamide-d_7.

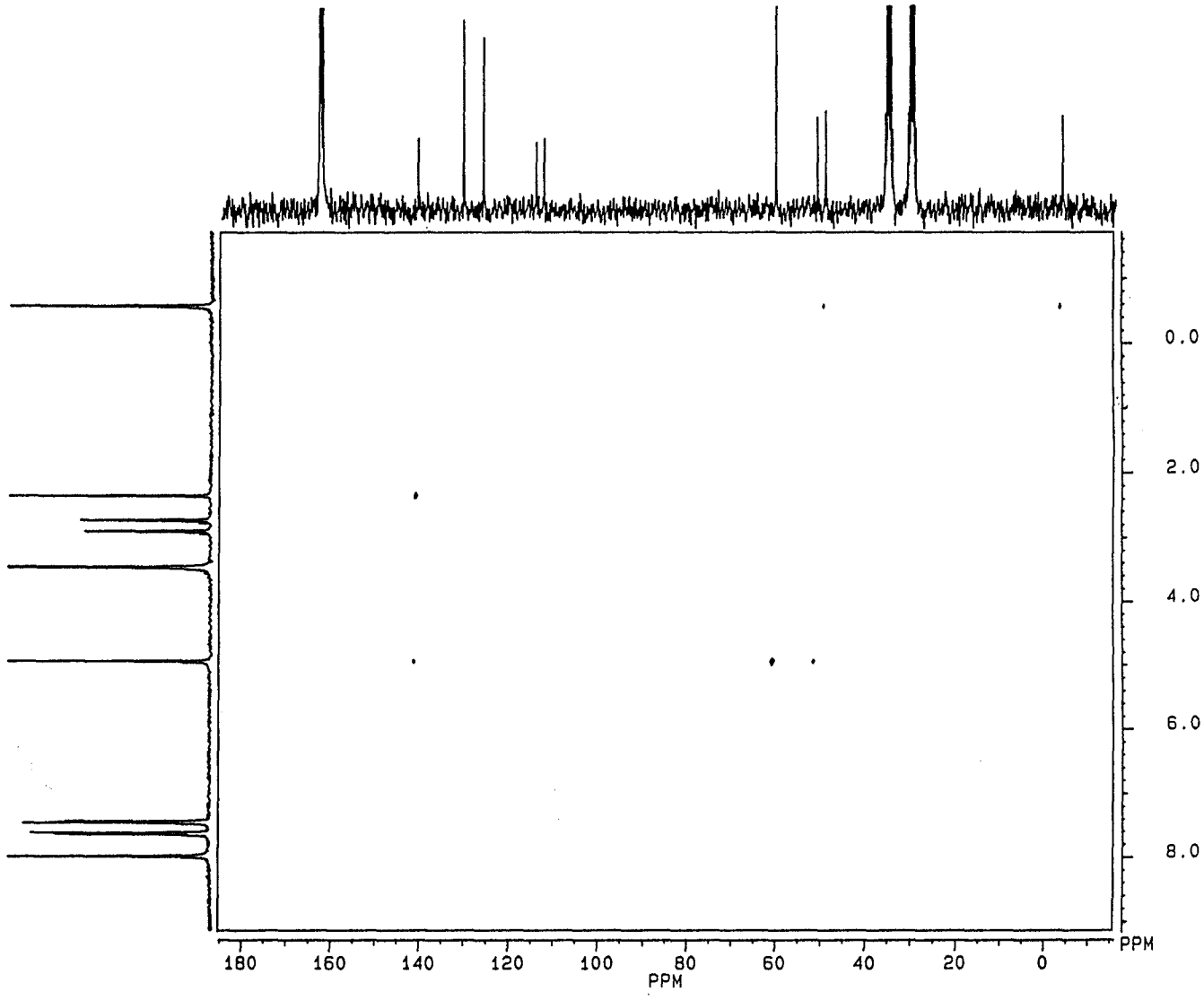

Figure 3.9 Long range ^{1}H - ^{13}C shift correlated spectrum of the double Diels-Alder adduct, **3.8**, in *N,N*-dimethylformamide-d_7.

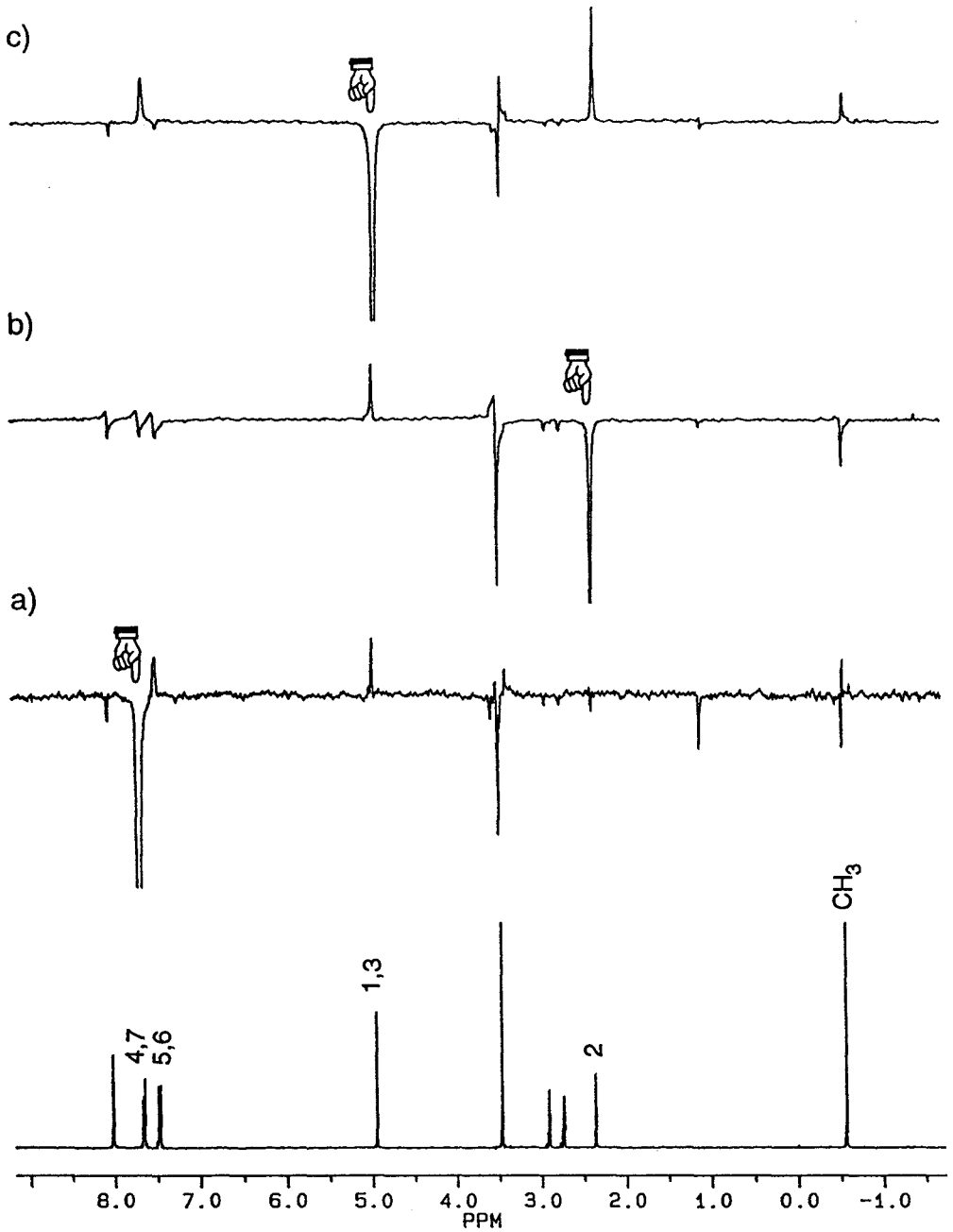

Figure 3.10 300.13 MHz NOE difference spectra of the double Diels-Alder adduct, **3.8**, in *N,N*-dimethylformamide-d_7. In a), irradiation of the H-4, H-7 resonance enhances the H-1,H-3 resonances, as well as the H-5, H-6 peak. In b), irradiation of the H-2 peak enhances the H-1, H-3 signal. In c), irradiation of the H-1, H-3 signal enhances the H-4, H-7, H-2 and methyl peaks.

observed at 300.13 MHz, and ^{13}C was observed at 75.47 MHz. All spectra were recorded on spinning samples, locked to a solvent signal. Peaks were referenced to a residual proton signal of the solvent, or to a ^{13}C solvent signal. Each temperature was measured by placing a copper-constantan thermocouple, contained in an NMR tube, into the probe.

All FID's were transferred to an IBM PC using the program NMRLINK. Spectra were Fourier transformed using the program NMR286.

Bis(1-indenyl)dimethylsilane

Following the method of Marechal[36], a 250 round-bottomed flask was charged with dry diethyl ether (50 mL) and butyllithium in hexanes (39.1 mL, 62.5 mmol) at -20 °C. A mixture of dry diethyl ether (25 mL) and freshly distilled indene (7.3 mL, 62.5 mmol) was added drop by drop, maintaining constant temperature. The mixture was allowed to warm up to -10 °C, and a mixture of dry diethyl ether (25 mL) and dichlorodimethylsilane (3.4 mL, 28.0 mmol) was added drop by drop, maintaining constant temperature. The mixture was warmed to room temperature, hydrolyzed, and the organic layer was dried over sodium sulphate. The ether was pumped off, and the resulting white solid was crystallized from diethyl ether and hexane at -78 °C.

The proton NMR chemical shifts correspond to those obtained by Chen and coworkers[8], for both the pure *d,l* enantiomers and for the mixture of *meso* and *d,l* diastereomers. Chen did not report a ^{13}C NMR spectrum, so a ^{1}H-^{13}C shift correlated 2D experiment (the full spectrum is shown in figure 3.11 and an expansion of the aromatic region in figure 3.12) was performed in order to assign the ^{13}C chemical shifts.

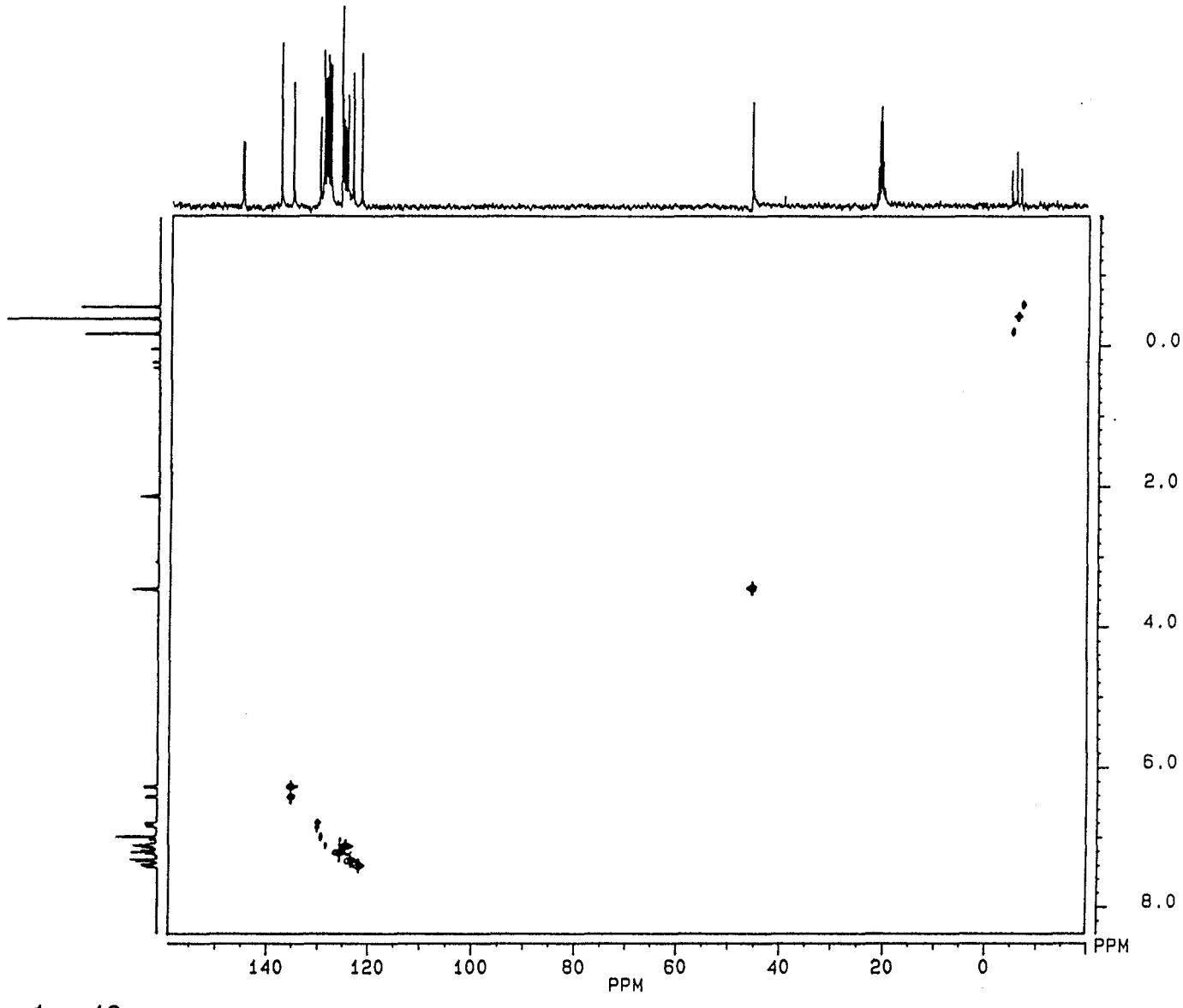

Figure 3.11 ^{1}H - ^{13}C shift correlated spectrum of the mixture of bis(1-indenyl)dimethylsilane isomers, **3.1a**, **3.2a**, in toluene-d_8.

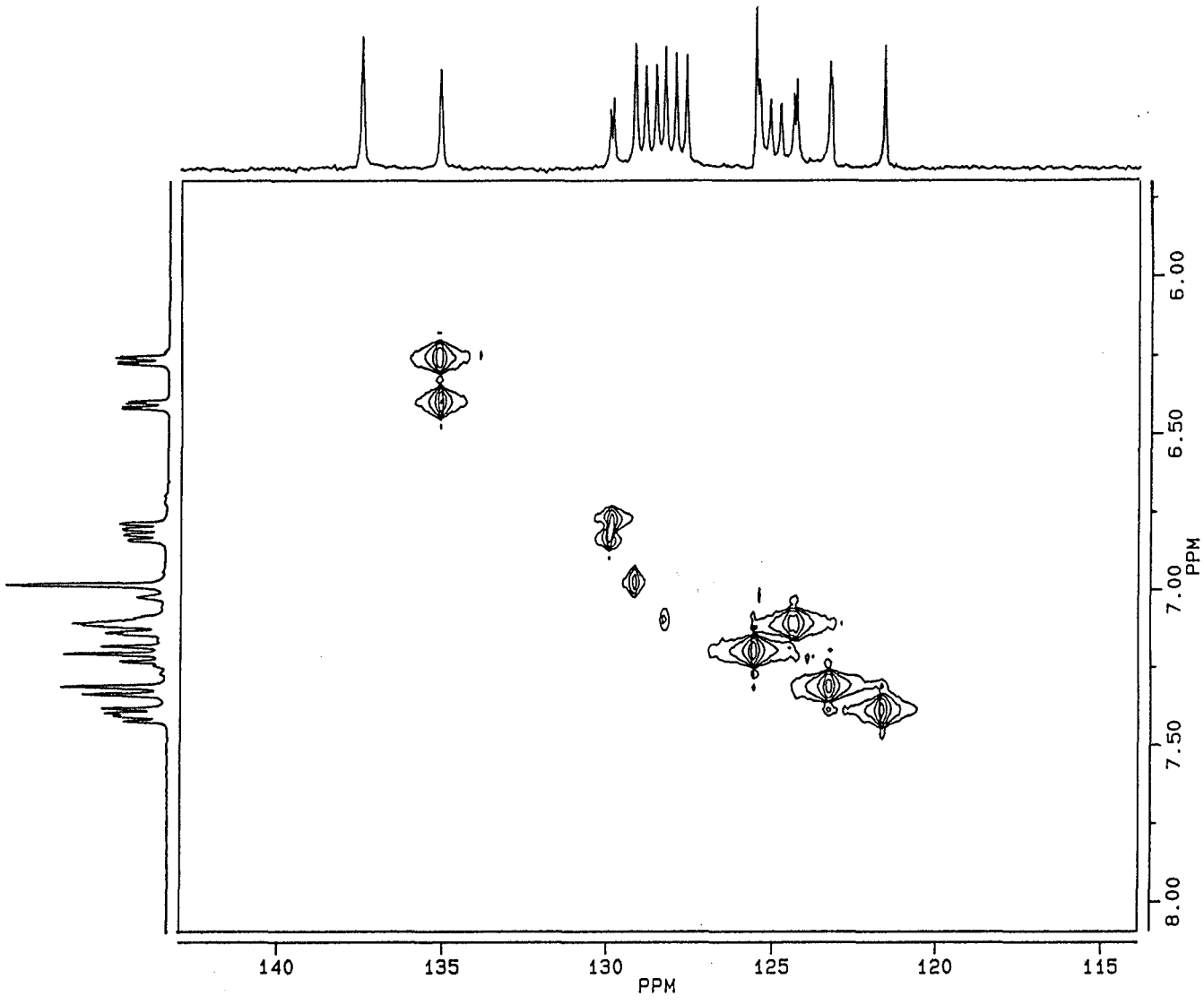

Figure 3.12 Aromatic region of the ^{1}H - ^{13}C shift correlated spectrum of the mixture of bis(1-indenyl)-dimethylsilane isomers, **3.1a**, **3.2a**, in toluene-d_8.

d,l enantiomers ^{1}H NMR (toluene-d_8) δ 7.41 (d, ^{3}J=7.6 Hz, 2H, H-4), 7.32 (d, ^{3}J=7.5 Hz, 2H, H-7), 7.20 (d, ^{3}J=7.6 Hz of d, ^{3}J=7.5 Hz, 2H, H-5), 7.10 (d, ^{3}J=7.5 Hz of d, ^{3}J=7.6 Hz, 2H, H-6), 6.83 (d, ^{3}J=5.3 Hz of d, ^{3}J=1.0 Hz, 2H, H-3), 6.40 (d, ^{3}J=1.9 Hz of d, ^{3}J=5.3 Hz, 2H, H-2), 3.42 (s, 2H, H-1), -0.43 (s, 6H, 2CH_3).

meso ^{1}H NMR (toluene-d_8) δ 7.39 (d, ^{3}J=7.6 Hz, 2H, H-4), 7.32 (d, ^{3}J=7.5 Hz, 2H, H-7), 7.20 (d, ^{3}J=7.6 Hz of d, ^{3}J=7.6 Hz, 2H, H-5), 7.10 (d, ^{3}J=7.5 Hz of d, ^{3}J=7.6 Hz, 2H, H-6), 6.79 (d, ^{3}J=5.3 Hz of d, ^{3}J=1.0 Hz, 2H, H-3), 6.26 (d, ^{3}J=5.3 Hz of d, ^{3}J=1.9 Hz, 2H, H-2), 3.42 (s, 2H, H-1), -0.21 (s, 3H, CH_3), -0.59 (s, 3H, CH_3).

d,l ^{13}C NMR (toluene-d_8) δ 145.15, 144.84 (C-8, C-9), 135.16 (C-2), 129.96 (C-3), 125.6 (C-5), 124.42 (C-6), 123.32 (C-7), 121.64 (C-4), 45.48 (C-1), -6.21 (methyl).

meso ^{13}C NMR (toluene-d_8) δ 145.15, 144.84 (C-8, C-9), 135.16 (C-2), 129.88 (C-3), 125.6 (C-5), 124.33 (C-6), 123.26 (C-7), 121.64 (C-4), 45.42 (C-1), -5.24, -7.11 (2 methyl).

Mass spectrum: *m/z* (relative intensity) 288 (10) $(M)^+$, 273 (5) $(M-CH_3)^+$, 173 (100) $(M-C_9H_7)^+$, 145 (50) $(M-C_9H_7)^+$, 115 (15) $(C_9H_7)^+$.

Trapping of Isoindene, 3.3, with Tetracyanoethylene

A 100 mL two-necked round bottom flask was charged with ethyl acetate (50 mL), bis(1-indenyl)dimethylsilane (240 mg, 0.83 mmol) and tetracyanoethylene (380 mg, 2.97 mmol). The mixture was stirred under N_2 for 72 hours. The Diels-Alder adduct was separated from excess TCNE using flash chromatography on silica by elution with methylene chloride to obtain the pure

double Diels-Alder adduct (200 mg, 0.37 mmol, 44%).

^{1}H NMR (acetonitrile-d_3) δ 7.66-7.64 (m, 4H, H-7, H-4), 7.48-7.45 (m, 4H, H-5, H-6), 4.93 (d, ^{3}J=1.05 Hz, 4H, H-1, H-3), 2.35 (tr, ^{3}J=1.05 Hz, 2H, H-2), -0.57 (s, 6H, 2CH_3). The assignment of the proton signals were confirmed by NOE difference experiments. ^{13}C chemical shifts were assigned on the basis of ^{1}H-^{13}C shift correlated experiments. ^{13}C NMR (acetonitrile-d_3) δ 140.69 (C-8, C-9), 130.46 (C-5, C-6), 126.04 (C-7, C-4), 114.27, 112.53 (exo and endo nitrile), 60.54 (C-1, C-3), 51.30 (C-10, C-11), 49.414 (C-2), -3.742 (2CH_3).
Mass spectrum: *m/z* (relative intensity) 544 (10) $(M)^+$, 416 (40) $(M-4CN)^+$, 288 (45) $(M-8CN)^+$.

NOESY Experiment

The program NOESYPH.AU was used, with the pulse sequence described in chapter one. The experiment was performed at 107 °C, with a mixing time of 1.6 seconds, 2K words in the f_2 dimension, and 1K words in the f_1 dimension. The sweep width in f_2 was 3184.713 Hz, with the 01 set at 6006.055 Hz. The 90° pulse width was determined to be 12.8 μsec. Four scans were collected for each spectrum. FID's were processed on the AC 300 with a Gaussian window function in both f_1 and f_2, and a line broadening of 3.2 Hz. The relaxation delay was set to 2 seconds, and the initial value for the 2D evolution was set to 10 μsec.

Selective Inversion Recovery Experiments

The samples were allowed to equilibrate in the magnet for one hour prior to making measurements. The ^{1}H 90° pulse width was calibrated at each

temperature. At 101.2 °C, it was 10 μsec. The program INVREC2P.AUR was used with the following pulse sequence:

D1 - 90° - D2 - 90° - VD - 90° - FID

where D2 is 1/2Δν, and Δν is the frequency difference between the signal being inverted (i.e. the *d,l* methyl signal), and the signal left unperturbed (one of the *meso* methyl signals). The fixed delay, D1, was set to 40 seconds. The sweep width was set to 5555.556 Hz, with the O1 set at the *d,l* methyl peak, typically 4782.312 Hz. The acquisition time was 1.36 seconds, with a digital resolution of 0.74 Hz/data point.

Spectra were Fourier transformed and the intensities of the methyl peaks were measured. The magnetization vs. variable delay data at each temperature were fitted using the non-linear least squares fitting program FLOPSI, to determine rate constants.

Rate constants were obtained at 101.2 and 107.2 °C with selective inversion experiments. In order to help fit the data thus obtained with the non-linear least squares fitting program FLOPSI, spin-lattice relaxation times were determined at 101.2 °C with a non-selective inversion recovery experiment. The values obtained are 4.6 seconds for the *d,l* methyl peak, 4.8 seconds for the high frequency *meso* methyl peak, and 4.9 seconds for the low frequency *meso* methyl peak.

Non-Selective Inversion Recovery Experiment

Spin-lattice relaxation times were measured for the methyl protons, by performing a non-selective inversion recovery experiment at 101.2 °C. Again, the program INVREC2P.AUR was used, as described previously. The delay D2

was set to a very small number, making the pulse sequence equivalent to 180°-variable delay-90°. The fixed delay D1 was set to 40 seconds. Each spectrum was acquired with a sweep width of 3521.13 Hz, with O1 set at 5978.8 Hz, over 16K data points. Four scans were collected for each variable delay, with an acquisition time of 2.33 seconds, giving a resolution of 0.43 Hz/point.

FID's were Fourier transformed and the intensities of the methyl peaks were measured. For each methyl peak, an input data file was created, consisting of variable delay times and the corresponding magnetizations. The input files were processed using the program T1cals to calculate approximate T_1's for each methyl site.

Classical Kinetics Experiments

For each of the temperatures 47.4, 57.2 and 68.3 °C, the magnet was allowed to equilibrate for one hour. A fresh sample of the *d,l* isomer in toluene-d_8 was prepared, and placed in the magnet. Spectra were recorded at regular intervals after locking and shimming. Two runs were performed at 57.2 °C, to ensure that the results were reproducible. Intensities of methyl signals were measured, and the data were processed using initial rates methods.

From the rate constants obtained over this sixty degree temperature range, using a combination of selective inversion experiments and classical kinetics methods, the Eyring plot, shown in figure 3.4 was calculated.

Heteronuclear Shift Correlated Experiments

A ^{13}C - ^{1}H shift correlated experiment was performed on the double Diels-Alder adduct. The program XHCORRDC.AU was used. The 90° ^{1}H pulse

width through the decoupler was determined to be 9.2 μsec, and the ^{13}C 90° pulse width was determined to be 4.3 μsec. The spectra in f_2 were recorded over a spectral width of 15151.515 Hz in 2K data points. The 256 FID's in f_1 were obtained over a ^1H spectral spectral width of 1633.987 Hz. Each FID was acquired in 160 scans. The relaxation delay was set to 1 second, the polarization transfer delay to 0.003571 s, and the refocussing delay to 0.001786 sec. The data were processed using a Gaussian window function in f_2, with 14.8 Hz line broadening, and a sine bell window function in f_1.

A long range ^{13}C - ^1H shift correlated experiment was performed on the double Diels-Alder adduct, using the program XHCORRC.AU. The FID's in f_2 were recorded over a spectral width of 15151.515 Hz in 2K data points. The 256 FID's in f_1 were obtained over a ^1H spectral spectral width of 1633.987 Hz. Each FID was acquired in 160 scans. The relaxation delay was set to 1 second, the polarization transfer delay to 0.0480 s, and the refocussing delay to 0.024 s. The data were processed using a Gaussian window function in f_2, with 14.8 Hz line broadening, and a sine bell window function in f_1. The 90° ^1H pulse width through the decoupler was determined to be 9.2 μsec, and the ^{13}C 90° pulse width was determined to be 4.3 μsec.

A ^{13}C - ^1H shift correlated experiment was performed on the mixture of diastereomers of bis(1-indenyl)dimethylsilane. The program XHCORRDC.AU was used. The 90° ^1H pulse width through the decoupler was determined to be 9.2 μsec, and the ^{13}C 90° pulse width was determined to be 4.3 μsec. The spectra in f_2 were recorded over a spectral width of 13513.514 Hz in 4K data points. The 256 FID's in f_1 were obtained over a ^1H spectral spectral width of 1533.742 Hz. Each FID was acquired in 128 scans. The relaxation delay was

set to 1 second, the polarization transfer delay to 0.003571 s, and the refocussing delay to 0.001786 s. The data were processed using a Gaussian window function in f_2, with 6.6 Hz line broadening, and a sine bell window function in f_1.

NOE Difference Experiments

NOE difference experiments were performed on the double Diels-Alder adduct. Spectra were obtained with a sweep width of 3267.974 Hz, over 16K data points, with an acquisition time of 2.507 s, giving a digital resolution of 0.399 Hz/pt. 128 scans were acquired for each spectrum. The O1 was set to 5783.181 Hz. The O2 was set to 6151.386 Hz in order to irradiate the bridgehead protons (H-1, H-3), 6966.385 Hz to irradiate the high field aromatic protons (H-4, H-7), and 5376.280 Hz to irradiate the other bridgehead proton (H-2). The 02 was set to 4241.345 Hz in order to irradiate baseline for the reference spectra.

CHAPTER FOUR

The Molecular Dynamics of $(\eta^1\text{-cpp})Mn(CO)_3(PEt_3)_2$

4.1 Introduction

Organometallic moieties can coordinate to 4*H*-cyclopenta[*def*]phenanthrene, cppH, **4.1**, in the η^6, η^5 or η^1 fashions.

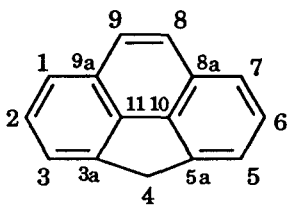

4.1

Examples of the first two have been characterized crystallographically, as shown below. The conversion of η^6 derivatives, such as $(\eta^6\text{-cppH})Cr(CO)_3$, **4.2**, or $[(\eta^6\text{-cppH})Mn(CO)_3]^+$ into the corresponding η^5-analogues, such as $(\eta^5\text{-cpp})$-$Mn(CO)_3$, **4.3**, occurs upon treatment with base.[37]

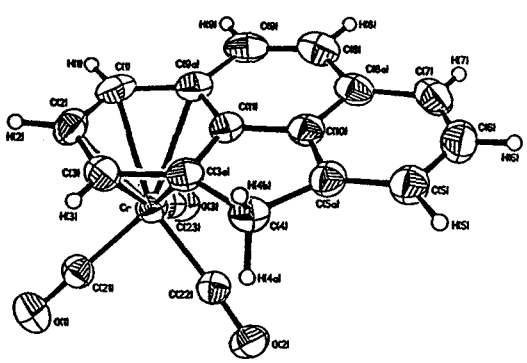

4.2

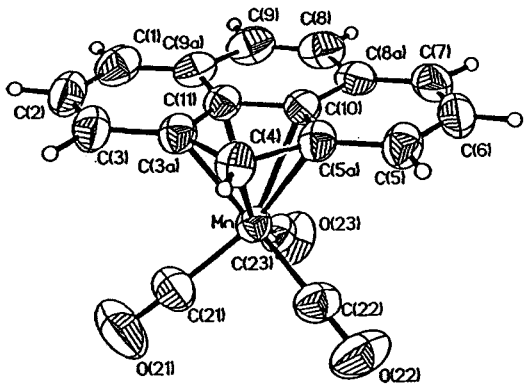

4.3

EHMO calculations suggest that the least-motion pathway joining the centers of the 6- and 5-membered rings is strongly disfavored.[37] Indeed, an energy hypersurface study indicates that an exocyclic η^3-transition state is the most viable. To this end, synthetic approaches to $(\eta^3\text{-cpp})ML_n$ complexes were investigated.

In the first approach, removal of one CO ligand from $(\eta^1\text{-cpp})\text{-}Fe(CO)_2(C_5H_5)$, to generate $(\eta^3\text{-cpp})Fe(CO)(C_5H_5)$, as in scheme 4.1, was not successful. Instead the reaction yielded the iron dimer $[(C_5H_5)Fe(CO)_2]_2$ and the interesting cpp trimer whose structure has been discussed elsewhere.[9]

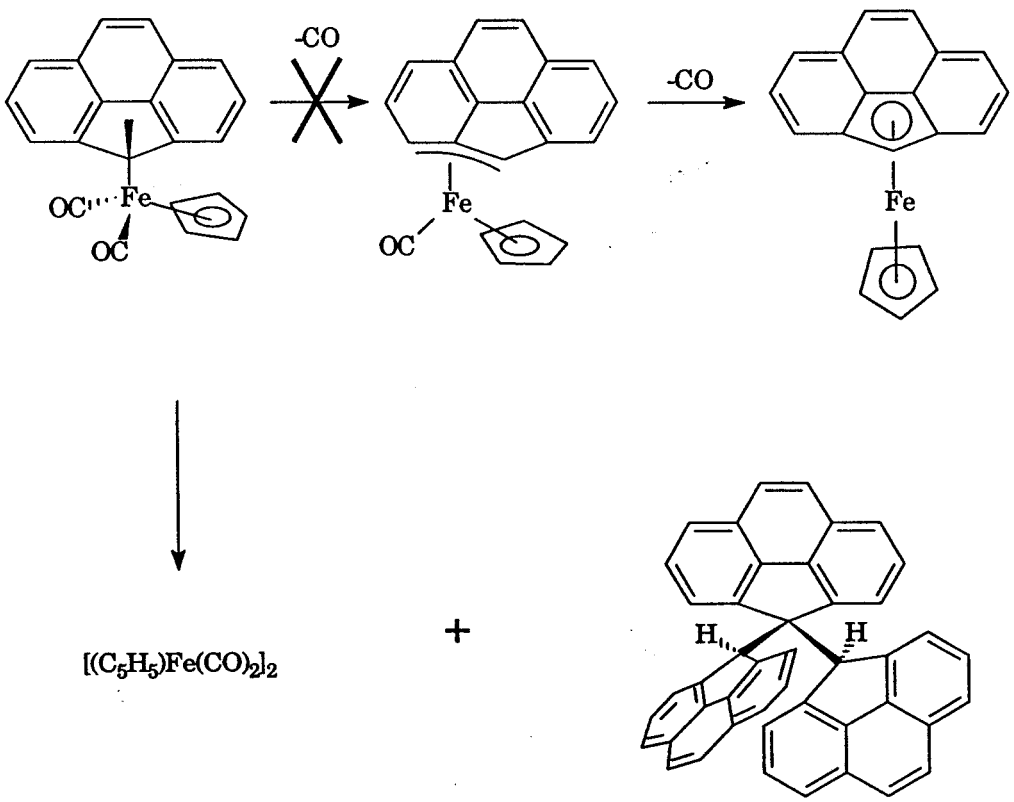

Scheme 4.1 Attempted synthesis of $(\eta^3\text{-cpp})Fe(CO)(C_5H_5)$ by removal of one CO ligand from $(\eta^1\text{-cpp})Fe(CO)_2(C_5H_5)$.

The second approach involved the attempted addition of a single mole of Et_3P to $(\eta^5\text{-cpp})Mn(CO)_3$.

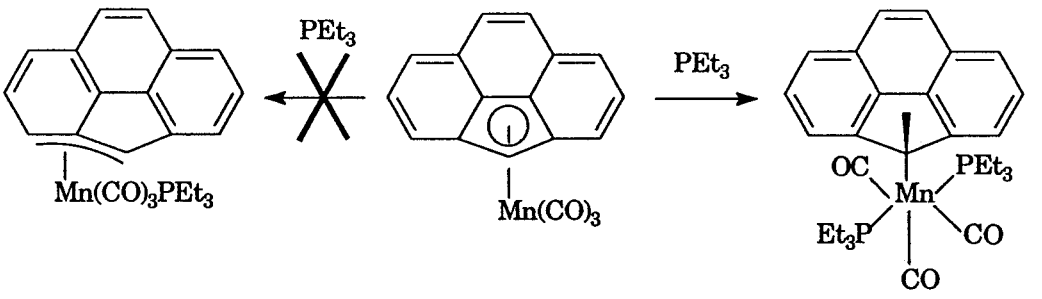

4.4

Scheme 4.2 Attempted synthesis of $(\eta^3\text{-cpp})Mn(CO)_3PEt_3$ by addition of a PEt_3 ligand to $(\eta^5\text{-cpp})Mn(CO)_3$.

One phosphine group was expected to add to the manganese, yielding the η^3- complex. However, it was not possible to stop the reaction at the $(\eta^3\text{-cpp})Mn(CO)_3PEt_3$ stage, and instead $(\eta^1\text{-cpp})Mn(CO)_3(PEt_3)_2$, **4.4**, was isolated. The ^1H, ^{13}C and ^{31}P NMR spectra indicated the existence of two phosphine environments, and the initial interpretation was in terms of an axial and an equatorial disposition of the phosphines. However, a subsequent x-ray crystal structure revealed that the phosphines were trans di-equatorial such that the P—Mn—P vector lies at about 37° with respect to the cpp mirror plane, as shown in figure 4.1.

Evidently, there must be hindered rotation of the $Mn(CO)_3(PEt_3)_2$ moiety about the Mn - C(4) sigma bond. To equilibrate the ^{31}P environments, it would be necessary to attain a C_S conformation in which the P—Mn—P vector straddles the cpp ligand's mirror plane, as shown in the PC-MODEL derived

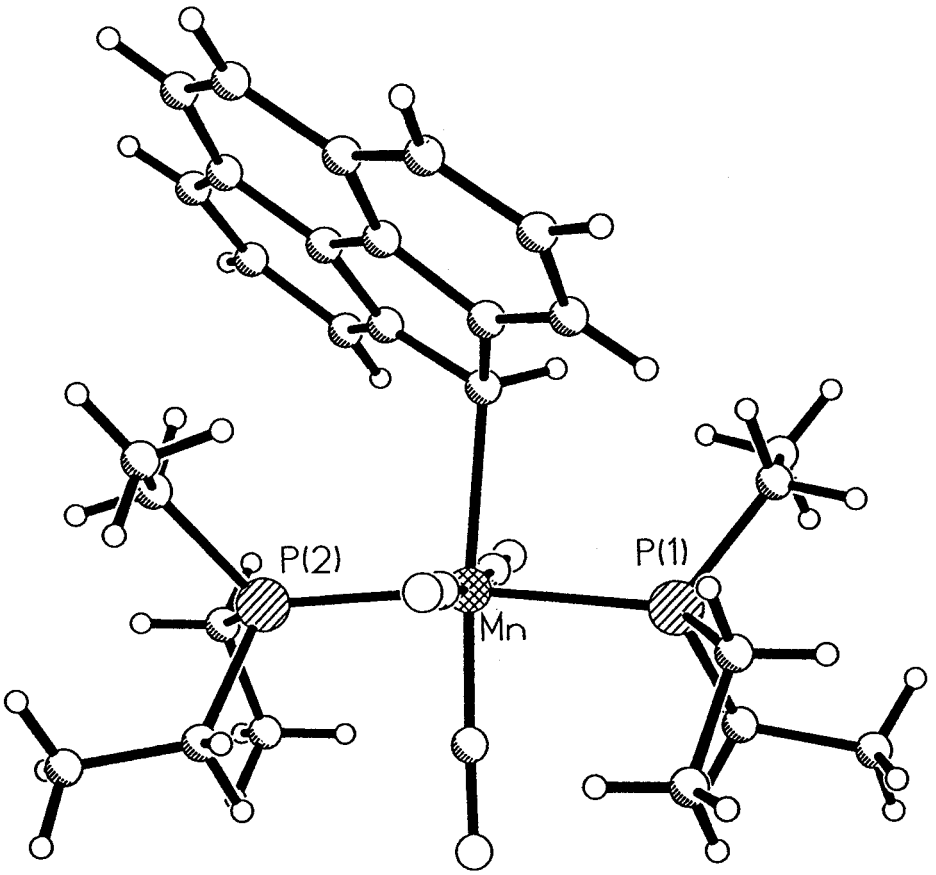

Figure 4.1 X-ray crystal structure of (η^1-cpp)Mn(CO)$_3$(PEt$_3$)$_2$, **4.4**,. This figure is reproduced from reference 9.

transition state structure shown in figure 4.2.

In order to determine if the phosphine groups were chemically exchanging, a 2-D ^1H NOESY spectrum was performed at room temperature. Figure 4.3 shows that the two methylene signals are exchanging, and that the two methyl signals are exchanging.

As the molecule decomposed above room temperature, the use of lineshape analysis was out of the question for determining the barrier to rotation about the Mn - C(4) bond. The author of this thesis used single selective inversion recovery experiments to determine the barrier to rotation about the Mn - C(4) bond.

4.2 Results and Discussion

^1H selective inversion experiments were performed in order to determine rate constants, at different temperatures, between the two methylene signals. The methyl signals could not be used because one of the methyl signals was overlapped with the free phosphine signal. One methylene signal was inverted, by placing the offset on that peak, and delivering a 180^o pulse to it. Following this, the time dependences of the intensities of both methylene signals were monitored, using a 90^o pulse, after a variable delay. Twenty-five variable delays were used, entered in random order.

Figure 4.4 shows the selective inversion initial state (upper spectrum), as well as the equilibrium (lower) spectrum. The non-linear least squares fitting program, FLOPSI was used to fit the data from the selective inversion experiments. Figure 4.5 shows a typical fit. Data from selective inversion experiments at different temperatures were used to compute an Eyring plot

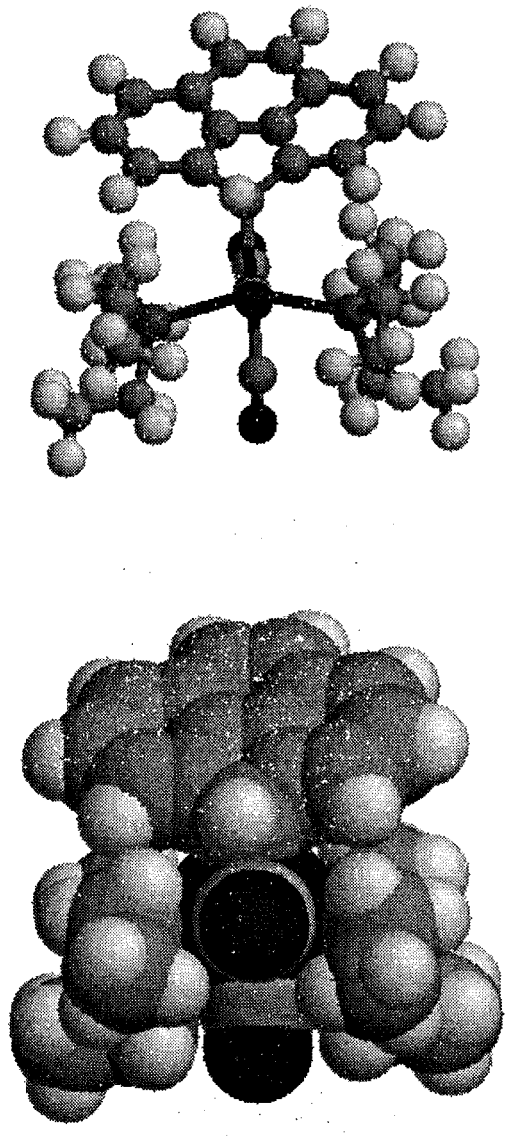

Figure 4.2 Ball and stick (upper) and space filling (lower) views of the transition state structure for (η^1-cpp)$Mn(CO)_3(PEt_3)_2$, **4.4**, as calculated by PC-MODEL. The molecule was constrained such that the P-Mn-P fragment straddled the mirror plane which bisected the cpp ligand. The minimized structure allowed the ethyl substituents to adopt their most favourable orientations.

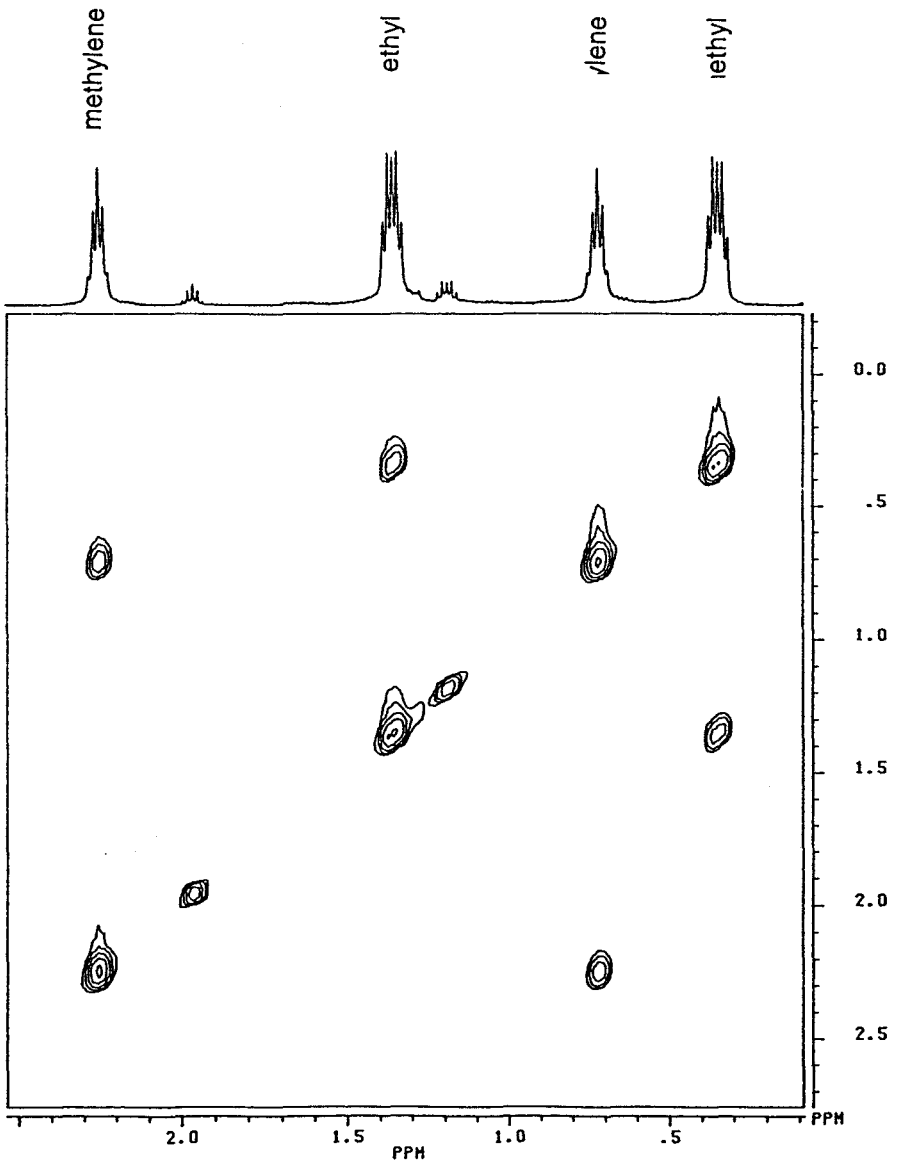

Figure 4.3 500.13 MHz ^{1}H NOESY spectrum of (η^1-cpp)Mn(CO)$_3$(PEt$_3$)$_2$, **4.4**, in CD_2Cl_2, recorded at ambient temperature. The mixing time was 0.05 s. This figure is reproduced from reference 9.

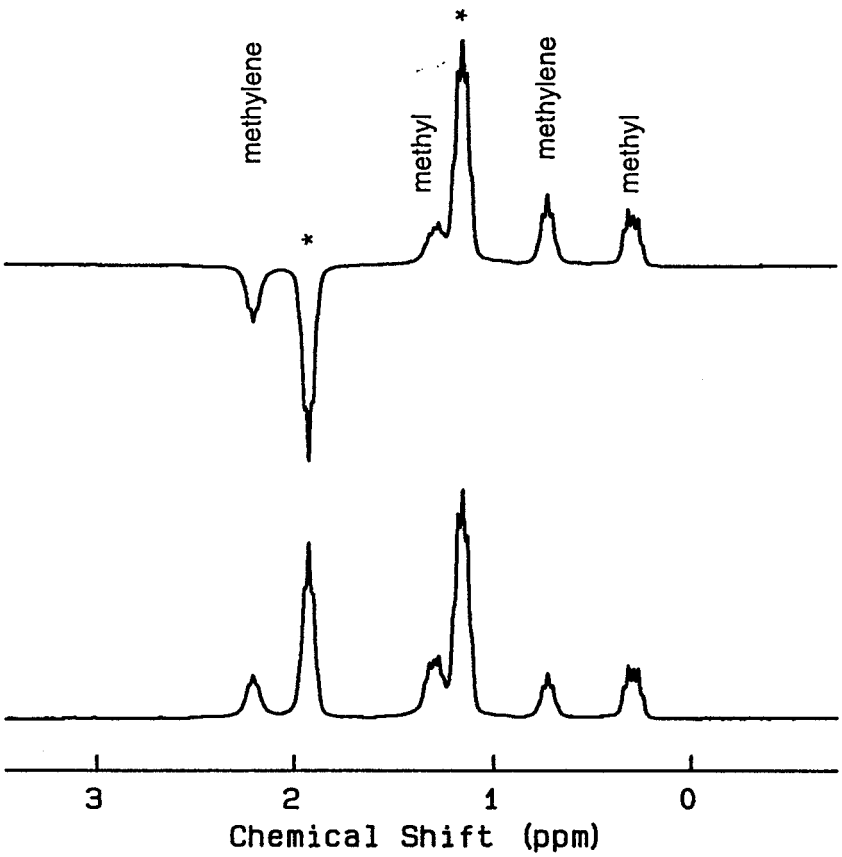

*free phosphine

Figure 4.4 300.13 MHz ^1H selective inversion initial state (upper) spectrum with equilibrium (lower) spectrum for (η^1-cpp)$Mn(CO)_3(PEt_3)_2$, **4.4**, in CD_2Cl_2.

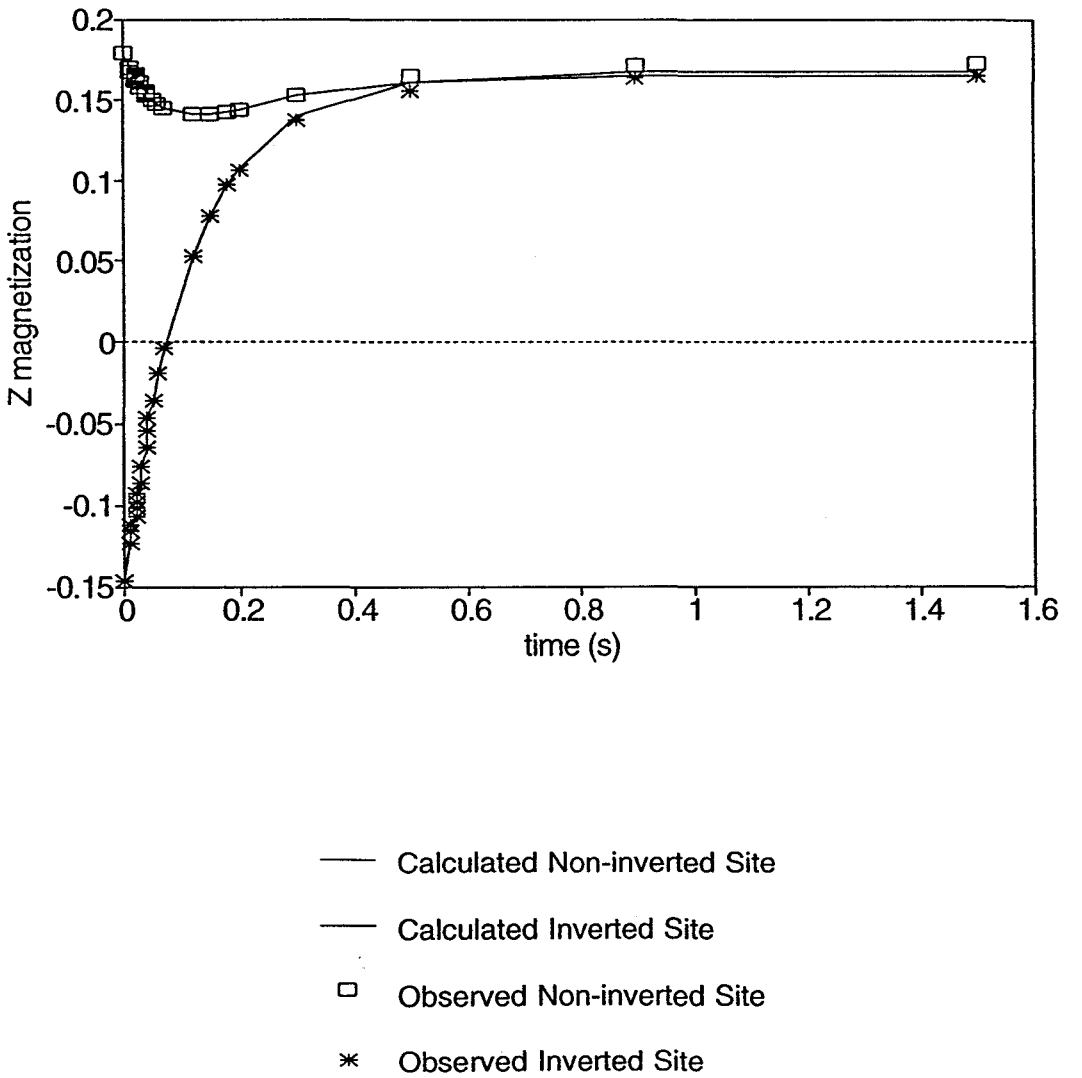

Figure 4.5 Experimental data vs. calculated data obtained from a selective inversion recovery experiment for $(\eta^1\text{-cpp})Mn(CO)_3(PEt_3)_2$, **4.4**.

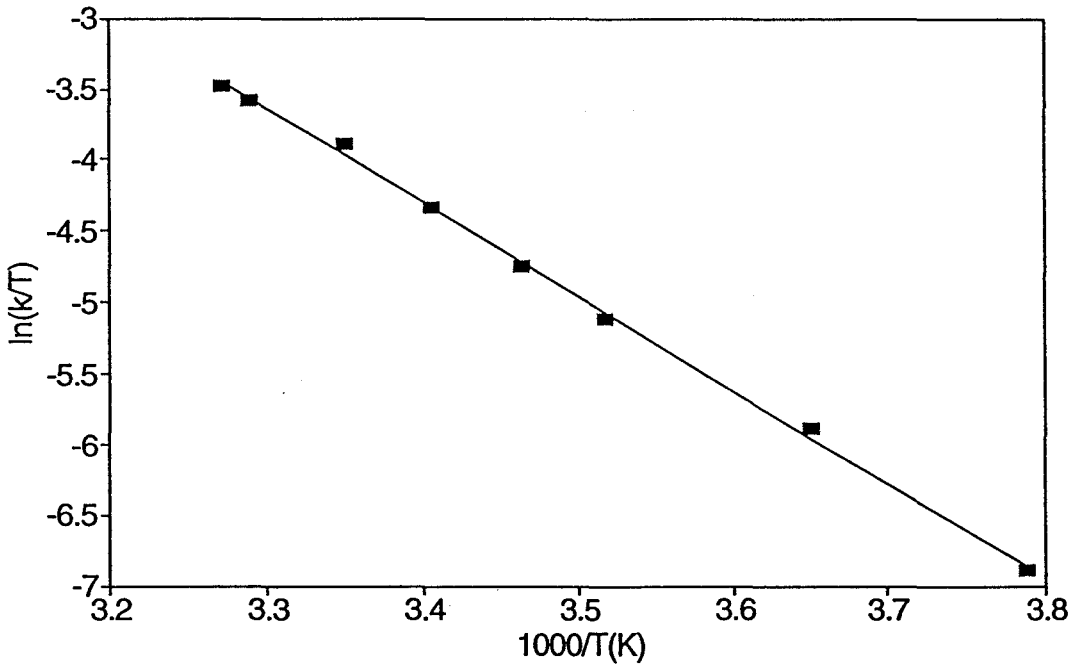

Figure 4.6 Eyring plot of ln(*k*/*T*) vs. 1000/*T* for the compound (η^1-cpp)-$Mn(CO)_3(PEt_3)_2$, **4.4**, in CD_2Cl_2. All of the rate constants were derived from ^1H selective inversion recovery experiments, performed at 300.13 MHz.

(figure 4.6).

According to the 1D NMR magnetization transfer experiments, there is hindered rotation about the Mn - C(4) bond in $(\eta^1\text{-Cpp})Mn(CO)_3(PEt_3)_2$, with $\Delta H^{\ddagger}$ of 13.1 ± 0.2 kcal/mol. $\Delta S^{\ddagger}$ was determined to be -11.2 ± 0.7 eu.

At all temperatures, the ^1H signal arising from H(4) remained a doublet of doublets. Therefore, coupling to the phosphorus atoms was retained, and exchange between bound triethylphosphine and free phosphine can be ruled out.

The molecular mechanics calculations undertaken are in good agreement with the experimentally determined barrier, resulting in a barrier of about 18 kcal/mol for the same rotation.[33] More interestingly, these calculations tell us why there is such a high barrier. The methylene protons of the triethylphosphine groups come into close contact with the protons at positions 3 and 5 on the ligand, during rotation about the Mn-C(4) bond.

Although the high barrier to rotation about the single bond seemed surprising at first, high rotational barriers have been observed for the 9-fluorenyl derivatives listed in table 4.1, and have been attributed to restricted rotation about the C(9)-aryl bond.

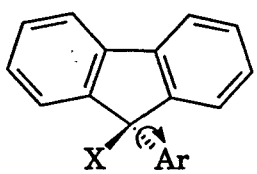

Table 4.1 Rotational Barriers in 9-Fluorenyl Derivatives

X	Ar	$\Delta G^{\ddagger}$ (kcal/mol)
H	2,4,6-trimethylphenyl	>25[38]
OH	2,4,6-trimethylphenyl	20.2[38]
Cl	2,4,6-trimethylphenyl	16.2[38]
H	2,6-dimethoxyphenyl	20.6[38]
OH	2,6-dimethoxyphenyl	14.4[38]
Cl	2,6-dimethoxyphenyl	9.2[38]
OH	2,6-dimethylphenyl	21.6[39]
H	2-methylphenyl	16.4[40]
H	2,6-dimethylphenyl	>26[40]
H	3-methylphenyl	>9[40]
2-methylphenyl	4-amino-2,5-dimethylphenyl	13[41]
2-methylphenyl	4-amino-2-isopropyl-5-methylphenyl	>20[41]
1-naphthyl	4-amino-2-isopropyl-5-methylphenyl	>20[41]

The steric demands of the fluorene ligand should be similar to those of the cppH ligand. In fact, the analogous fluorenyl compound, $(\eta^1\text{-}C_{13}H_9)$-$Mn(CO)_3(PEt_3)_2$, has been prepared by Biagioni and coworkers.[42] They did not obtain an x-ray crystal structure, but their NMR evidence points to the trans-meridional isomer, as in the cpp complex. The NMR spectra showed two phosphine environments, and Biagioni noted that they could be accounted for by either the cis-meridional isomer, or the trans-meridional isomer. He concluded that he had the trans-meridional isomer on the basis of the equivalent $^2J_{PC}$ couplings. If the complex were cis-meridional, the $^2J_{PC}$ couplings would likely be different. Biagioni also realized that VT NMR would distinguish between the two scenarios, as the phosphine signals for the trans-meridional isomer would coalesce at elevated temperatures, while the phosphine signals for the cis-

meridional isomer would not. His compound, like the cpp complex, decomposed above room temperature, so he was not able to perform any VT NMR experiments. It should be possible to measure the barrier to rotation about the Mn-C(9) bond in Biagioni's molecule through magnetization transfer methods, as was done with the analogous cpp complex, and it would be interesting to compare the two barriers.

In conclusion, there is hindered rotation about the Mn - C(4) sigma bond in $(\eta^1\text{-Cpp})Mn(CO)_3(PEt_3)_2$, with $\Delta H^{\ddagger}$ of 13.1 ± 0.2 kcal/mol. $\Delta S^{\ddagger}$ was determined to be -11.2 ± 0.7 eu.

4.3 Experimental Section

Selective Inversion Experiments

The selective inversion experiments were performed on a Bruker AC-300 spectrometer, with a 7.65 T superconducting magnet, equipped with a Bruker B-VT 2000 temperature controller, and a 5 mm QNP probe. Protons were observed at 300.13 MHz.

All spectra were recorded spinning, locked on the signal of the solvent CD_2Cl_2. Chemical shifts were referenced to the residual proton signal of the solvent at 5.32 ppm, regardless of temperature. Each temperature was measured by placing a copper-constantan thermocouple, contained in an NMR tube, into the probe. Typically, forty minutes to one hour were allowed for the temperature to equilibrate.

All FID's were transferred to an IBM PC using the program NMRLINK.

The spectra were Fourier transformed under the same conditions, with absolute intensity set to one, using the program NMR286

Selective inversion recovery experiments were performed using the program INVREC2P.AU, which makes use of the pulse sequence described in chapter two. Experiments were performed over the temperature range -9.2 to 32.5 °C. The 90^{o} pulse width varied with temperature. At 5.2 °C, it was 7.8 µsec. Each spectrum was acquired over a SW of 4807.692 Hz, with O1 set at 4614.506 Hz, over 16K data points. Eight scans were collected for each spectrum, with an acquisition time of 1.7039 s, giving a resolution of 0.587 Hz/point.

For each temperature, an input file consisting of delay time and corresponding magnetization was prepared. The data were then fitted using the non-linear least squares fitting program FLOPSI, to obtain rate constants at each temperature.

Measurement of ^{1}H Spin-Lattice Relaxation Times

A ^{1}H non-selective inversion-recovery experiment was performed on the AC-300, in order to measure spin-lattice relaxation times (T_1's), at 5.2 °C. Spin-lattice relaxation times were needed as input for the fitting program FLOPSI.

The program INVREC2P.AUR was again used, with D2 set to a very small number. Each spectrum was acquired over a SW of 3496.50 Hz, with O1 set at 5215.0 Hz, over 16 K data points. Eight scans were collected for each spectrum, with an acquisition time of 2.342 s, giving a resolution of 0.427 Hz/data point. The 90^{o} pulse width was 7.8 µsec.

The spectra were Fourier transformed under the same conditions, with

absolute intensity set to one, using the program NMR286. An input data file consisting of variable delay times and corresponding magnetizations (as measured from transformed spectra) for each methyl and methylene peak was created. This data was then fitted with the non-linear least squares fitting program T1cals to calculate T_1's for each aliphatic ^1H site. Methyl T_1's were determined to be 0.22 s, while methylene T_1's were 0.16 s.

CHAPTER FIVE

The Molecular Dynamics of

N,N'-[dimethyl-(2,2'-dithiobisacetyl)]ethylenediamine

5.1 Introduction

The compound *N,N'*-[dimethyl-(2,2'-dithiobisacetyl)]ethylenediamine, **5.1**, hereafter abbreviated to DADS, was prepared by Bell and Maharajh.[10] The compound was found to have a very complex NMR spectrum, arising from several chemically exchanging conformations.

DADS was prepared as a conformational model for 10-membered diamide disulfide cyclic ligands. These asymmetric medium-sized, heterocycles were prepared as precursors to complexing reagents for technetium, to be used in ^{99m}Tc radioimaging. Bell and Maharajh noted that the NMR spectra of these compounds were very complex.[10] Thus they prepared the symmetric title compound, DADS, hoping that it would help in the conformational analysis of the asymmetric ligands.

The approximate DNMR methods used by Maharajh warranted a re-examination of this interesting molecule, and the complexity of this slowly exchanging system was expected to provide a challenging test for the single selective inversion recovery method.[6,7]

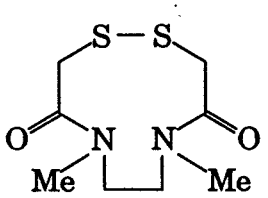

5.1

5.2 Summary of Maharajh's DNMR Results and Conformational Analysis

As mentioned, DADS was expected to give a much simpler NMR spectrum than the related asymmetric ligands, however, the ^{1}H (figure 5.1) and ^{13}C (figure 5.2) NMR spectra show that it is also a very complex system.

Maharajh attributed the complexity to the presence of different ring conformers. In principle, the cyclic disulfide could adopt three conformations with respect to the amide functional groups. Both amide groups could be *Z* (*ZZ*), both amide groups could be *E* (*EE*), or one amide could be *Z* and the other *E* (*ZE*).

To verify that the system was chemically exchanging, Maharajh obtained ^{1}H NMR spectra up to 127.4 °C, and noted that the signals broadened. He estimated the coalescence temperature to be 127 °C, and estimated $\Delta G^{\ddagger}$ to be 19.3 kcal/mol. This barrier was attributed to restricted amide rotation.

Based on the variable temperature NMR and 2D experiments, Maharajh concluded that there were three ring conformers in solution. Two were symmetrical, each giving rise to one NCH_3 signal, one NCH_2 signal, and one SCH_2 signal in the ^{13}C NMR spectrum. The other conformer was asymmetric, giving rise to two NCH_3, NCH_2, and SCH_2 signals in the ^{13}C spectrum. NOE difference experiments were performed on the asymmetric and the more populated of the two symmetric isomers. He concluded that the symmetric isomer contained two *Z* amide groups, and named it *ZZ1*. The asymmetric conformer contained one *Z* and one *E* amide group, and thus was named *ZE*. Aromatic solvent induced shift experiments were then performed in order to determine the amide stereochemistry of the minor symmetric isomer. Both

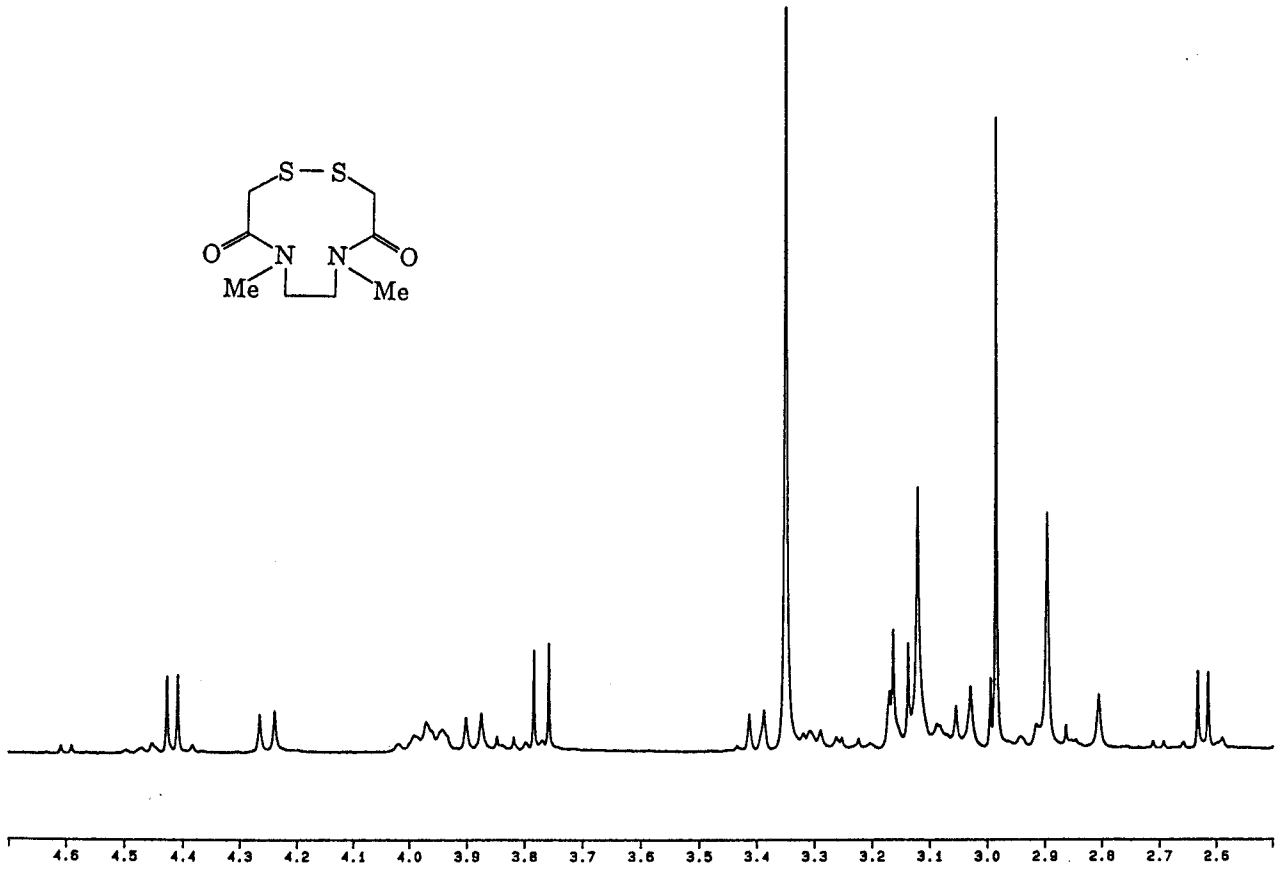

Figure 5.1 500.13 MHz ^{1}H NMR spectrum of DADS, **5.1**, at 303 K, in dimethylsulfoxide-d_6.

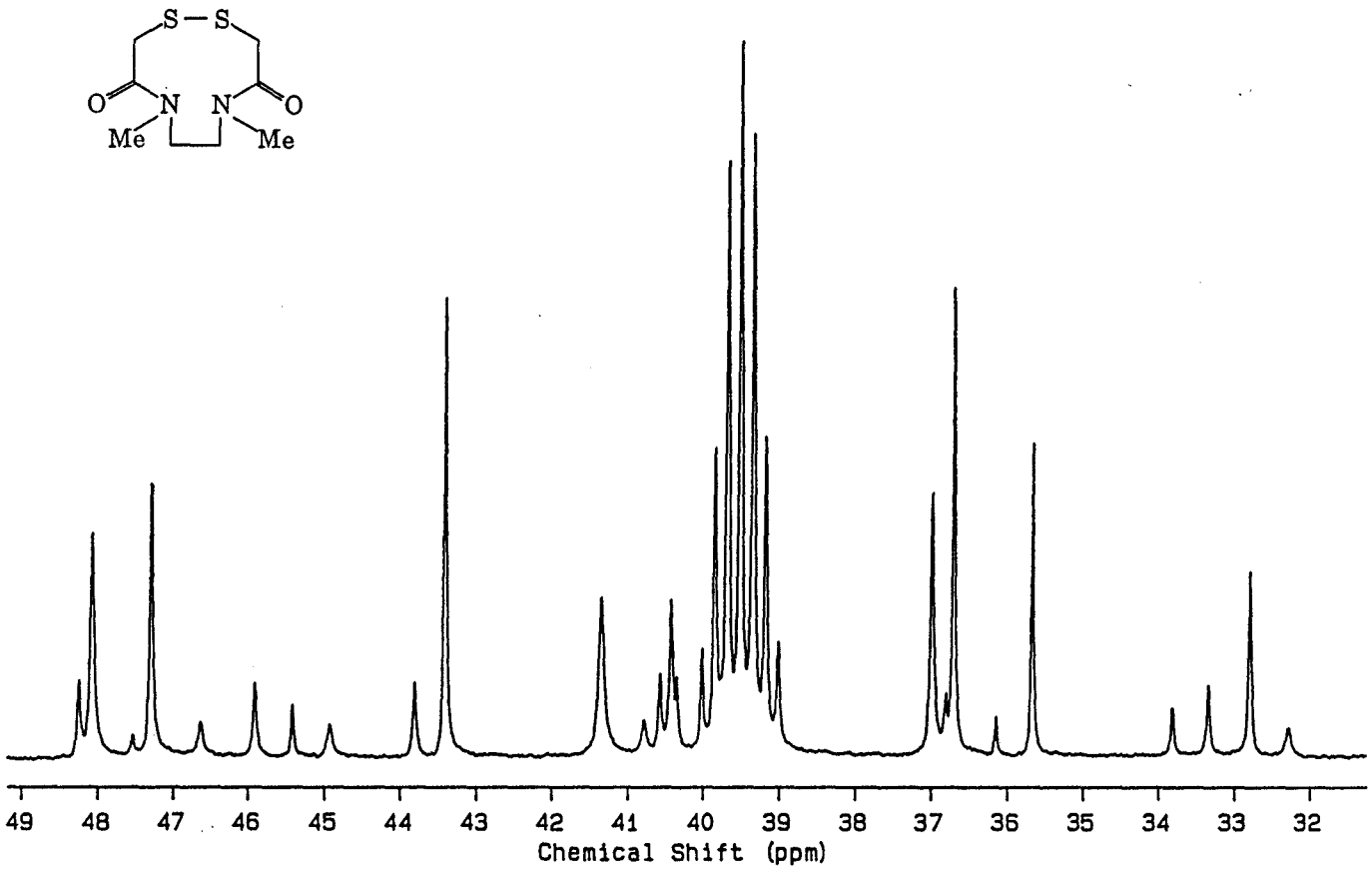

Figure 5.2 125.76 MHz ^{13}C NMR spectrum of DADS, **5.1**, at 303 K, in dimethylsulfoxide-d_6.

amide groups were *Z*, and it was called *ZZ2*.

Maharajh grew crystals and obtained an x-ray structure of DADS. It had crystallized in the *ZE* geometry, as shown in figure 5.3. He noted that the disulfide and amide torsional angles were close to the ground state values of 90 ° for the disulfide group and 0 and 180 ° for the amide groups.

After performing some PC-MODEL calculations, Maharajh suggested that the *ZZ1* and *ZZ2* conformations arose via restricted rotation about the disulfide bond. He then went on to perform variable temperature ^{13}C NMR experiments. Lineshape analysis led to a $\Delta G^{\ddagger} = 14.5 \pm 1.3$ kcal/mol for the barrier to rotation about the disulfide bond.

As an aid to understanding the behavior of the DADS ligand, the barrier to rotation about the amide bond in the uncyclized precursor to DADS, *N,N'*-[dimethylbis[2-(triphenylmethyl)thioethanoyl]]ethylenediamine, **5.2**, was determined. The barrier was estimated to be $\Delta G^{\ddagger} = 15.1$ kcal/mol, by Maharajh, using the coalescence method.

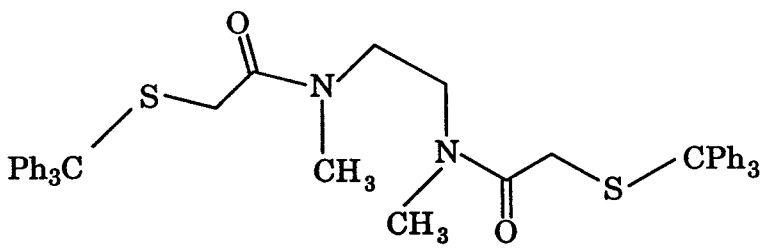

5.2

As mentioned above, the preliminary results obtained by Maharajh warranted further study of the complex DADS system, as well as the uncyclized precursor to DADS, **5.2**. The DADS used in this work was obtained from Bell and Maharajh, and the uncyclized precursor used for this work was obtained

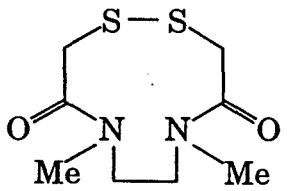

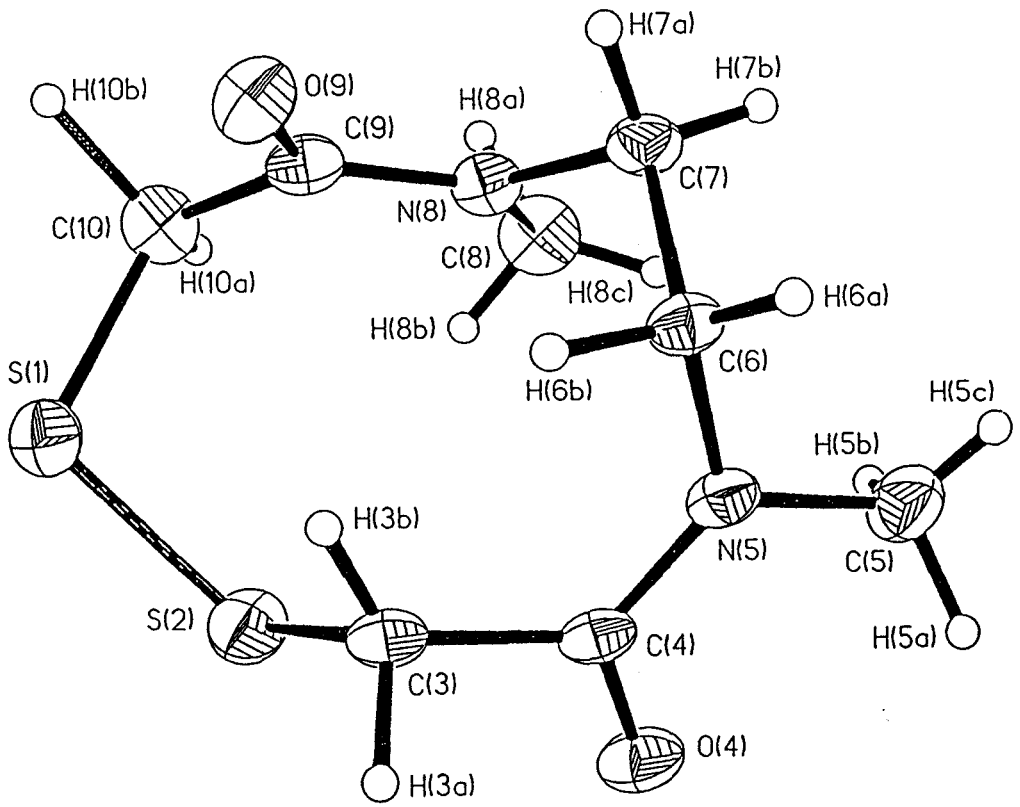

Figure 5.3 X-ray crystal structure of DADS, **5.1**. The figure is reproduced from reference 10.

from Bell and Valliant.

The following results and discussion section will describe the assignment of the ^{1}H and ^{13}C NMR spectra for compounds **5.1** and **5.2**. The exchange mechanisms as determined by 2D NOESY spectra, for each molecule, will be given. Finally, the determination of rate constants and thermodynamic parameters for both molecules will be discussed. Rate constants were determined using a combination of single selective inversion recovery experiments in the slow exchange regime and lineshape analysis in the intermediate regime.

5.3 Results and Discussion

5.3.1 *N,N'*-{dimethylbis[2-(triphenylmethyl)thioethanoyl]}-ethylenediamine

Using a combination of DEPT, ^{1}H - ^{13}C shift correlated (figures 5.4 - 5.6), and 2D ^{1}H NOESY (figure 5.7) experiments, the ^{13}C and ^{1}H chemical shifts for the molecule *N,N'*-{dimethylbis[2-(triphenylmethyl)thioethanoyl]}ethylenediamine, were assigned. The chemical shifts are listed in table 5.1. It was determined that there are two symmetric conformations, one ZZ, the other *EE*, and one asymmetric conformation, *ZE*, in a solution of dmf-d_7. This solvent was used because the compound was not very soluble in dmso-d_6. It should be noted that there were some impurities present in the sample, but since they were not chemically exchanging with the compound of interest, they were ignored in this work.

From the 2D ^{1}H NOESY spectrum at 42.2 °C, the exchange pathways were determined. At 42.2 °C, the *ZE* conformer was exchanging with both the

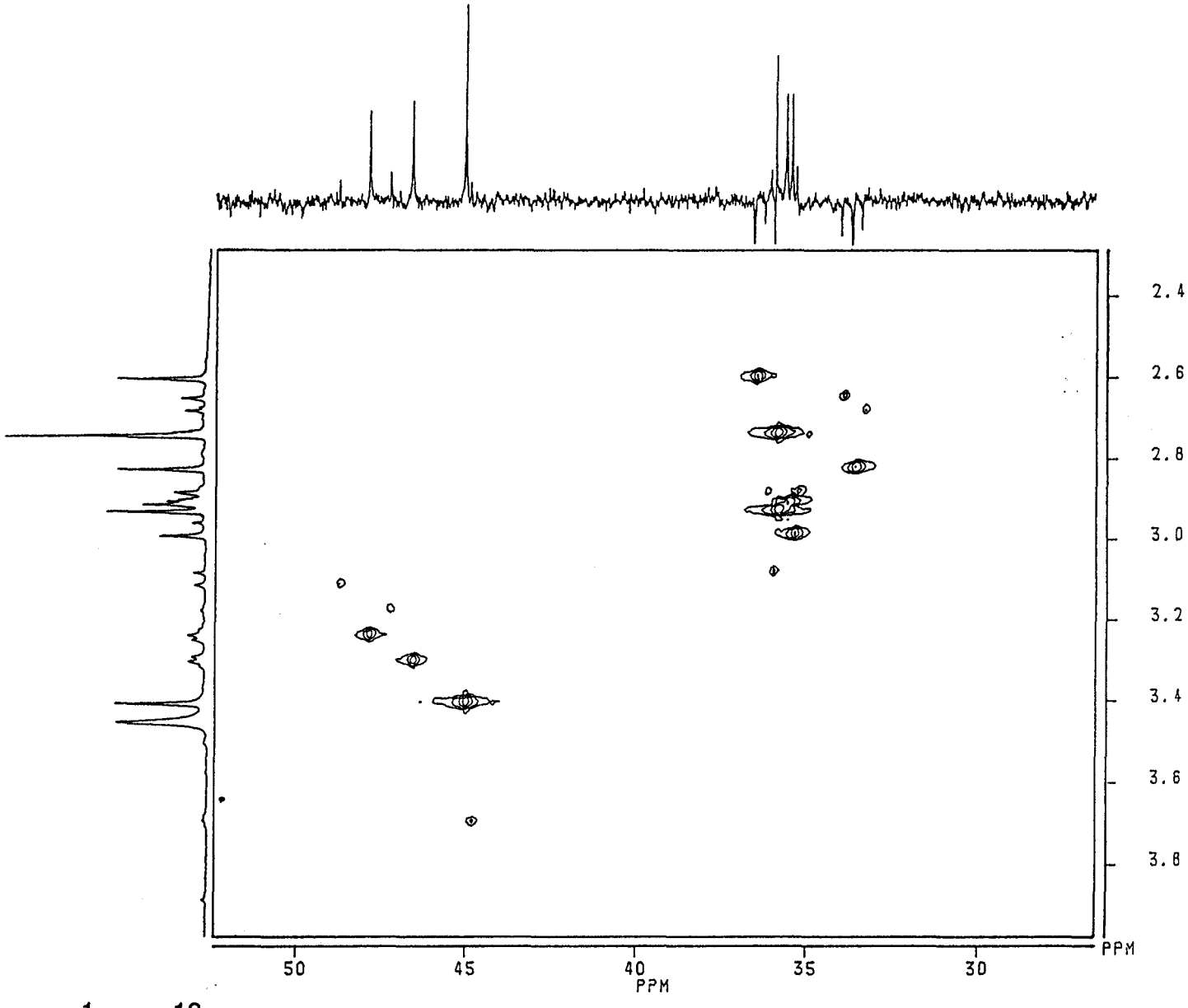

Figure 5.4 ^{1}H - ^{13}C shift correlated spectrum of *N,N'*-{dimethylbis[2-(triphenylmethyl)thioethanoyl]}-ethylenediamine, **5.2**, in *N,N*-dimethylformamide-*d7*.

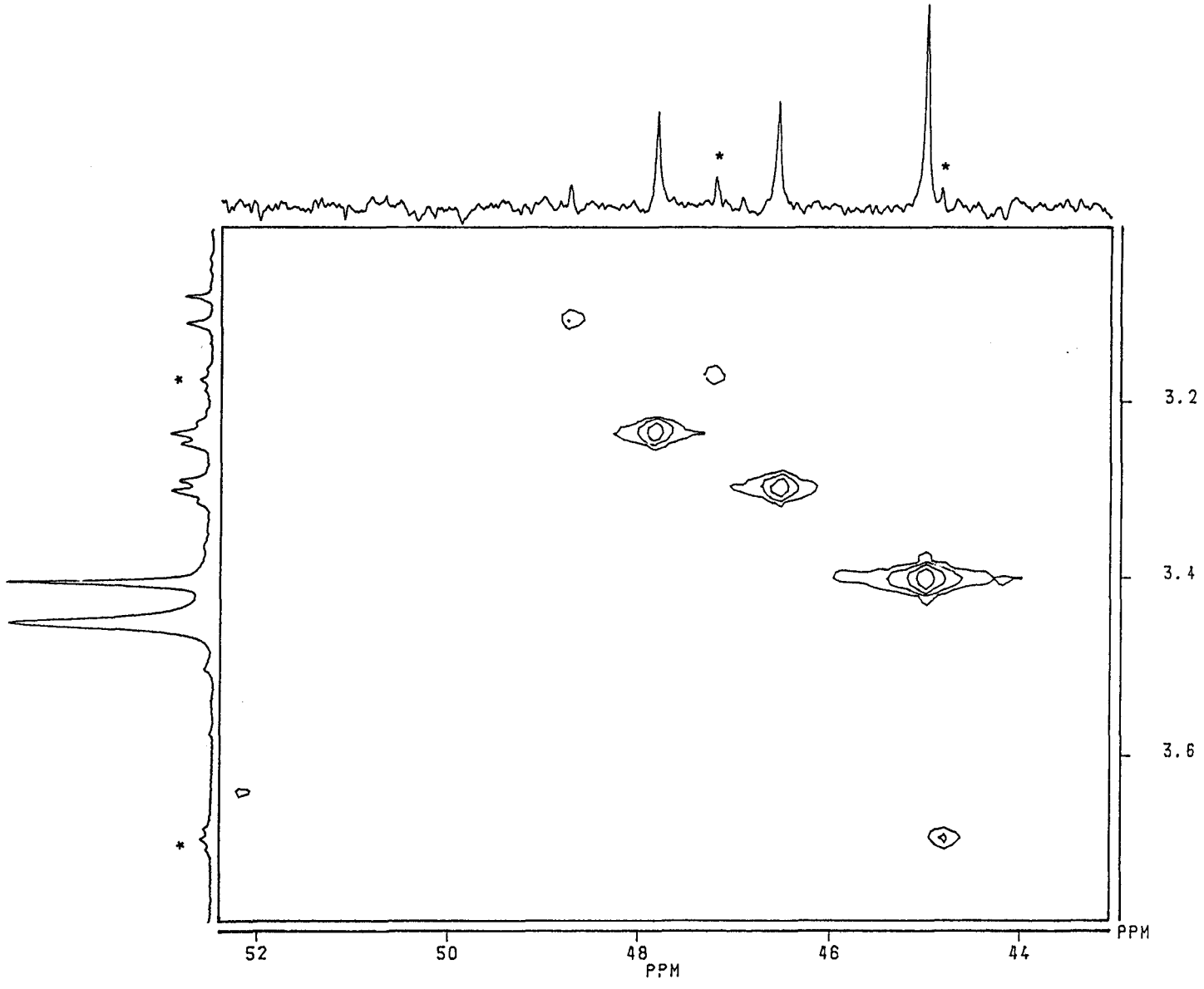

Figure 5.5 N-methylene region of the ^{1}H - ^{13}C shift correlated spectrum of *N,N'*-{dimethylbis[2-(triphenylmethyl)-thioethanoyl]}ethylenediamine, **5.2**, in *N,N*-dimethylformamide-d_7.

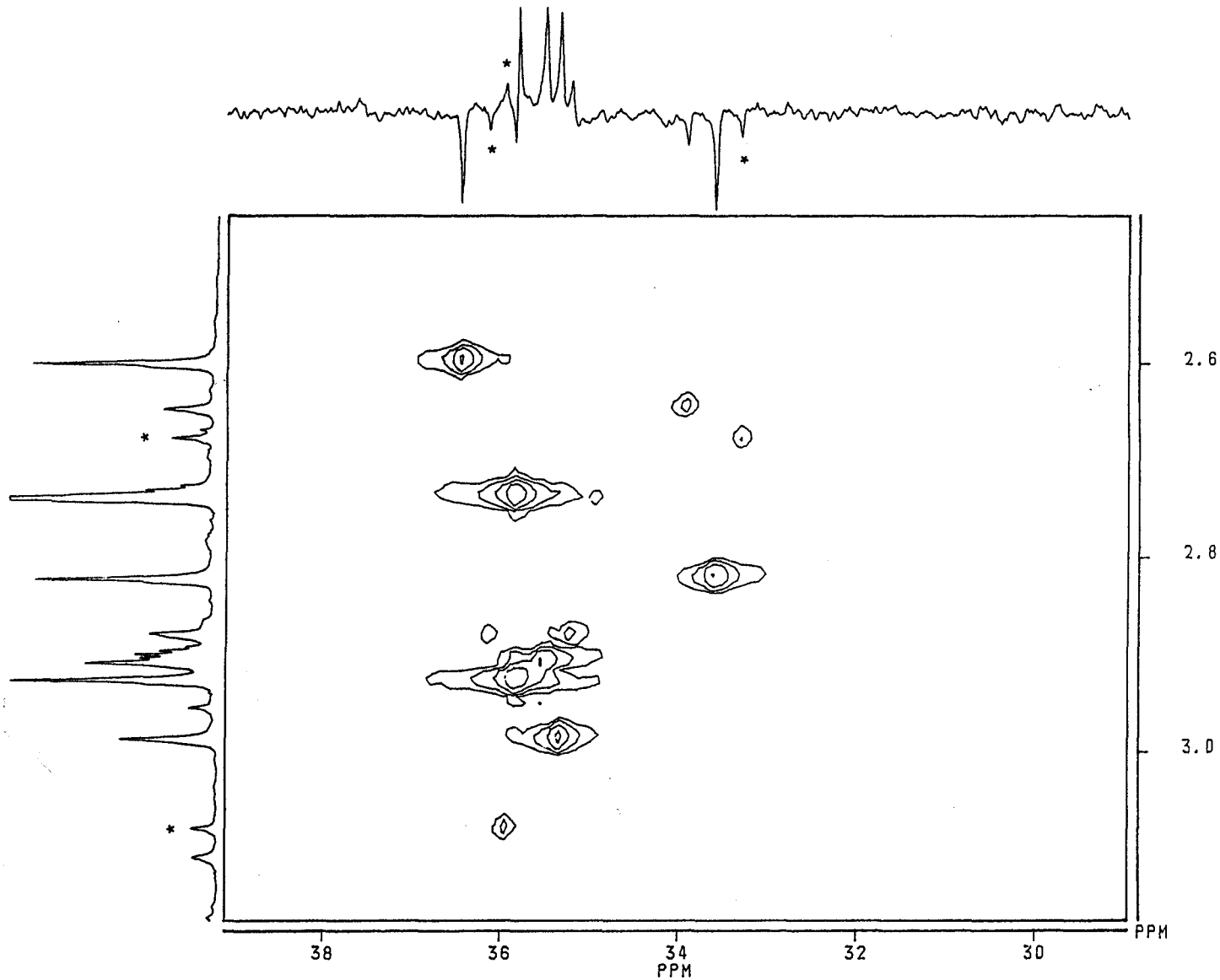

Figure 5.6 S-methylene and methyl region of the ^{1}H - ^{13}C shift correlated spectrum of *N,N'*-{dimethylbis-[2-(triphenylmethyl)thioethanoyl]}ethylenediamine, **5.2**, in *N,N*-dimethylformamide-d_7.

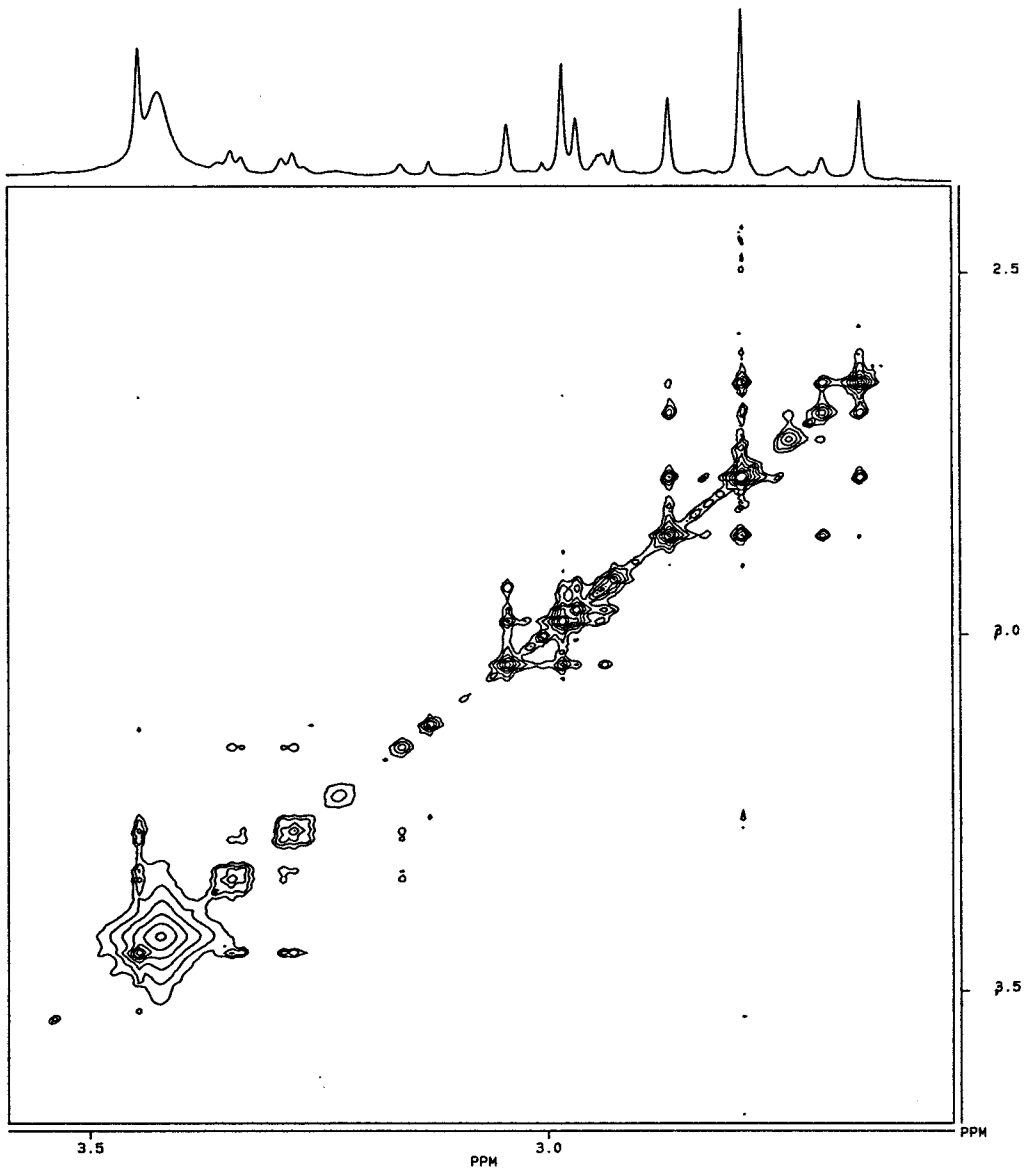

Figure 5.7 500.13 MHz ^{1}H NOESY spectrum of *N,N'*-{dimethylbis[2-(triphenylmethyl)thioethanoyl]}ethylenediamine, **5.2**, in *N,N*-dimethylformamide-d_7.

ZZ conformer, and the *EE* conformer, as expected for rotation about an amide C-N partial double bond. This process is represented in figure 5.8.

Table 5.1 ^{1}H and ^{13}C Chemical Shifts for *N,N'*-{dimethylbis[2-(triphenylmethyl)thioethanoyl]}ethylenediamine

Resonance	^{13}C chemical shift (ppm)	^{1}H chemical shift (ppm)
N-methylene		
ZZ	44.97	3.401
ZE	47.80	3.233
ZE	46.53	3.299
EE	48.70	3.107
S-methylene		
ZZ	35.80	2.923
ZE	35.49	2.906
ZE	35.33	2.983
EE	35.20	2.876
N-methyl		
ZZ	33.82	2.733
ZE	36.42	2.594
ZE	33.57	2.818
EE	33.89	2.643

Kinetic Data

Since the methyl proton resonances for the three conformations were well separated at temperatures below about 45 °C, single selective inversion recovery experiments were performed on these peaks at 29.6, 41.6 and 42.2 °C.

T_1's for the methyl protons were determined at 42.2 °C. They are listed in table 5.2.

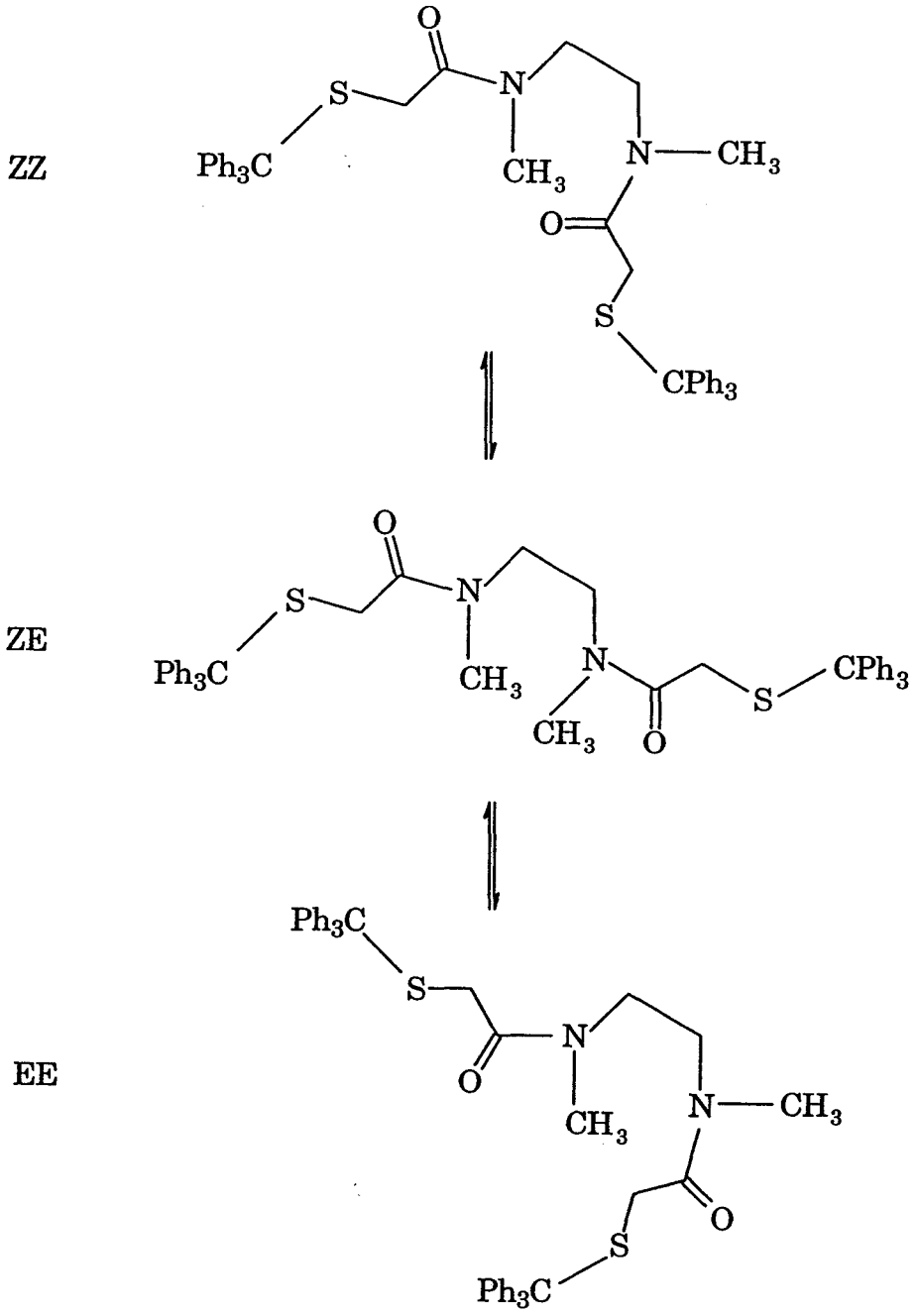

Figure 5.8 Possible rotamers of *N,N'*-{dimethylbis[2-(triphenyl-methyl)thio-ethanoyl]}ethylenediamine, **5.2**, arising from restricted rotation about the two amide bonds.

Table 5.2 T_1's for the Methyl Protons of *N,N'*-{dimethylbis[2-(triphenylmethyl) thioethanoyl]}ethylenediamine

^1H Resonance	T_1 (s)
ZZNMe	.95
ZENMe	.89
ZENMe	.93
EENMe	.95

There was some overlap between the $ZZNCH_3$ peak and one of the dmf solvent peaks in the ^1H spectrum, so a ^{13}C selective and a non-selective inversion experiment were performed on the NCH_2 peaks at 42.2 °C, as there was no overlap in that region. The ^{13}C NCH_2 T_1's are listed in table 5.3. The calculated rates for all of the ^1H and for the ^{13}C selective inversions at 42.2 °C were essentially the same. Therefore the overlapped dmf peak was ignored in the ^1H selective inversion work. There is a precedent for this. When McClung presented his multisite magnetization transfer experiment, he noted that there was significant overlap of a peak involved in the exchange process that he was studying, with a peak that was not exchanging. The data for that site was fit just as well as for the other exchanging sites, that were not overlapped. [23]

Table 5.3 T_1's for the N-methylene Carbons of *N,N'*-{dimethylbis[2-(triphenylmethyl)thioethanoyl]}ethylenediamine

^{13}C Resonance	T_1 (s)
$ZZNCH_2$	.33
$ZENCH_2$	.30
$ZENCH_2$	.32
$EENCH_2$	.25

^{13}C spectra were obtained at 53.0, 64.7, 72.6 and 82.9 °C, in the NCH_2 region, for lineshape analysis. ^{1}H spectra were recorded at the same temperatures, for future use in lineshape analysis.

The ^{13}C spectra were then compared to spectra calculated using Bain's program, to obtain temperature dependent rate constants. The experimental and calculated spectra are shown in figure 5.9.

The rate constants obtained from the selective inversion experiments and the lineshape analysis are listed in table 5.4.

Table 5.4 Rate Constants Derived From Selective Inversion Experiments and Lineshape Analysis for the Barrier to Rotation about the Amide Bond in *N,N'*-{dimethylbis[2(triphenylmethyl)thioethanoyl]}ethylene-diamine.

Temperature (°C)	Rates from Selective Inversion Experiments	Rates from Lineshape Analysis
29.6	0.27 ± 0.03	
41.6	0.32 ± 0.08	
42.2	0.96 ± 0.04	
53.0		5
64.7		9
72.6		18
82.9		35

The Eyring plot calculated from this data is shown in figure 5.10. $\Delta H^{\ddagger}$ was determined to be 19.3 ± 0.7 kcal/mol, while $\Delta S^{\ddagger}$ was determined to be 2.5 ± 2.1 eu. From these values, $\Delta G^{\ddagger}$ at 25 °C is 18.5 ± 0.7 kcal/mol, which is considerably higher than the barrier obtained by Maharajh ($\Delta G^{\ddagger}$ = 15.1 kcal/mol).

To summarize, the ^{1}H and ^{13}C chemical shifts for **2** were assigned using

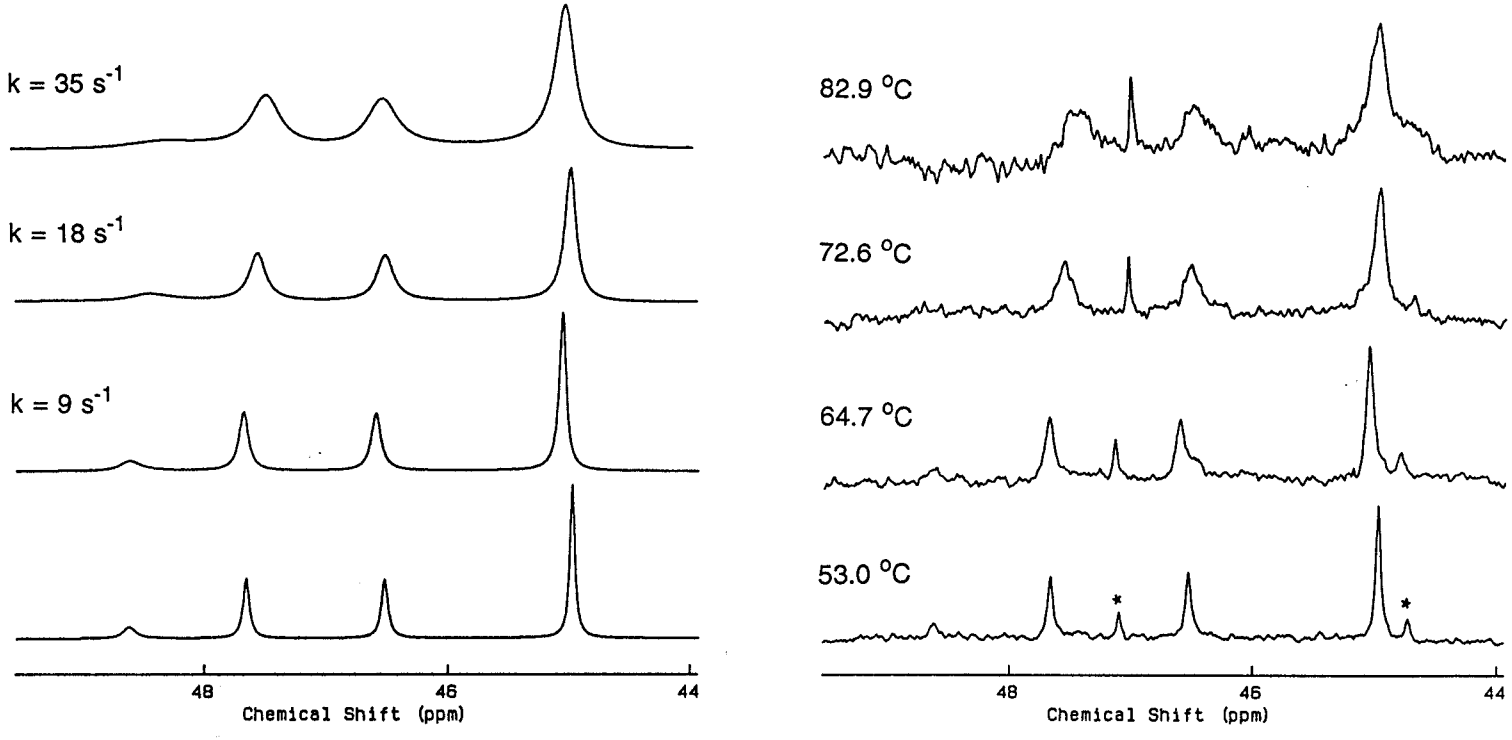

Figure 5.9 N-methylene region of the calculated spectra (left) and experimental 125.76 MHz ^{13}C NMR spectra (right) for *N,N'*-{dimethylbis[2-(triphenylmethyl)thioethanoyl]}ethylenediamine, **5.2**, in *N,N*-dimethylformamide-d_7.
* impurity

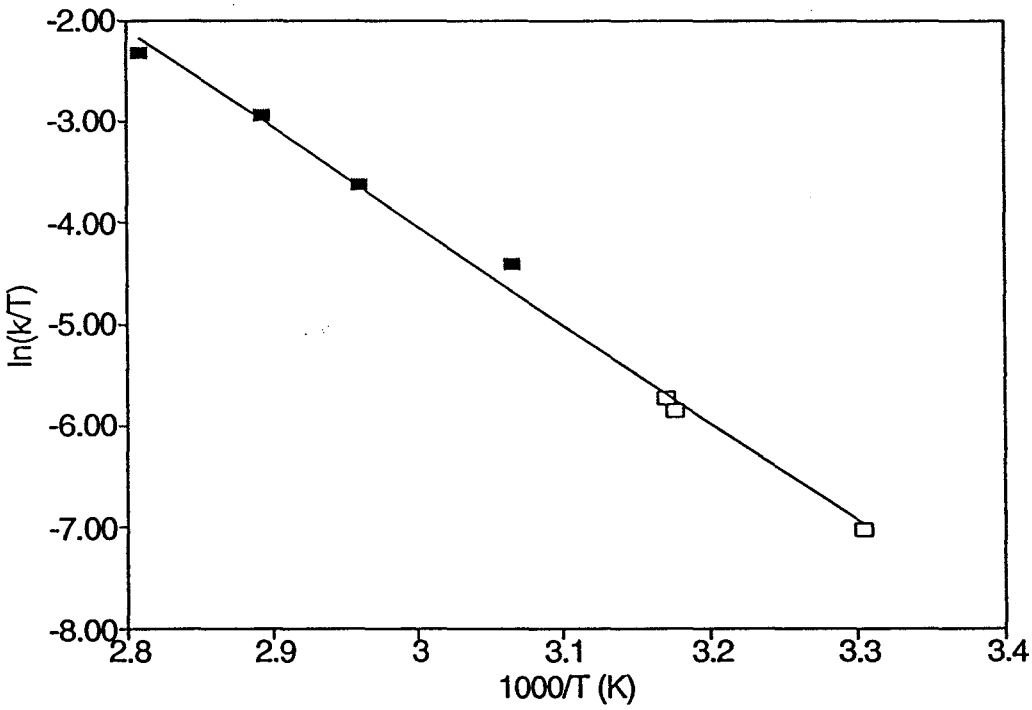

Figure 5.10 Eyring plot of ln(*k*/*T*) vs. 1000/*T* for the amide process in *N,N'*-{dimethylbis[2-(triphenylmethyl)thioethanoyl]}ethylenediamine, **5.2**. The filled squares represent rate constants derived from ^{13}C lineshape analysis, while the open squares represent rate constants derived from ^{13}C selective inversion experiments.

a DEPT and a ^{1}H - ^{13}C shift correlated experiment. A ^{1}H NOESY spectrum provided the exchange pathways for the system, as well as helping to confirm the chemical shift assignments. Spin-lattice relaxation times were determined using non-selective inversion recovery experiments. Rate constants for the hindered rotation about the amide bond were determined in the slow exchange regime using selective inversion recovery experiments, and in the intermediate regime using ^{13}C lineshape analysis. Thermodynamic parameters were then obtained from Eyring plots. This methodology was then applied to the DADS system, which is discussed below.

5.3.2 DADS

Further to the preliminary findings of Maharajh, DADS was found to exist as five conformations, two symmetric, and three asymmetric amide conformations in a solution of dmso-d_6. The ^{13}C and ^{1}H assignments were made through a combination of DEPT (figure 5.11), ^{1}H - ^{13}C shift correlated (figure 5.12), and 2D ^{13}C NOESY experiments.

In keeping with Maharajh's nomenclature the symmetric rotamers are referred to as *ZZ1* (the more populated site) and *ZZ2* (the less populated site). Similarly, the asymmetric rotamers are referred to as *ZE1* (most populated site), *ZE2* and *ZE3* (least populated site). Figure 5.13 shows the exchange pathways for the DADS system. The different conformations shown are taken from Maharajh's PC-MODEL calculations. They are the five lowest energy conformations that were obtained, but as yet no correlation can be made between these conformations and the actual rotamers of DADS in solution.

The ^{13}C chemical shifts and the ^{13}C T_1's for the five rotamers are listed

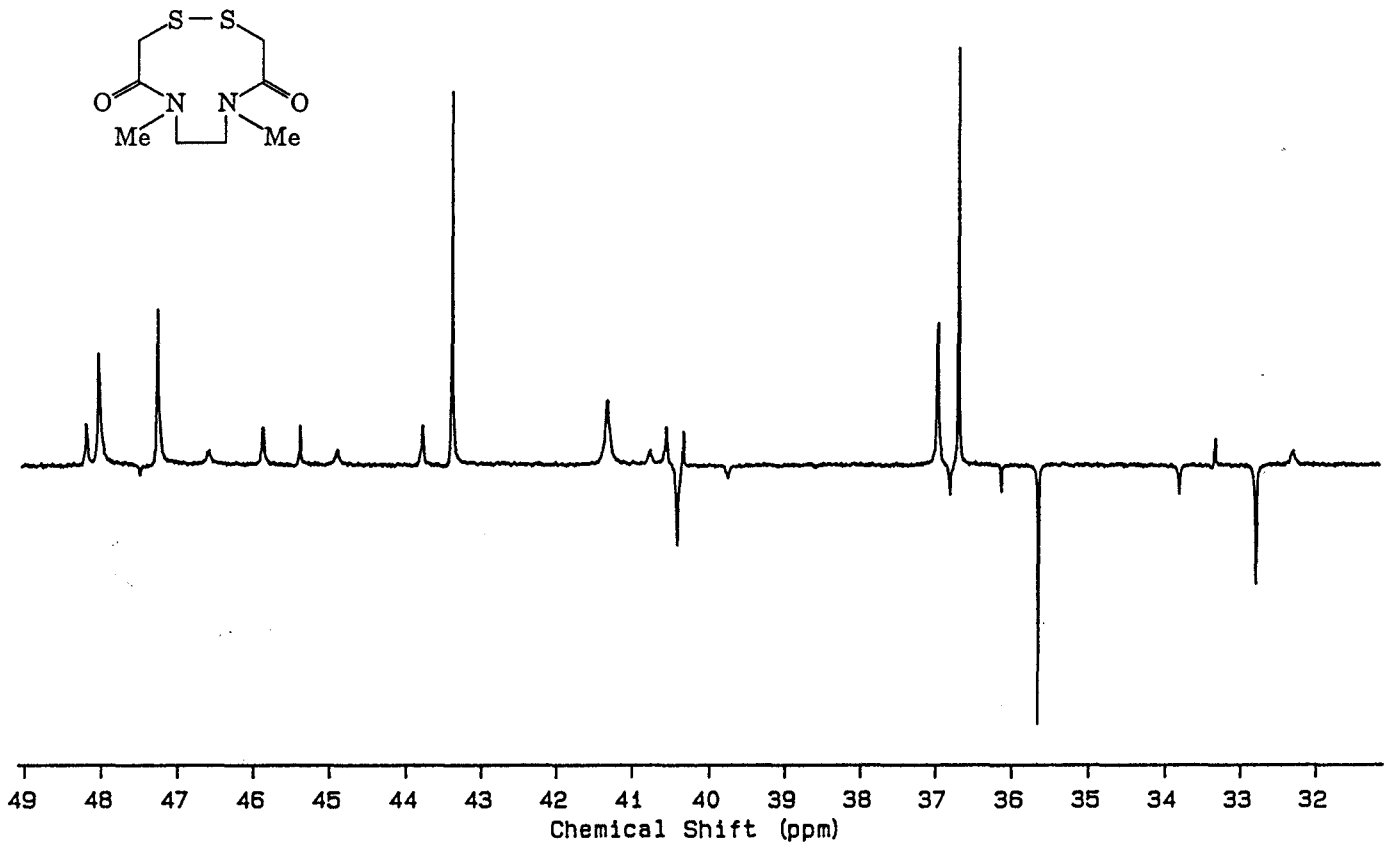

Figure 5.11 125.76 MHz ^{13}C DEPT spectrum of DADS, **5.1**, at 303 K, in dmso-d_6.

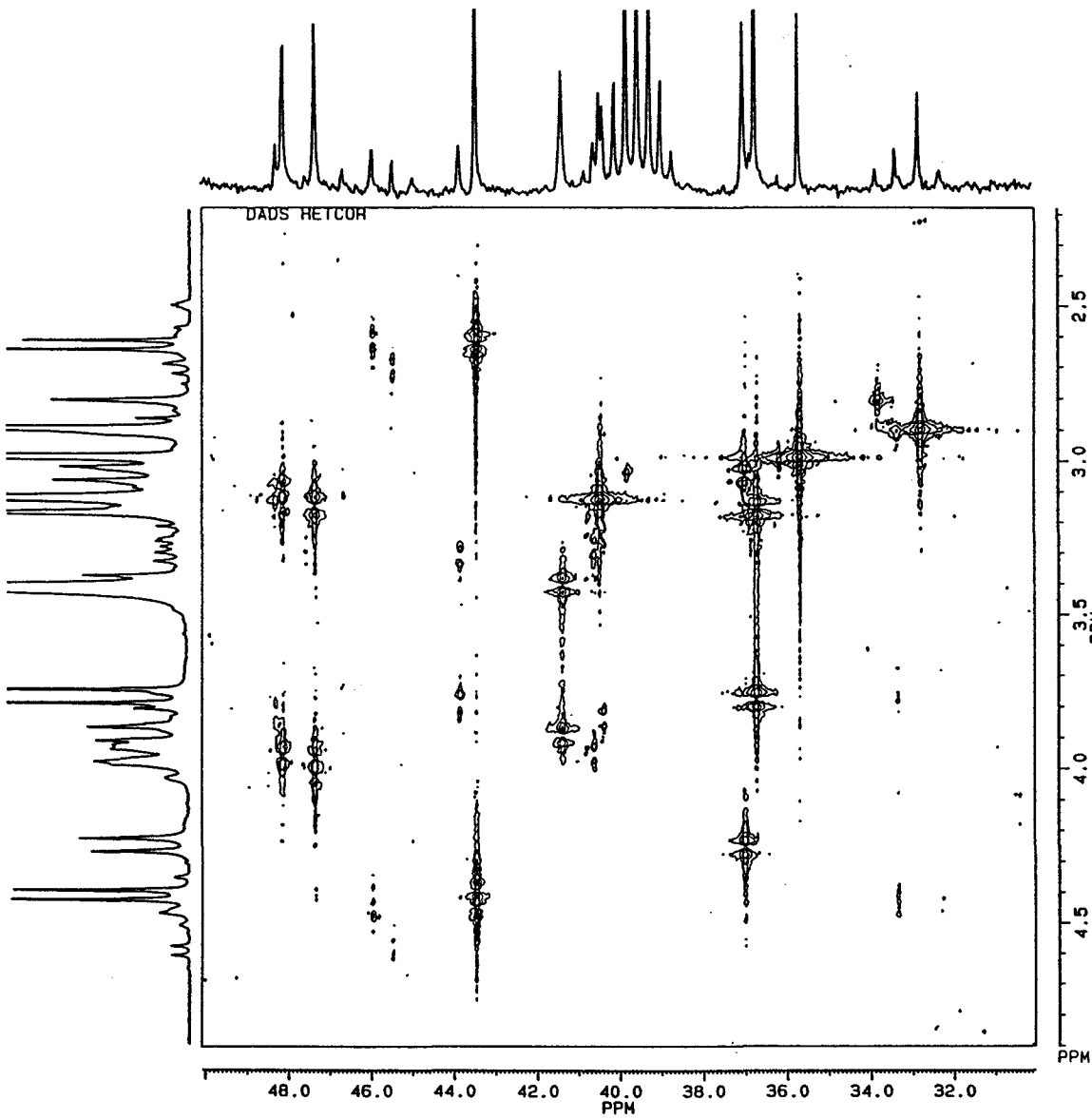

Figure 5.12 ^{1}H - ^{13}C shift correlated spectrum of DADS, **5.1**, at 300 K, in dmso-d_6.

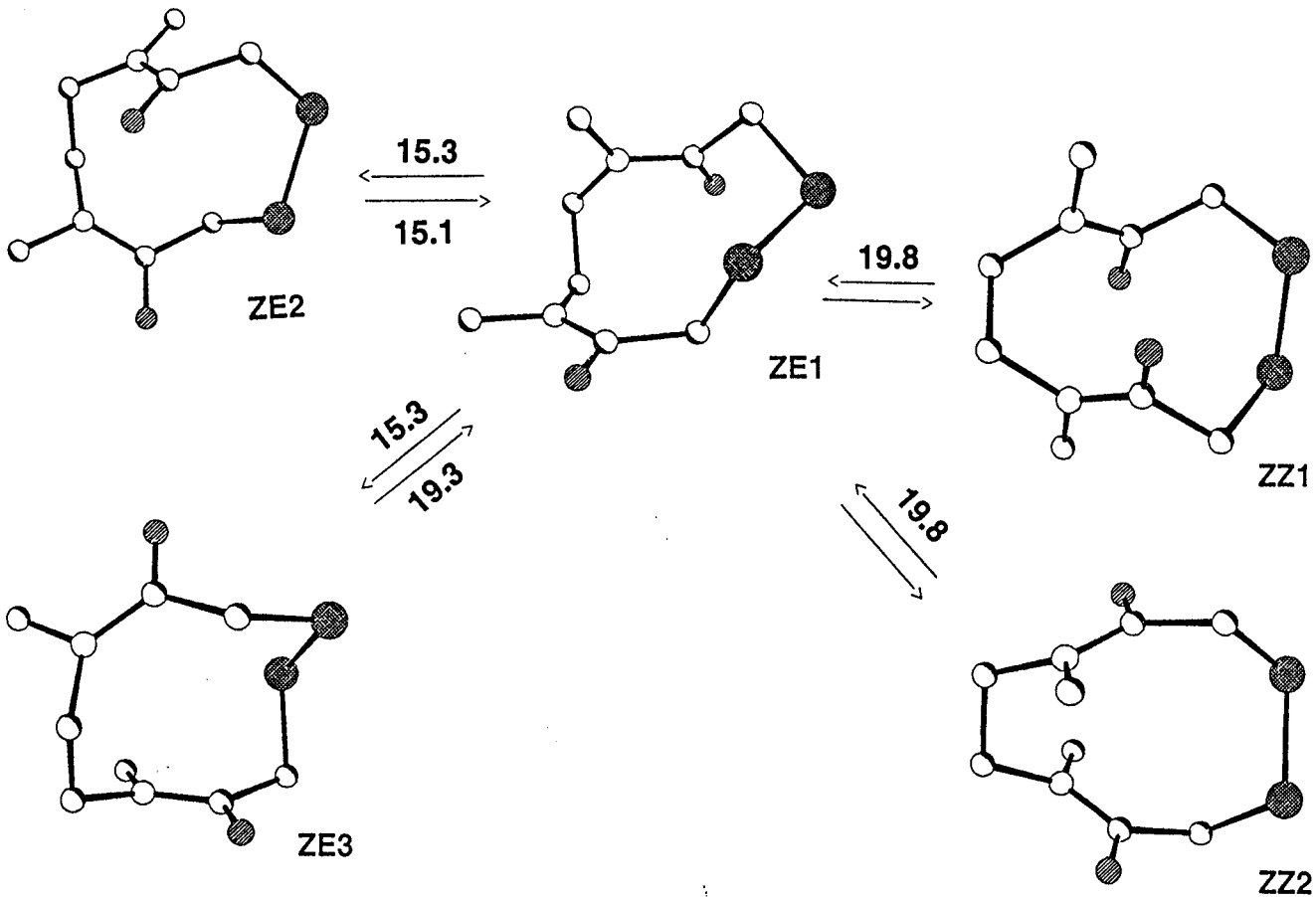

Figure 5.13 Exchange pathways for DADS, **5.1**.
Barriers are enthalpies of activation in kcal/mol

in table 5.5.

Table 5.5 ^{13}C Chemical Shifts and T_1's for DADS Rotamers

DADS Species	C-13 Chemical Shift (ppm)	T_1 (sec)
N-methylene		
ZE1	48.06	0.67
ZE1	47.28	0.64
ZE2	48.23	0.53
ZE2	45.89	0.51
ZE3	46.62	0.57
ZE3	44.90	0.40
ZZ1	43.40	0.78
ZZ2	45.40	0.63
S-methylene		
ZE1	41.33	0.63
ZE1	36.97	0.65
ZE2	40.55	0.67
ZE2	43.79	0.56
ZE3	40.76	0.37
ZE3	32.27	-
ZZ1	36.69	0.83
ZZ2	40.33	1.14
N-methyl		
ZE1	40.41	3.22
ZE1	32.77	3.42
ZE2	36.80	2.68
ZE2	33.79	3.43
ZE3	39.75	-
ZZ1	35.65	3.91
ZZ2	36.13	3.34

The exchange pathways were determined from the ^{13}C NOESY spectra, which are shown in figures 5.14, 5.15 and 5.16. At room temperature, *ZE1* is slowly exchanging with both *ZE2* and *ZE3*, but there is no apparent exchange

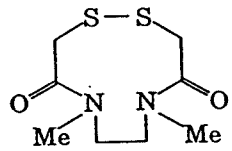

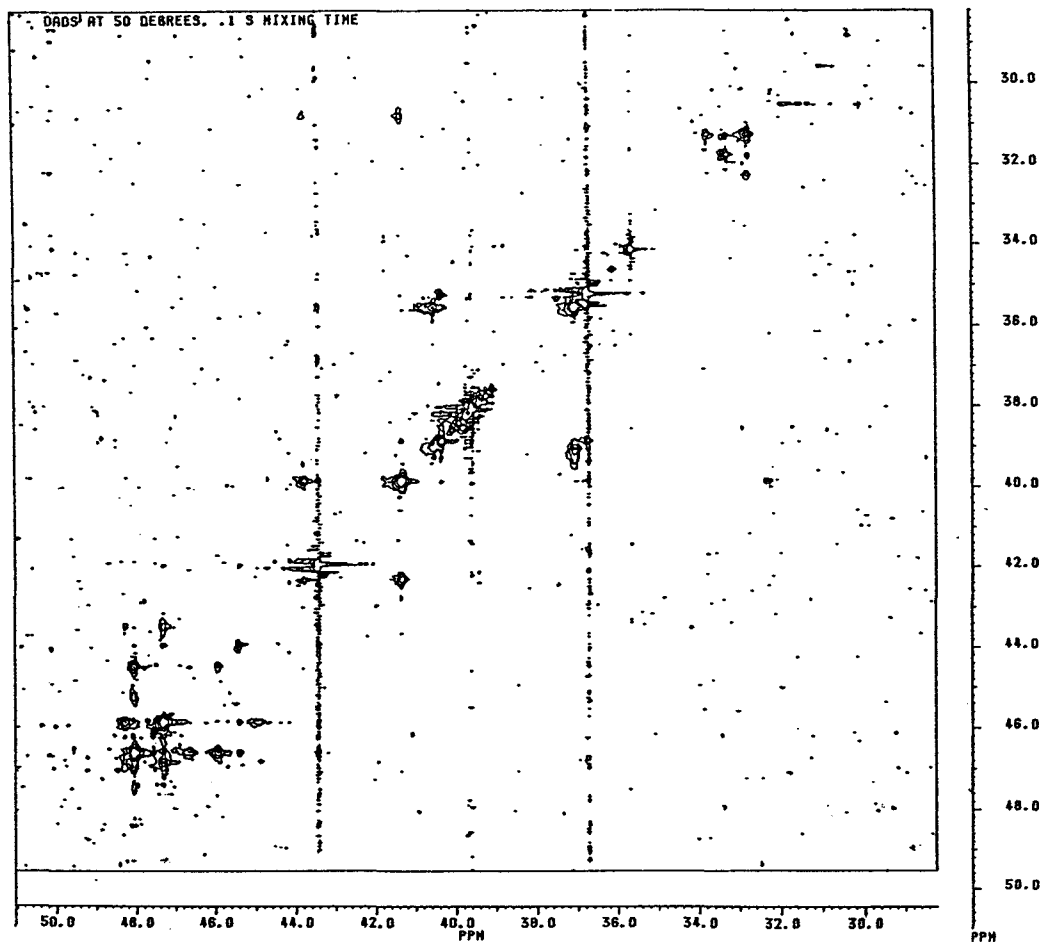

Figure 5.14 125.76 MHz ^{13}C NOESY spectrum of DADS, **5.1**, in dmso-d_6, at 323 K, in the aliphatic region. The mixing time was 0.1 s.

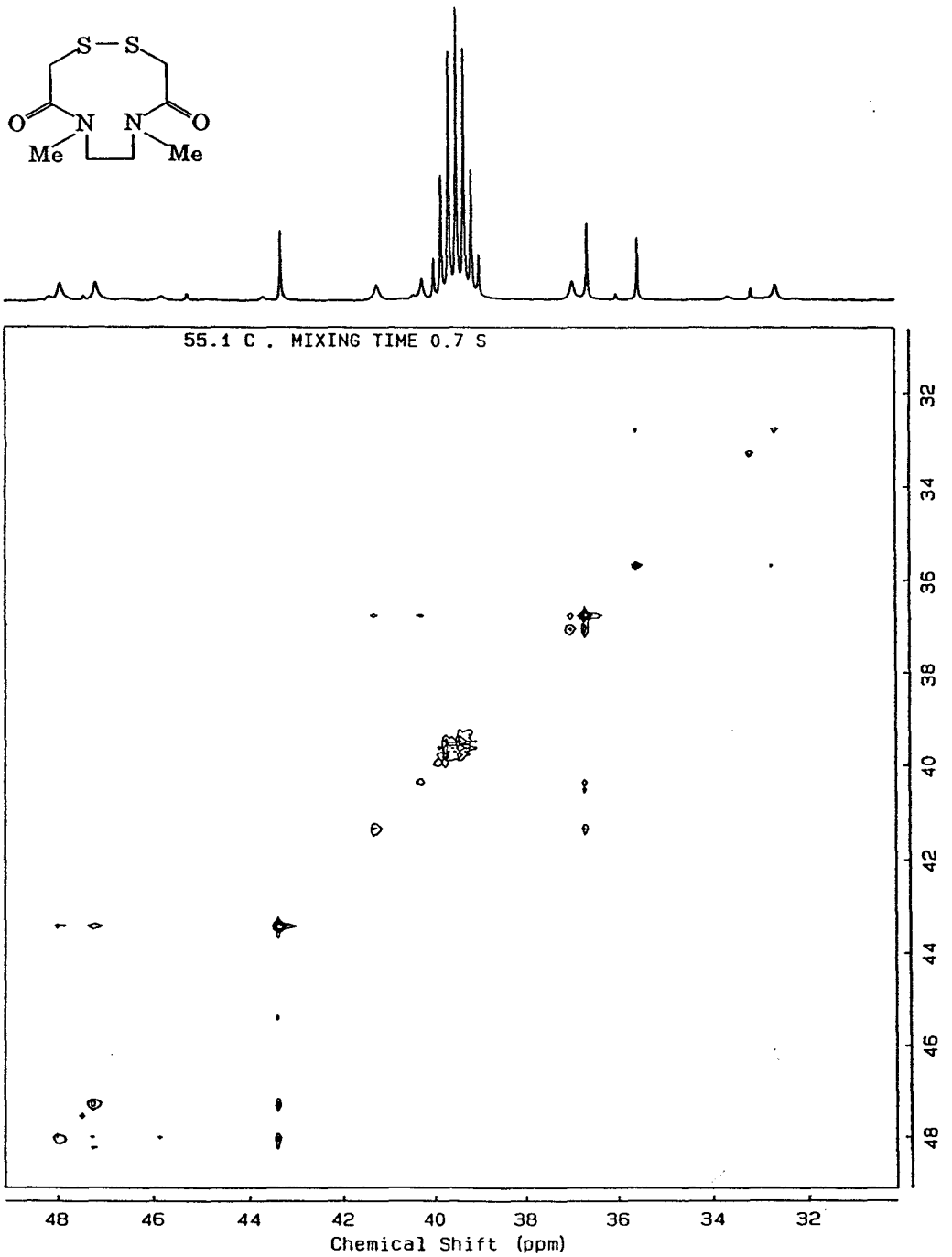

Figure 5.15 125.76 MHz ^{13}C NOESY spectrum of DADS, **5.1**, in dmso-d_6, at 328 K, in the aliphatic region. The mixing time was 0.7 s.

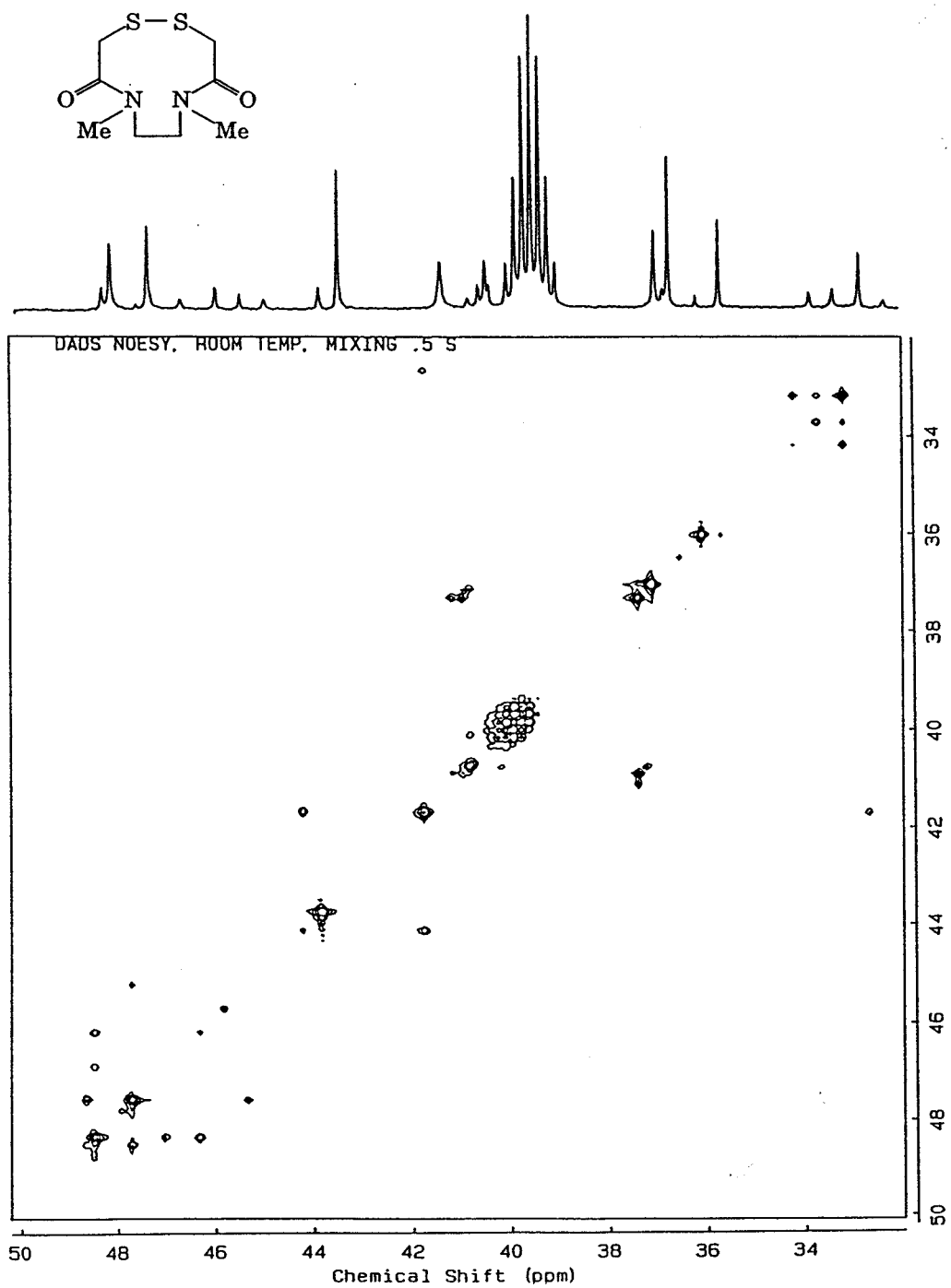

Figure 5.16 125.76 MHz ^{13}C NOESY spectrum of DADS, **5.1**, in dmso-d_6, at 303 K, in the aliphatic region. The mixing time was 0.5 s.

between *ZE2* and *ZE3*. At 50.1 °C, *ZZ2* is exchanging with *ZE1*, and at 55.1 °C, *ZZ1* is exchanging with *ZE1*. According to the NOESY spectra, there is no chemical exchange between the rotamers *ZZ1* and ZZ2, up to 55.1 °C, as put forth by Maharajh. The line broadening that he observed (and measured) in the ^{13}C NCH_2ZZ2 resonance was actually a result of the *ZZ2-ZE1* exchange.

It seems that the three *ZE* rotamers interconvert by rotation about the disulfide bond. Interconversion of the asymmetric rotamers (*ZE*'s) with the symmetric rotamers (*ZZ*'s) must occur via rotation about the amide C-N partial double bonds, at higher temperatures.

Kinetic Studies

Once the exchange pathways were known, kinetic studies were undertaken, in order to determine the barriers to rotation about the disulfide bond and the amide bonds. Normally, when cyclic systems are studied by DNMR, one barrier is obtained, for ring inversion.[5] In the DADS system, it was possible to obtain barriers for the two different processes, restricted rotation about the disulfide bond, and restricted rotation about the amide bonds, although both processes must contribute to both barriers.

A ^{13}C non-selective inversion recovery experiment was performed, in order to determine the ^{13}C spin-lattice relaxation times. The T_1's are listed in table 5.5, along with the chemical shifts for each site.

^{13}C single selective inversion recovery experiments were performed to determine temperature dependent rate constants for the *ZE1-ZE2,* and *ZE1-ZE3* processes.

A typical initial state spectrum and equilibrium ^{13}C spectrum are shown in

figure 5.17. Note that a *ZE1* and *ZE2* resonance are inverted, and the *ZE3* resonance is unperturbed. Consequently, this experiment would probe the *ZE1-ZE3* and *ZE2-ZE3* processes. Figure 5.18 shows a typical fit obtained by FLOPSI for the time dependence of an initially inverted and an initially unperturbed peak.

As well as giving rate constants for these processes, the selective inversion experiments confirmed that there was no measurable exchange between the *ZZ1 and* ZZ2 rotamers, or the *ZE2-ZE3* rotamers, up to 41.6 °C. Also, at 41.6 °C, the rate constant for the *ZZ2-ZE1* process was determined to be $0.19 \pm 0.08\ s^{-1}$. Although the error in this rate is large, it helps to determine an upper limit on the rate of exchange at 41.6 °C, and ties down the low temperature end of the Eyring plot for the amide process.

Table 5.6 lists the parameters for the single selective inversion experiments. Table 5.7 lists the values obtained for $k_{forward}$, while table 5.8 lists the values obtained for $k_{reverse}$.

Table 5.6 Parameters for ^{13}C Selective Inversion Experiments for DADS

Temp (°C)	Inverted Peak	^{13}C shift	Obs. Peak	^{13}C shift	O1 (Hz)	# data points	# scans
19.0	NCH2ZZ1	43.4	NCH2ZE2	45.9	-10733.329	24	350
29.9	NCH2ZZ1	43.4	NCH2ZE2	45.9	-10734.595	26	400
37.5	NCH2ZE1	48.0	NCH2ZE2	45.9	-10149.975	21	300
37.5	NCH2ZE2	45.9	NCH2ZE3	46.6	-10420.445	18	400
37.5	NCH2ZE1	48.0	NCH2ZE2	45.9	-10145.188	10	750
41.6	NCH2ZE1	48.0	NCH2ZE2	45.9	-10146.243	15	750
30.7	NCH2ZE1	48.1	NCH2ZE3	46.6	-10148.317	13	900
30.7	NCH2ZE3	44.9	NCH2ZE1 NCH2ZE2	47.3 48.2	-10550.153	13	675

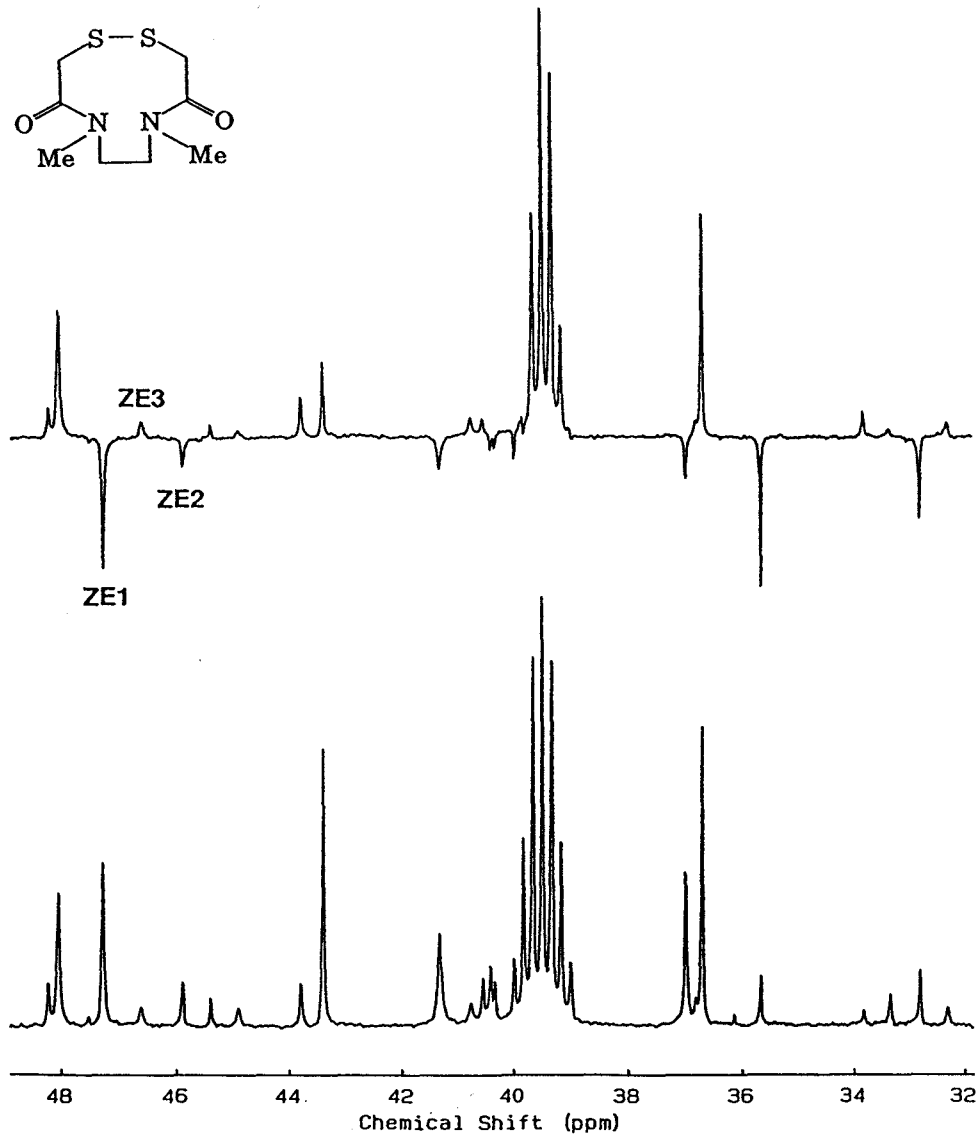

Figure 5.17 Typical 125.76 MHz ^{13}C selective inversion initial state (upper spectrum) with equilibrium (lower) spectrum, for DADS, **5.1**, in dmso-d_6. This experiment probes the *ZE1-ZE3* and *ZE2-ZE3* processes.

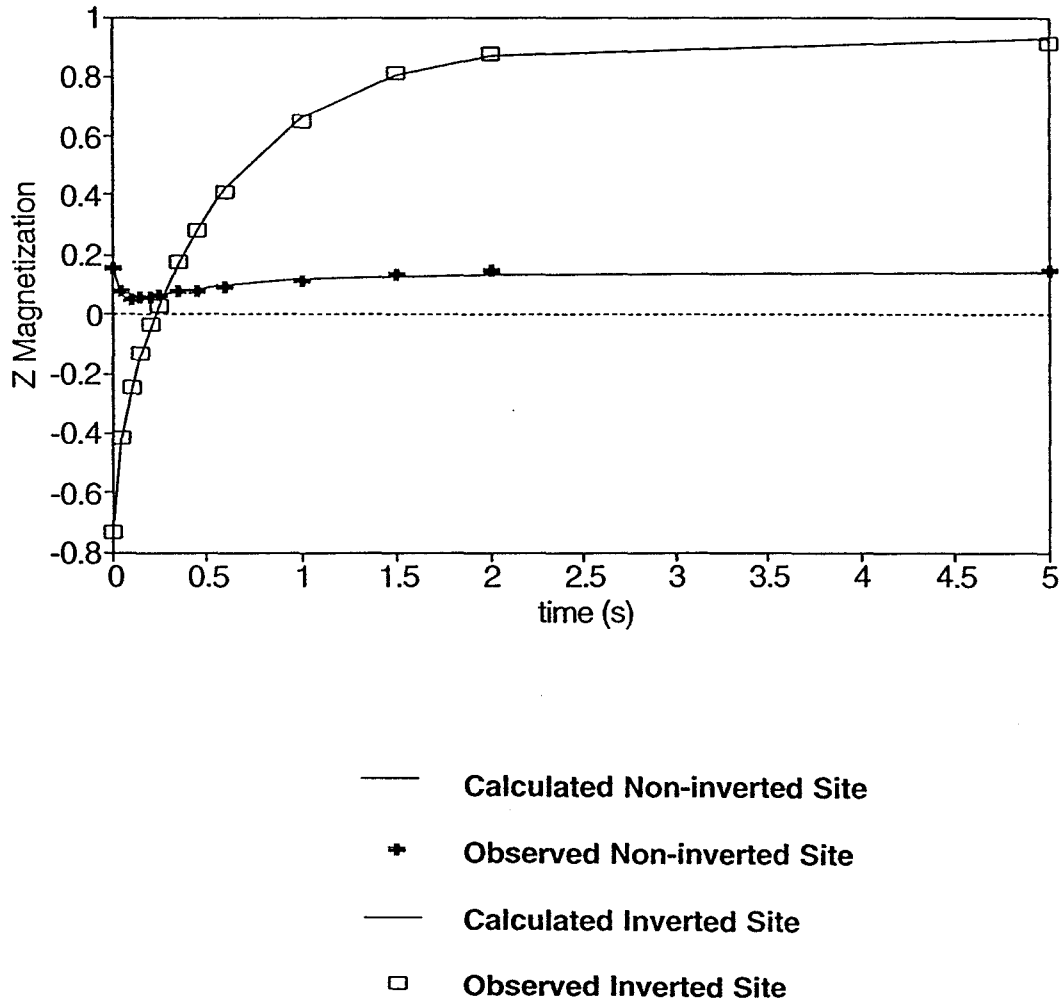

Figure 5.18 Experimental data vs. calculated data obtained from a ^{13}C selective inversion recovery experiment for DADS, **5.1**.

Table 5.7 Rate Constants ($k_{forward}$) Derived From Selective Inversion Experiments for the Barrier to Rotation About the Disulfide Bond in DADS

Temp (°C)	Rate 1-2 (s^{-1})	Rate 1-3 (s^{-1})
19.0	0.9 ± 0.1	0.9 ± 0.1
30.7	2.1 ± 0.1	2.1 ± 0.1
37.5	4.4 ± 0.4	4.4 ± 0.4
41.6	5.5 ± 0.4	5.5 ± 0.4

Table 5.8 Rate Constants ($k_{reverse}$) Derived From Selective Inversion Experiments for the Barrier to Rotation About the Disulfide Bond in DADS

Temp (°C)	Rate 2-1 (s^{-1})	Rate 3-1 (s^{-1})
19.0	2.7 + 0.3	5.1 + 0.6
30.7	8.0 + 0.6	23.5 + 2.4
37.5	13.5 + 2.1	39.8 + 21.6
41.6	17.9 + 1.2	59.3 + 16.3

^{13}C lineshape analysis was performed at four temperatures, calculating only the N-methylene region of the spectrum. The rate constants obtained are listed in table 5.9. The calculated and the N-methylene region of the experimental spectra are shown in figure 5.19. The complete ^{13}C experimental spectra at these temperatures are shown in figure 5.20.

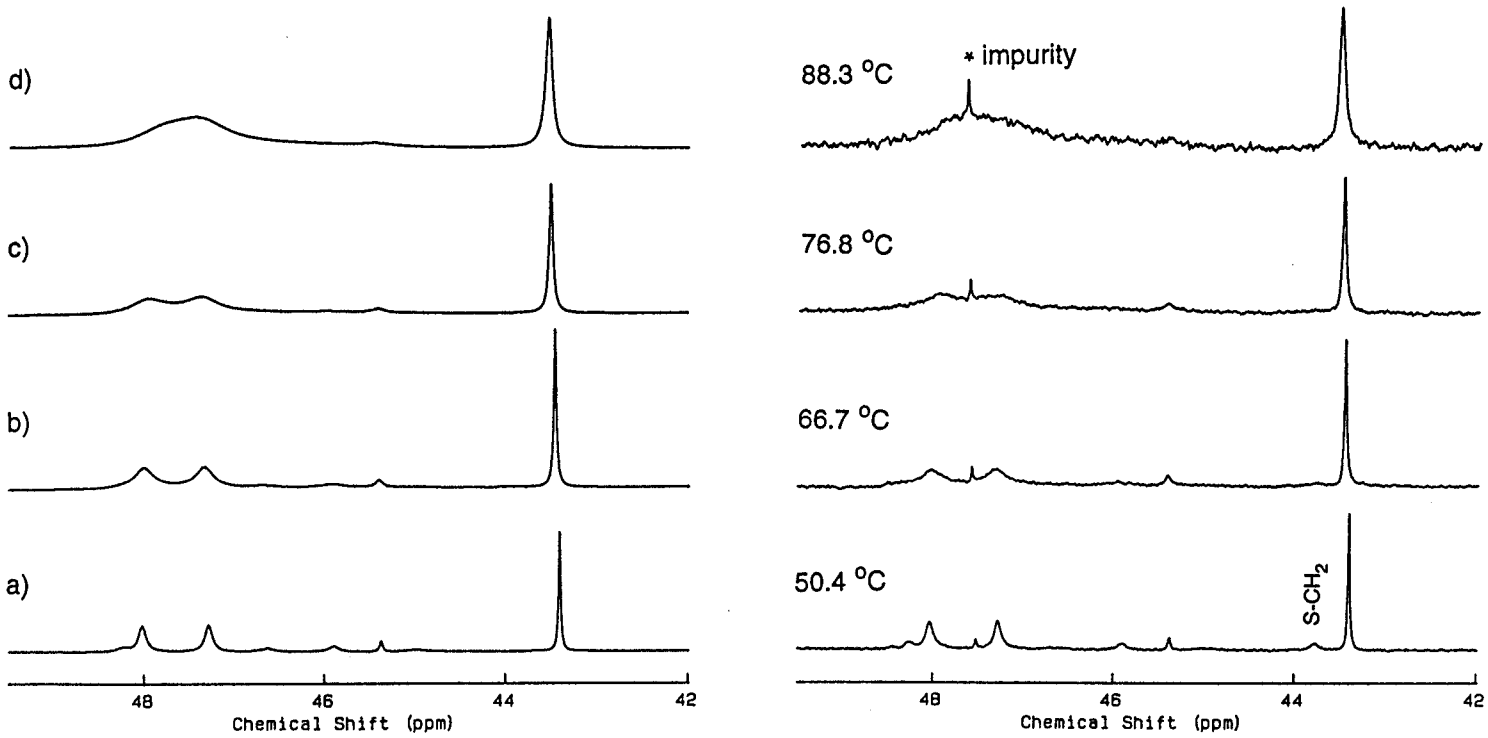

Figure 5.19 N-methylene region of the calculated spectra (left) and the experimental 125.76 MHz ^{13}C NMR spectra, in dmso-d_6 (right) for DADS, **5.1**. In a), the rate of exchange for the disulfide process is 14 s^{-1}, and the rate of exchange for the amide process is 0.4 s^{-1}. In b), the rate for the disulfide process is 40 s^{-1}, and the rate for the amide process is 2 s^{-1}. In c), the rate for the disulfide process is 80 s^{-1}, while the rate for the amide process is 5 s^{-1}. Finally, in d), the rate for the disulfide process is 160 s^{-1}, while the rate for the amide process is 12 s^{-1}.

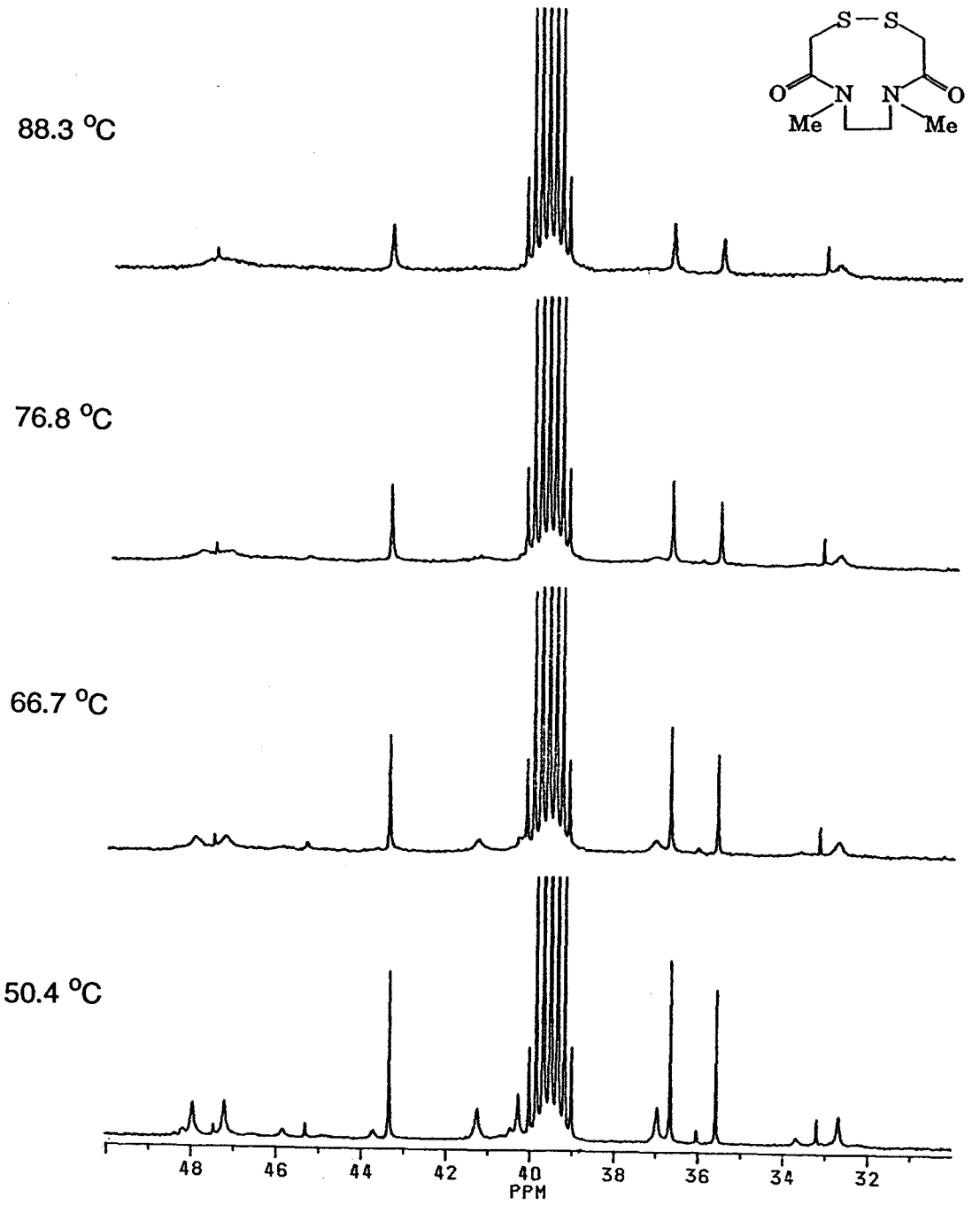

Figure 5.20 Variable temperature 125.76 MHz ^{13}C NMR spectra for DADS, **5.1**, in dmso-d_6, showing all of the resonances.

Table 5.9 Rate Constants Derived from ^{13}C Lineshape Analysis

Temperature (°C)	Rate (s^{-1}) for Disulfide Process	Rate (s^{-1}) for Amide Process
50.4	14	0.4
66.7	40	2
76.8	80	5
88.3	160	12

An Eyring plot (figure 5.21) was computed for the disulfide processes, *ZE1-ZE2* and *ZE1-ZE3* and gives $\Delta H^{\ddagger}$= 15.3 ± 0.4 kcal/mol. $\Delta S^{\ddagger}$ is -6.3 ± 1.1 eu.

The Eyring plot (figure 5.22) using $k_{reverse}$ yields $\Delta H^{\ddagger}$ = 15.1 ± 0.6 kcal/mol for the *ZE2-ZE1* disulfide process, and $\Delta H^{\ddagger}$ = 19.3 ± 1.4 kcal/mol for the *ZE3-ZE1* process. $\Delta S^{\ddagger}$ = -4.9 ± 2.0 eu for the *ZE2-ZE1* process, and $\Delta S^{\ddagger}$ = 10.8 ± 4.6 eu for the *ZE3-ZE1* process.

An Eyring plot (figure 5.23) was computed for the amide processes, *ZZ1-ZE1* and *ZZ2-ZE1* and gives $\Delta H^{\ddagger}$ = 19.8 ± 0.4 kcal/mol. $\Delta S^{\ddagger}$ is 0.7 ± 1.2 eu.

5.3.3 Discussion of the Thermodynamic Parameters

Typical amide rotational barriers for amides are $\Delta H^{\ddagger}$ = 20.5 kcal/mol, with $\Delta S^{\ddagger}$ = -1.4 ± 1 eu for *N,N*-Dimethylformamide, and $\Delta H^{\ddagger}$ = 18.3 kcal/mol, with $\Delta S^{\ddagger}$ = 0.7 ± 1 eu for *N,N*-Dimethylacetamide.[43] The results obtained for both the uncyclized precursor to DADS, and for DADS itself are consistent with these numbers.

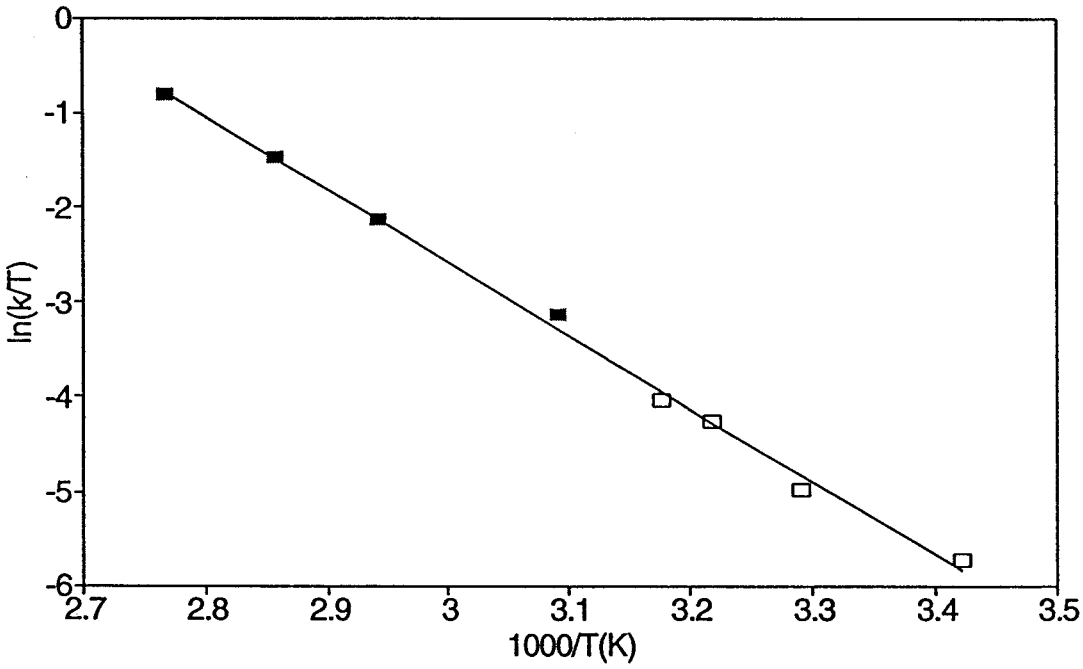

Figure 5.21 Eyring plot of ln(*k*/*T*) vs. 1000/*T* for the disulfide process in DADS, **5.1**. The filled squares represent rate constants derived from ^{13}C lineshape analysis, while the open squares represent rate constants derived from ^{13}C selective inversion experiments.

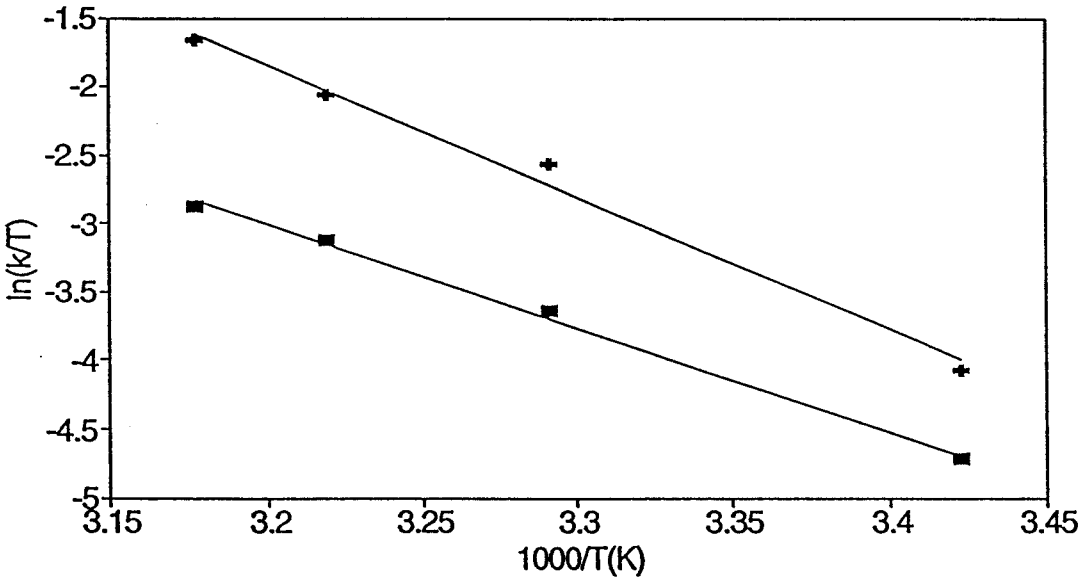

Figure 5.22 Eyring plot of $\ln(k_{reverse}/T)$ vs. $1000/T$ for the disulfide process in DADS, **5.1**. The filled squares represent the *ZE2-ZE1* process, while the crosses represent the *ZE3-ZE1* process. All rate constants were derived from ^{13}C selective inversion experiments.

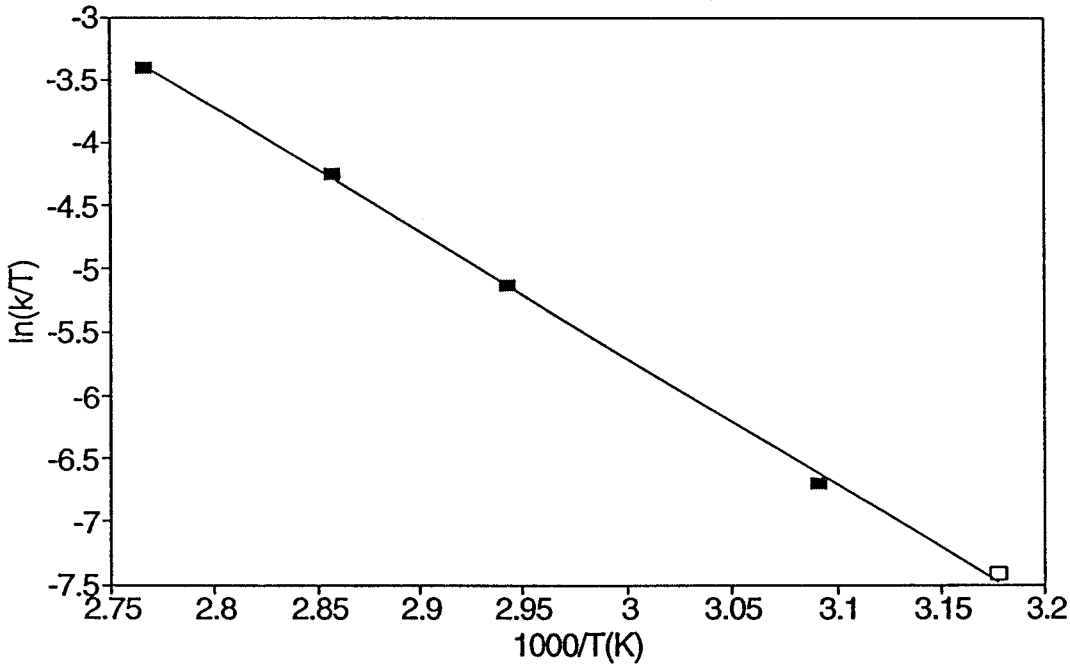

Figure 5.23 Eyring plot of ln(k/T) vs. 1000/T for the amide process in DADS, **5.1**. The filled squares represent rate constants derived from ^{13}C lineshape analysis, while the open square represents a rate constant derived from a ^{13}C selective inversion experiment.

Barriers to rotation about the S-S bond of disulfides are not so readily compared to literature values, as they have not been studied extensively, and barriers vary widely, depending upon the molecule under study.

Theoretical studies investigating disulfide bridges commonly use dimethyl disulfide because it is the simplest model compound containing the C-S-S-C sequence found in the disulfide bridge regions of cysteine containing peptides and proteins.[44] These computations result in two energy barriers for rotation about the S-S bond. Both the cis and trans transition states are produced by a 90^{o} rotation (in opposite directions) about the S-S bond from the ground state configuration.[45] Minimum energy conformations have a C-S-S-C dihedral angle of $80\text{-}90^{o}$.[46] The trans barrier is found to be lower than the cis barrier.

Actual values for the barriers vary widely. Values for the cis barrier range from 9.4-24.1 kcal/mol, while trans barriers have been calculated to be anywhere from 5.72 to 12.7 kcal/mol, depending upon the level of the calculations.[47]

Experimental Results

Fraser *et al* have reported barriers to rotation about the S-S bond in eight unhindered acyclic disulfides.[45] The disulfides have the structure $C_6H_5CH_2SSR$, and Fraser determined $\Delta G^{\ddagger}$ values from 7 to 9.4 kcal/mol, increasing with the size of R, using the coalescence method. Fraser concluded that the size of the disulfide barrier for acyclic disulfides would be 7 kcal/mol or less, if there are no steric effects.

$\Delta G^{\ddagger}$'s increase for more hindered acyclic disulfides. For example, for the molecule bis(4-methyl-2,6-di-tert-butylphenyl) disulfide,

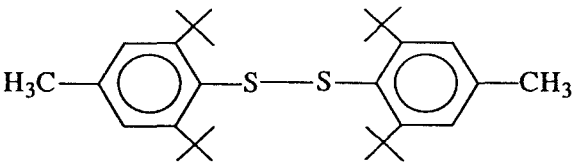

Kessler and Rundel used the coalescence method to determine a $\Delta G^{\ddagger}$ of 15.7 kcal/mol.[48]

Constraining the S-S bond to a ring appears to increase the energy barrier by several kcal/mol.[46] For instance, Claeson found the barrier to inversion in the six-membered ring, 1,2-dithiane to be $\Delta G^{\ddagger}$ =11.6 kcal/mol[49,50], while Weiss-Lopez found the barrier to inversion in the nine-membered 1,2-dithiacyclononane to be $\Delta G^{\ddagger}$ =11.7 kcal/mol, using lineshape analysis.[51] Claeson found a barrier to inversion of $\Delta G^{\ddagger}$ =16.1 kcal/mol in the more hindered molecule, 3,3,6,6-tetramethyl-1,2-dithiane, using lineshape analysis.[50]

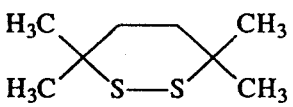

Barriers to inversion have been reported in several rings containing more than one disulfide bond. Bushweller found a barrier for chair to twist equilibration of $\Delta G^{\ddagger}$ =16.5 kcal/mol in tetramethyl-s-tetrathiane (duplodithioacetone), using a combination of the lineshape method and kinetic data obtained by allowing the isolable twist form to equilibrate to the chair conformer.[52]

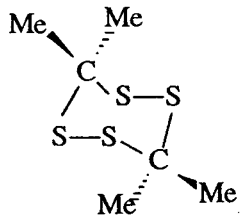

Chenard *et al.* found barriers to ring inversion in tetrathiepins, with $\Delta G^{\ddagger}$ ranging from 17.5 - 21.2 kcal/mol, depending on the relative location of the sulfur atoms.[53]

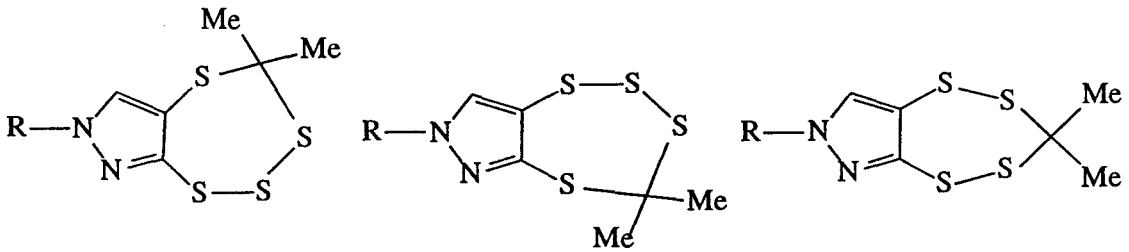

The tetrathiepins with trisulfide bridges have the lower barriers, while the tetrathiepin with the two disulfide bonds has the higher barrier. He used lineshape and selective inversion experiments.

Finally, in a cyclic system with 2 disulfide bonds and two amide groups, Lidert found a barrier to inversion of $\Delta G^{\ddagger}$ =17.3 kcal/mol, using lineshape analysis, which he attributes to disulfide rotation.[54] He completely discounts hindered rotation about the C-N amide bond.

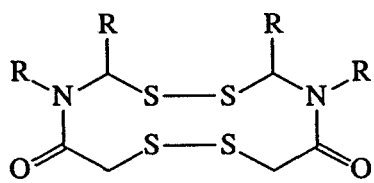

In conclusion, a combination of ^{13}C NOESY, ^{13}C single selective inversion, and ^{13}C lineshape analysis experiments identified the exchange pathways and determined temperature-dependent rate constants for the DADS system. DADS exists as five exchanging rotamers in solution. Two of the conformers are symmetric, with C_2 symmetry (*ZZ1* and *ZZ2*). The other three conformers are asymmetric, with one amide group cis and the other trans (*ZE1, ZE2, ZE3*).

The NOESY experiments gave a site-to-site map of the exchange processes at several temperatures. At room temperature, *ZE1* is exchanging with both *ZE2* and *ZE3*, but there appears to be no exchange between *ZE2* and *ZE3*. This process seems to occur via hindered rotation about the disulfide bond, with $\Delta H^{\ddagger} = 15.3 \pm 0.4$ kcal/mol, and $\Delta S^{\ddagger} = -6.3 \pm 1.1$ eu. This is not an unusual barrier for a disulfide bond that is constrained in a ring.

At higher temperatures, *ZZ1* and *ZZ2* start to exchange with *ZE1* via hindered rotation about the amide bonds. $\Delta H^{\ddagger}$ for the process was determined to be 19.8 ± 0.4 kcal/mol, and $\Delta S^{\ddagger}$ was found to be 0.7 ± 1.2 eu. These values are in accord with amide barriers reported in the literature. Further, the barrier agrees quite well with that measured for the uncyclized precursor to DADS, **5.2.** $\Delta H^{\ddagger}$ was found to be 19.3 ± 0.7 kcal/mol, while $\Delta S^{\ddagger}$ was determined to be 2.5 ± 2.1 eu.

While the kinetics for this system are now well defined, there is little known about the actual structures of the conformations in solution. Maharajh gained some insight into the stereochemistry of the two major rotamers using NOE difference experiments. Future work includes slowing the chemical exchange down enough to perform NOE difference experiments on the minor

conformations. It may also be possible to obtain some structural information from the N-methylene coupling constants.

5.4 Experimental Section

5.4.1 DADS

Approximately fifty milligrams of *N,N'*-[dimethyl-(2,2'-dithiobisacetyl)]-ethylenediamine, were dissolved in about 0.5 mL dmso-d_6 (MSD Isotopes) in a thin-walled NMR tube, by Rob Maharajh.

All spectra were recorded spinning, locked on the signal of the solvent dmso-d_6. Peaks were referenced to the residual proton signal of the solvent at 2.49 ppm, or to the ^{13}C solvent signal at 39.5 ppm, regardless of temperature.

All experiments except the ^{1}H - ^{13}C shift correlated experiment have been performed on a Bruker AM-500 spectrometer, with an 11.744 T superconducting magnet, using a five mm dual frequency ^{1}H - ^{13}C probe. Proton spectra were run at 500.135 MHz, while ^{13}C spectra were run at 125.759 MHz. The spectrometer was equipped with a Bruker B-VT 1000 temperature controller. Each temperature was measured by placing a copper-constantan thermocouple, contained in an NMR tube, into the probe. Typically, forty minutes to one hour were allowed for the temperature to equilibrate.

For processing, all 1D FID's were transferred to a PC using the program NMRLINK. Spectra were then processed on a PC using the program NMR286.

^{13}C Broadband Decoupled Spectrum

The spectrum was recorded with a sweep width of 20,000.00 Hz, O1 set at -4194.623 Hz, over 16K data points, at ambient temperature (30 °C).

Composite pulse decoupling was used, with the decoupler power set at 17H. A ^{13}C pulse width of 2.5 µsec was used, which is a flip angle of approximately 35 degrees. The relaxation delay was 0.5 seconds. 26,108 scans were acquired, with an acquisition time of 0.4096 seconds, giving a resolution of 2.441 Hz/data point.

DEPT Experiment

The ^{13}C 90° pulse width was determined to be 6 µsec, and the proton 90° pulse width was determined to be 18 µsec. The experiment was performed at ambient temperature (30 °C). Only the aliphatic region of the spectrum was acquired, between 50 - 20 ppm, ignoring the low field carbonyl signals. The program used was DEPT.AUR. A 135 ° pulse was used, so that CH and CH_3 peaks would be positive, while CH_2 peaks would be negative. The spectrum was acquired with a sweep width of 5000 Hz, and O1 set at -11282.253 Hz, over 8K data points. 2048 scans were acquired with an acquisition time of 0.819 sec, giving a resolution of 1.221 Hz/data point.

Measurement of ^{13}C Spin-lattice Relaxation Times

The program INVREC2P.AUR was used, as described in chapter two. Variable delays of 0.001, 0.1, 0.3, 0.5, 0.75, 1.0, 2.0, 3.0, 5.0, 10.0 and 20.0 seconds were used, with the values being entered randomly. Each spectrum was acquired over a sweep width of 5000 Hz, with O1 set at -11282.253 Hz, over 8K data points. Three hundred scans were collected for each spectrum, with an acquisition time of 0.819 seconds, giving a resolution of 1.221 Hz/data point.

The spectra were Fourier transformed under identical conditions, with absolute intensity set to one, using the program NMR286. Exponential multiplication, with a line broadening of 4 Hz was used.

An input data file consisting of variable delay times and corresponding magnetizations (as measured from transformed spectra) for each peak in the ^{13}C spectrum was created. This data was fitted with the non-linear least squares fitting program, T1cals, to calculate T_1's for each site.

^{13}C Selective Inversion Experiments

The same program INVREC2P.AUR was used, as described in chapter two. Experiments were performed over the temperature range 19.0 to 41.6 °C. Only the aliphatic region of the spectrum was acquired, with a typical sweep width of 5000 Hz, over 8K data points, with an acquisition time of 0.786 sec and resolution of 1.271 Hz/data point. The number of scans accumulated for each spectrum varied between 400-800, depending on the time available on the spectrometer. In early experiments, more spectra were acquired with fewer scans, in later experiments, less spectra were acquired with more scans. The spectra were recorded decoupled with a decoupler power of 17H. The ^{13}C 90^o pulse width was determined before each experiment. Typically, it was 6 µsec at 30 °C, varying slightly with temperature.

All FID's were transferred to an IBM PC using the program NMRLINK, then Fourier transformed under identical conditions using the program NMR286. Exponential multiplication was applied to the FID's, typically with 5 Hz line broadening.

For each selective inversion experiment, an input file was created,

consisting of variable delay times, and the corresponding magnetizations for each site involved in the exchange process. This data was fitted using the non-linear least squares fitting program, FLOPSI.

Rate constants for the disulfide process were determined using twelve sites, the N-methylene and the S-methylene carbons for each of the ZE1, ZE2 and ZE3 rotamers. The methyl signals could not be used because one of them is buried under the dmso-d_6 signal, and intensities could not be measured for it. Both the *ZE1-ZE2* and the *ZE1-ZE3* rates were varied simultaneously, along with M_∞ and M_∞-M_0 for each site. The T_1's have not as yet been varied along with the other parameters.

At 41.6 °C, it was also possible to determine a rate constant for the *ZZ2* to *ZE1* exchange. It had just begun, but there was no measurable exchange between *ZZ1* and *ZE1* occurring at this temperature.

^{13}C NOESY Experiments

The program NOESYPH.AUR was used with the pulse sequence described in chapter one. The first NOESY experiment was performed at 30 °C, with a mixing time of 0.5 seconds, 1024 words in the f_1 dimension, and 512 words in the f_2 dimension. As only the aliphatic region of the spectrum was acquired, the sweep width was 3676.471 Hz, with O1 at -11658.864 Hz. Eighty scans were collected for each spectrum. FID's were processed on the AM-500 with Gaussian window function in both f_1 and f_2 and a line broadening of 10 Hz. The ^{13}C 90^o pulse width was 6 µsec. The relaxation delay (D1) was set to 1 sec, and the initial value for the 2D evolution was set to 10 µsec.

A second NOESY experiment was performed with the same parameters

as above, except that the mixing time was 1 second, f_1 = 512 words, f_2 = 256 words, and the number of scans per spectrum was 104. The relaxation delay was set to 1.5 sec.

A NOESY was performed at 45.6 °C, with a mixing time of 0.1 seconds, f_1 equal to 1K, f_2 equal to 512 words, and relaxation delay equal to 2 sec. 80 scans were collected per spectrum. The ^{13}C 90° pulse width was determined to be 6 μsec.

A NOESY was then recorded at 55.1 °C on the AM-500. The 90° pulse width was determined to be 7 μsec. The mixing time was set to 0.7 s. The aliphatic region was again acquired, but excluding the DCU peaks at high field, thus a sweep width of 2196.014 Hz was used, with O1 set at -11143.623 Hz. F_1 was set to 512 words, f_2 was set to 256 words, and 96 scans were collected per spectrum.

A NOESY was recorded at 50.1 °C on the AM-500. The 90° pulse width was determined to be 6.4 μsec. The mixing time was set to 0.1 s. Spectra were acquired over the aliphatic region, with a SW of 2873.563 Hz, O1 set at -11206.486 Hz, and an acquisition time of 0.178 s. F_1 was set to 1K, f_2 was set to 512 words, and 300 scans were collected per spectrum.

^{13}C Variable Temperature Spectra

Variable temperature ^{13}C spectra were acquired on the AM-500 at 50.4, 66.7, 76.8 and 88.3 °C. The aliphatic region of the spectrum was recorded, with a sweep width of 4000 Hz, with the O1 set at -11279.779 Hz, over 16K data points, giving a resolution of 0.488 Hz/pt. 9,500 scans were collected for each spectrum. Composite pulse decoupling was used with a decoupler power of

17H.

^{1}H - ^{13}C Shift Correlation Experiment

A ^{1}H - ^{13}C shift correlation experiment experiment was performed on a Bruker AC-300, with a 7.65 T superconducting magnet, equipped with a Bruker B-VT 2000 temperature controller. Protons were observed at 300.13 MHz, and ^{13}C was observed at 75.47 MHz.

The program XHCORRC.AU was used, in an attempt to see vicinal couplings. The ^{13}C 90^{o} pulse width was determined to be 4.4 μsec. The decoupler 90^{o} ^{1}H pulse width was determined to be 9 μsec, using the DEPT program.

The sweep width in f_1 was 408.50 Hz, recorded in 512 words. 256 spectra in f_2 were recorded with a sweep width of 1510.57 Hz. 160 scans were collected for each spectrum. The relaxation delay was set to 1 sec, the polarization transfer delay was set to 3.5 msec (t_2= $1/2^{1}J_{CH}$) and the refocussing delay was set to 1.7 msec ($1/4^{1}J_{CH}$). The data was processed on the AC-300 spectrometer using a shifted sine bell squared window function in f_1 and a Gaussian window function in f_2.

^{1}H Spectra

Spectra were acquired at room temperature and at 20 °C, with a sweep width of 1700.68 Hz, over 8K data points. Ninety scans were collected for each spectrum, with an acquisition time of 2.408 sec, giving a resolution of 0.4152 Hz/data point.

5.4.2 *N,N'*-{dimethylbis[2-(triphenylmethyl)thioethanoyl]}ethylenediamine

Approximately 100 mg of *N,N'*-{dimethylbis[2-(triphenylmethyl)-thioethanoyl]}ethylenediamine was dissolved in 0.5 mL dmf-d_7. N_2 was bubbled through the solution to degas it.

All NMR experiments have been performed on a Bruker AM-500 spectrometer, equipped with a Bruker B-VT 1000 temperature controller, and a dual frequency ^1H -^{13}C probe. All spectra were recorded spinning, locked on the solvent signal of the solvent dmf-d_7. Chemical shifts were referenced to the residual proton signal of dmf-d_7, regardless of temperature. Each temperature was measured by placing a copper-constantan thermocouple, contained in an NMR tube, into the probe. Typically, forty minutes to one hour were allowed for the temperature to equilibrate.

Single Selective Inversion Recovery Experiments

Selective inversion recovery experiments were performed using the program INVREC2P.AU, as described previously.

At 29.6 °C, the high frequency ^1H *ZE* resonance at 2.818 ppm was inverted, while observing the *EE* peak at 2.643 ppm. Each spectrum was acquired with a sweep width of 7042.254 Hz, with the O1 at 9084.4 Hz, over 32K data points. Eight scans were collected for each spectrum, with an acquisition time of 2.326 s, giving a resolution of 0.430 Hz/pt. The variable delays used were 0.001, 25, 0.8, 20, 0.2, 0.5, 0.01, 0.05, 0.3, 5, 10, 0.08, 3, 1, 4, 0.09, 15, 1.2, 2, 1.5, 12 and 8 seconds.

A selective inversion experiment was performed at 41.6 °C, with the same parameters as at 29.6 °C.

At 42.2 °C, four ^{1}H selective inversion experiments were performed. Only the aliphatic region of the NMR spectrum was acquired. Typically, the spectra were acquired with a sweep width of 952.381 Hz, over 8K data points. Four scans were collected for each spectrum, with an acquisition time of 4.30 s, giving a digital resolution of 0.233 Hz/point. The position of the O1 varied as listed in table 5.10.

Table 5.10 Parameters for ^{1}H Selective Inversion Experiments for *N,N'*-{dimethylbis[2-(triphenylmethyl)-thioethanoyl]}ethylenediamine

Inverted Peak	O1 (Hz)	Observed Peak
NCH_3ZZ	9043.895	NCH_3ZE (high frequency)
NCH_3ZZ	9043.895	NCH_3ZE (low frequency)
NCH_3ZE (high frequency)	9084.12	EE
NCH_3ZE (low frequency)	8978.791	EE

The variable delays used were 0.001, 10, 0.01, 0.09, 8, 0.5, 0.05, 5, 0.08, 1.2, 0.9, 0.2, 0.8, 3, 1.5, 2, 0.3 and 1 second.

At 42.2 °C, one ^{13}C selective inversion experiment was performed. The NCH_2ZZ peak was inverted, while the low frequency NCH_2ZE peak was observed. Each spectrum was acquired with a sweep width of 2100.84 Hz, and the O1 set at -10685.982 Hz, over 4K data points. 1024 scans were collected for each spectrum, with an acquisition time of 0.975 s, giving a resolution of 1.026 Hz/pt. The variable delays used were 0.001, 3, 1, 0.5, 0.01, 0.1, 0.4, 0.08, 0.2, 0.3, 0.6, 0.05, 0.15, 0.8 and 0.25 seconds.

Spin-lattice Relaxation Times

A ^{13}C non selective inversion recovery experiment, using the program INVREC2P.AU, was performed at 42.2 °C, in order to determine the spin-lattice relaxation times for the N-methylene carbons. Each spectrum was acquired with a sweep width of 1319.261 Hz, with the O1 set at -10303.345 Hz, over 2K data points. 1024 scans were collected for each spectrum, with an acquisition time of 0.776 seconds, giving a digital resolution of 1.288 Hz/pt. The variable delays used were 0.001, 10, 0.1, 7, 0.5, 5, 0.01, 0.2, 1, 0.4, 0.3 and 2 seconds.

^{1}H T_1's were determined at 42.2 °C. Each spectrum was acquired with a sweep width of 633.371 Hz, and O1 set at 9162.245 Hz, over 8K data points. Four scans were collected for each spectrum, with an acquisition time of 6.463 seconds, giving a digital resolution of 0.155 Hz/pt. The variable delays used were the same as for the selective inversion experiment at 29.6 °C, described above.

Variable Temperature NMR Spectra

Spectra for use in lineshape analysis were collected at four temperatures, 53.0, 64.7, 72.6 and 82.9 °C.

The ^{13}C spectra were acquired only over the N-methylene region of the spectrum. The sweep width was set to 2304.147 Hz, with O1 set at -10647.002 Hz. Each spectrum was acquired over 4K data points, with an acquisition time of 0.888 s, giving a digital resolution of 1.125 Hz/pt. The number of scans varied, increasing with temperature, as the peaks became increasingly more exchange broadened.

The ^{1}H spectra were acquired over the entire spectral region, with the

sweep width set at 4201.681 Hz, and O1 set at 10282.703 Hz. Each spectrum was acquired over 32K data points, with an acquisition time of 3.899 s, giving a digital resolution of 0.256 Hz/pt. Sixteen scans were collected for each spectrum.

The experimental ^{13}C spectra were compared to spectra that were calculated using Bain's program, to obtain temperature dependent rate constants.

An Eyring plot was computed, to obtain activation parameters.

^{1}H - ^{13}C Shift Correlation Experiment

A ^{13}C-^{1}H shift correlated experiment was run on a Bruker AM 500, using the program XHCORRDC.AU.

The ^{13}C 90° pulse width was determined to be 6.4 μsec. The decoupler 90° pulse width was determined to be 18.6 μsec, using the DEPT sequence. The sweep width in f_1 was 424.448 Hz, recorded in 256 words. 512 spectra were recorded in f_2, with a sweep width of 3267.974 Hz. 725 scans were acquired for each spectrum. The relaxation delay was set to 1 sec, the polarization transfer delay was set to 3.57 msec, and the refocussing delay was set to 1.78 msec. The data was processed on the AM 500 using a shifted sine bell squared window function in f_1, and a Gaussian function in f_2, with 12.8 Hz line broadening.

^{1}H NOESY Spectrum

A NOESY spectrum was recorded at 42.2 °C, with a mixing time of 0.1 seconds, 1024 words in the f_1 dimension, and 512 words in the f_2 dimension.

The sweep width was 819.672 Hz, with the O1 set at 9249.988 Hz. The 90^{o} ^{1}H pulse width was determined to be 18.25 μsec. Four scans were collected for each spectrum. The relaxation delay was set to 2 seconds, and the initial value for the 2D evolution was set to 10 μsec. The data were processed on the AM 500 with Gaussian window functions in both f_1 and f_2, and a line broadening of 1.6 Hz.

References

1) Jeener, J.; Meier, B.H.; Bachmann, P.; Ernst, R.R. *J. Chem. Phys.*, **1979**, *71*, 4546-4553.

2) Perrin, C.L.; Dwyer, T. *Chem. Rev.*, **1990**, *90*, 935-967.

3) Sandström, J., *Dynamic NMR Spectroscopy*; Academic Press: London, 1982.

4) Orrell, K.G.; Sik, V.; Stephenson, D. *Prog. Nucl. Magn. Reson. Spectrosc.*, **1990**, *22*, 141-208.

5) Jackman, L.M.; Cotton, F.A., *Dynamic Nuclear Magnetic Resonance Spectroscopy*; Academic Press: New York, 1975.

6) Bain, A.D.; Cramer, J.A. *J. Magn. Reson.*, **1993**, *A 103*, 217-222.

7) Bain, A.D.; Cramer, J.A. *J. Phys. Chem.*, **1993**, *97*, 2884-2887.

8) Chen, Y-X.; Rausch, M.D.; Chien, J.C.W. *Organometallics*, **1993**, *12*, 4607-4612.

9) Decken, A.; Girard, L.; Rigby, S.S.; McGlinchey, M.J.; Bain, A.D. manuscript in progress.

10) Maharajh, R.B. *Ph.D. Thesis*, McMaster University, 1993.

11) Derome, A.E., *Modern NMR Techniques for Chemistry Research*; Pergamon Press: Oxford, 1988.

12) Sanders, J.K.M.; Hunter, B.K., *Modern NMR Spectroscopy - A Guide For Chemists*; Oxford University Press: Oxford, 1988.

13) Harris, R.K., *Nuclear Magnetic Resonance Spectroscopy*; Pitman Books Limited: London, 1983.

14) Stephenson, D.S.; Binsch, G. *J. Magn. Reson.*, **1978**, *32*, 145-152.

15) Forsén, S.; Hoffman, R.A. *J. Chem. Phys.*, **1964**, *40*, 1189-1196.

16) Hoffman, R.A.; Forsén, S. *J. Chem. Phys.*, **1966**, *45*, 2049-2060.

17) Forsén, S.; Hoffman, R.A. *J. Chem. Phys.*, **1963**, *39*, 2892-2901.

18) Dahlquist, F.W.; Longmuir, K.J.; DuVernet, R.B. *J. Magn. Reson.*, **1975**, *17*, 406-410.

19) Alger, J.R.; Prestegard, J.H. *J. Magn. Reson.*, **1977**, *27*, 137.

20) Led, J.J.; Gesmar, H. *J. Magn. Reson.*, **1982**, *49*, 444-463.

21) Gesmar, H.; Led, J.J. *J. Magn. Reson.*, **1986**, *68*, 95-101.

22) Grassi, M.; Mann, B.E.; Pickup, B.T.; Spencer, C.M. *J. Magn. Reson.*, **1986**, *69*, 92-99.

23) Muhandiram, D.R.; McClung, R.E.D. *J. Magn. Reson.*, **1987**, *71*, 187-192.

24) Morris, G.A.; Freeman, R. *J. Magn. Reson.*, **1978**, *29*, 433-462.

25) Bodenhausen, G.; Freeman, R.; Morris, G.A. *J. Magn. Reson.*, **1976**, *23*, 171-175.

26) McConnell, H.M. *J. Chem. Phys.*, **1958**, *28*, 430-431.

27) McConnell, H.M.; Thompson, D.D. *J. Chem. Phys.*, **1957**, *26*, 958-959.

28) Gutowsky, H.S.; Holm, C.H. *J. Chem. Phys.*, **1956**, *25*, 1228-1234.

29) Farrugia, L.J.; Rae, S.E. *Organometallics*, **1992**, *11*, 196-206.

30) Perrin, C.L. *J. Magn. Reson.*, **1989**, *82*, 619-621.

31) McMaster, A.D.; Stobart, S.R. *J. Am. Chem. Soc.*, **1982**, *104*, 2109-2112.

32) Davison, A.; Rakita, P.E. *J. Organomet. Chem.*, **1970**, *23*, 407-426.

33) Girard, L. private communication with.

34) Larrabee, R.B.; Dowden, B.F. *Tet. Lett.*, **1970**, *12*, 915-918.

35) Ashe, A.J.III *Tet. Lett.*, **1970**, 2105-2138.

36) Marechal, E.; Tortal, J.-P. *C. R. Acad. Sci. Paris*, **1968**, *267*, 467-470.

37) Decken, A.; Britten, J.F.; McGlinchey, M.J. *J. Am. Chem. Soc.*, **1993**, *115*, 7275-7284.

38) Rieker, A.; Kessler, H. *Tet. Lett.*, **1969**, 1227-1230.

39) Siddall, T.H.; Stewart, W.E. *Tet. Lett.*, **1968**, 5011-5014.

40) Siddall, T.H.; Stewart, W.E. *J. Org. Chem.*, **1969**, *34*, 233-237.

41) Siddall, T.H.; Stewart, W.E. *J. Chem. Soc. ,Chem. Commun.*, **1968**, 1116-1117.

42) Biagioni, R.N.; Lorkovic, I.M.; Skelton, J.; Hartung, J.B. *Organometallics*, **1990**, *9*, 547-551.

43) Drakenberg, T.; Dahlqvist, K-I.; Forsén, S. *J. Phys. Chem.*, **1972**, *76*, 2178-2190.

44) Renugopalakrishnan, V.; Walter, R. *Z. Naturforsch.*, **1984**, *39(a)*, 495-498.

45) Fraser, R.R.; Boussard, G.; Saunders, J.K.; Lambert, J.B.; Mixan, C.E. *J. Am. Chem. Soc.*, **1971**, *93*, 3822-3823.

46) Guttenberger, H.G.; Bestmann, H.J.; Dickert, F.L.; Jorgenson, F.S.; Snyder, J.P. *J. Am. Chem. Soc.*, **1981**, *103*, 159-168.

47) Jiao, D.; Barfield, M.; Combariza, J.E.; Hrubny, V.J. *J. Am. Chem. Soc.*, **1992**, *114*, 3639-3643.

48) Kessler, H.; Rundel, W. *Chem. Ber.*, **1968**, *101*, 3350-3357.

49) Claeson, G.; Androes, G.M.; Calvin, M. *J. Am. Chem. Soc.*, **1960**, *82*, 4428-4429.

50) Claeson, G.; Androes, G.M.; Calvin, M. *J. Am. Chem. Soc.*, **1961**, *83*, 4357-4361.

51) Weiss-Lopez, B.; Nash, C.P.; True, N.S. *Spectrochimica Acta*, **1989**, *45A*, 321-327.

52) Bushweller, C.H.; Golini, J.; Rao, G.U.; O'Neil, J.W. *J. Am. Chem. Soc.*, **1970**, *92*, 3055-3058.

53) Chenard, B.L.; Dixon, D.A.; Harlow, R.L.; Roe, D.C.; Fukunga, T. *J. Org. Chem.*, **1987**, *52*, 2411-2420.

54) Lidert, Z. *Tetrahedron*, **1981**, *37*, 967-969.